DOCKETED

Docket Number:	15-AFC-01
Project Title:	Puente Power Project
TN #:	218900
Document Title:	Expert Declaration of Phillip Mineart in Response to March 10, 2017 Committee Orders
Description:	N/A
Filer:	Patty Paul
Organization:	Latham & Watkins LLP
Submitter Role:	Applicant Representative
Submission Date:	6/15/2017 4:30:53 PM
Docketed Date:	6/15/2017

Michael J. Carroll
LATHAM & WATKINS LLP
650 Town Center Drive, 20th Floor
Costa Mesa, California 92626-1925
Tel.: (714) 540-1235
michael.carroll@lw.com

Attorneys for Applicant

State of California

Energy Resources

Conservation and Development Commission

In the Matter of: Application for Certification for the PUENTE POWER PROJECT	Docket No. 15-AFC-01 EXPERT DECLARATION OF PHILLIP MINEART IN RESPONSE TO MARCH 10, 2017 COMMITTEE ORDERS

I, Phillip Mineart, declare as follows:

1. I am employed by AECOM, which has been retained by the Applicant in these proceedings to conduct certain analyses associated with the proposed Puente Power Project (Project) and am duly authorized to make this declaration.

2. I earned a Bachelor of Science degree in Environmental Engineering from Humboldt State University in 1979 and a Master of Science degree in Civil Engineering from Cornell University in 1983. I have over 30 years of experience in the fields of hydrologic, hydraulic and hydrodynamic analysis, coastal engineering, erosion and sediment transport modeling, environmental restoration, risk assessments, climate change and sea level rise. A copy of my current curriculum vitae was previously submitted in these proceedings. Based on my education, training and experience, I am qualified to provide expert testimony as to the matters addressed herein.

3. Except where stated on information and belief, the facts set forth herein and in the attachments hereto are true of my own personal knowledge, and the opinions set forth herein and in the attachments hereto are true and correct articulations of my opinions. If called as a witness,

I could and would testify competently to the facts and opinions set forth herein and in the attachments hereto.

4. On March 10, 2017, the Committee ordered submission of additional evidence on a limited number of specific issues identified in the "Committee Orders for Additional Evidence and Briefing Following Evidentiary Hearings" (TN #216505) (the "March 10 Orders").

5. The March 10 Orders direct the California Energy Commission (CEC) staff and Applicant to prepare and submit specific additional evidence pertaining to four topic areas, including "Soil and Water Resources." With respect to the topic of Soil and Water Resources, the March 10 Orders direct the CEC staff and the Applicant to take certain actions and submit additional evidence, including the following:

- Develop and provide specified information pertaining to the CoSMoS 3.0 model utilized by CEC staff to analyze potential coastal hazards affecting the Puente Power Project.
- Conduct a noticed workshop to discuss and identify the best approach or approaches to supplement the assessment of coastal flooding risk for the Puente Power Project through 2050.
- Identify the best approach or approaches for assessing coastal flooding risk, and conduct an analysis using that approach or approaches, taking into consideration the effects of potential dune erosion, beach erosion, and change in beach angle.

6. Applicant participated in the workshop called for in the March 10 Orders which was held on March 28, 2017, at which it presented the document attached hereto as Attachment A and entitled "Applicant's March 28, 2017 CEC Workshop Presentation" (TN #216784).

7. The document attached hereto as Attachment B and entitled "Supplemental Coastal Hazards Analysis" was prepared by me and is submitted in response to the above-referenced requests in the March 10 Orders.

8. I hereby sponsor this declaration and the attached documents into evidence in these proceedings.

Executed on June 14, 2017, at San Francisco, California.

I declare under penalty of perjury of the laws of the State of California that the foregoing is true and correct.

Phillip Mineart

ATTACHMENT A

DOCKETED

Docket Number:	15-AFC-01
Project Title:	Puente Power Project
TN #:	216784
Document Title:	Applicant's March 28, 2017 CEC Workshop Presentation
Description:	N/A
Filer:	Paul Kihm
Organization:	Latham & Watkins LLP
Submitter Role:	Applicant Representative
Submission Date:	4/3/2017 3:46:44 PM
Docketed Date:	4/3/2017

Puente Power Project

CEC Public Workshop
March 28, 2017

Questions

1. What is the minimum flooding (inundation depth and time duration) and/or wave impact that would result in Puente unable to operate, for example due to mechanical failure or worker safety?

2. *What is the maximum flow of storm water before the project's drainage system becomes overwhelmed and cannot perform as designed?*

3. *What are the proposed facility features (e.g. construction on piles) and/or any operational activities that are intended to ensure the plant could operate reliably*?

Applicant Response Q1

- Puente's storm water system will be designed to manage more than a 500-year storm without impact to operations
- Puente's storm water system will incorporate Mandalay facilities including site drainage, retention basins, and sumps
- Applicant's extensive coastal hazards/wave run-up analysis has indicated that inundation would not occur
- Irrespective of potential modeled flood scenarios (i.e., rain or inundation), Applicant does not show a scenario that could result in flood or wave impacts to Puente
- If standing water accumulated and storm water management systems were unable to temporarily manage water, Puente would operate with a water level of approximately 15 ft (i.e., 1.5 ft above finished grade of approximately 13.5 ft)

Applicant Response Q2

- Puente's storm water system will be designed to manage a maximum of 5,600 GPM of runoff, more than a 500-year storm event NOAA Atlas Data for Oxnard Airport is as follows:
  - 25-year rainfall event is 4.89 inches in 24 hours – 1844 GPM
  - 100-year rainfall event is 5.93 inches in 24 hours – 2172 GPM
  - 500-year rainfall event is 7.04 inches in 24 hours - 2650 GPM
- As designed, the storm water system is not anticipated to become overwhelmed

Applicant Response Q3

- Puente will be engineered and graded to move water away from all critical infrastructure.
- Operations and Maintenance practices will ensure that storm water management infrastructure are fully available for modeled flood and/or inundation scenarios
- Critical infrastructure will be elevated above 14 ft to ensure the plant can operate reliably,
- Minimum water level where plant operations will cease to operation will be 15 ft

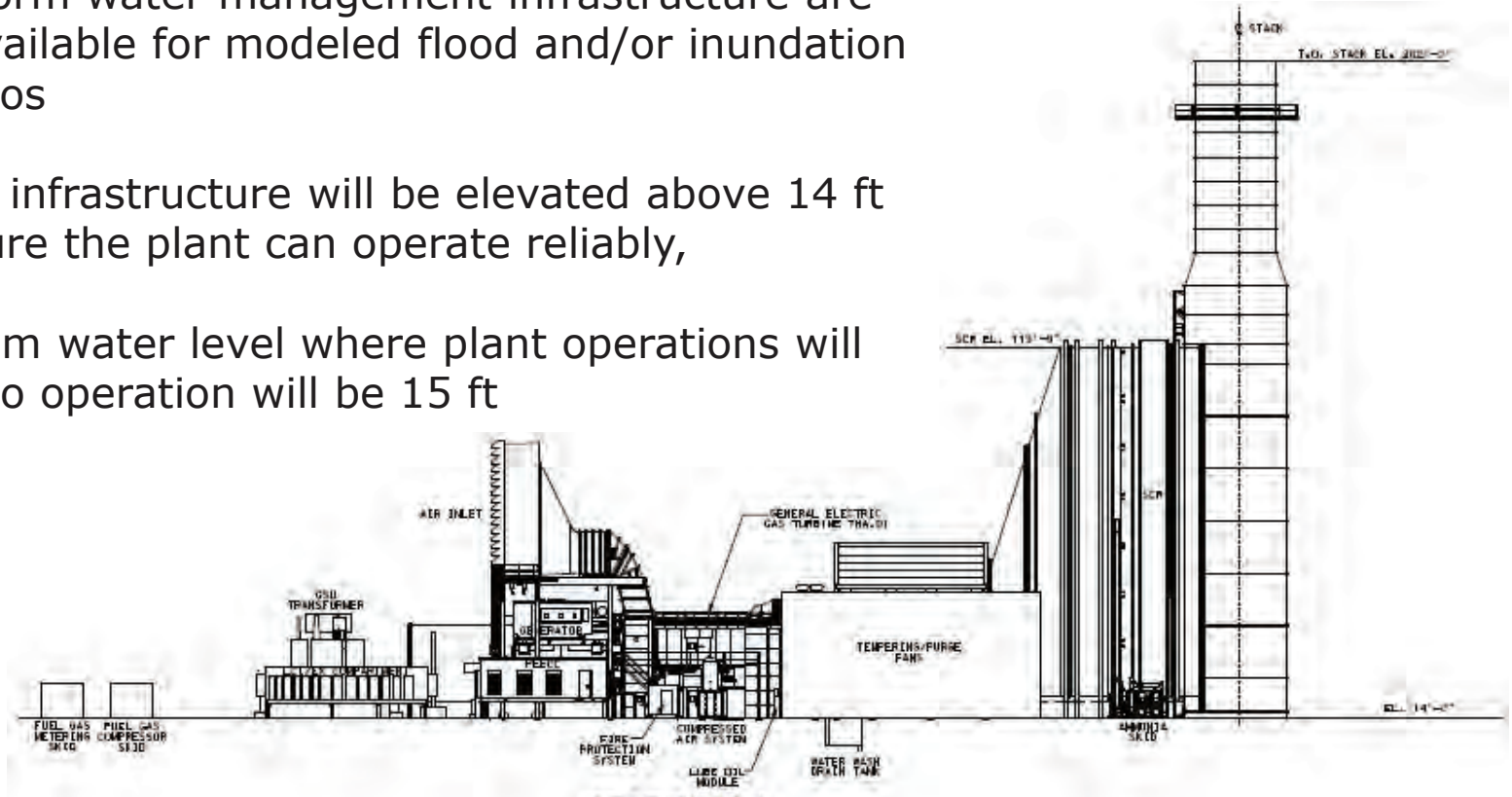

Applicant Response Q3

- Gas Turbine features:
  - ❖ Gas Turbine and auxiliary equipment foundations will be at 14 ft
  - ❖ Lowest critical component (15 ft) is an electronic instrument cabinet for gas valve control;
  - ❖ All other critical electrical equipment will be above 15.5 ft
  - ❖ Gas turbine bottom (16 ft), will be supported by a 2-foot steel support structure

- Power Distribution Center will be elevated 5 to 8 feet above grade (i.e., ~19 to 22 ft) to allow for bottom entry of electrical control cables.

- Other Features:
  - ❖ Ammonia Tank, Generator Step-Up Transformer and Auxiliary Transformer containments will be at a minimum of 15.5 ft
  - ❖ Storm water and waste water basins will be at elevation 17 ft
  - ❖ Air inlet to the Gas Turbine will be elevated above the generator

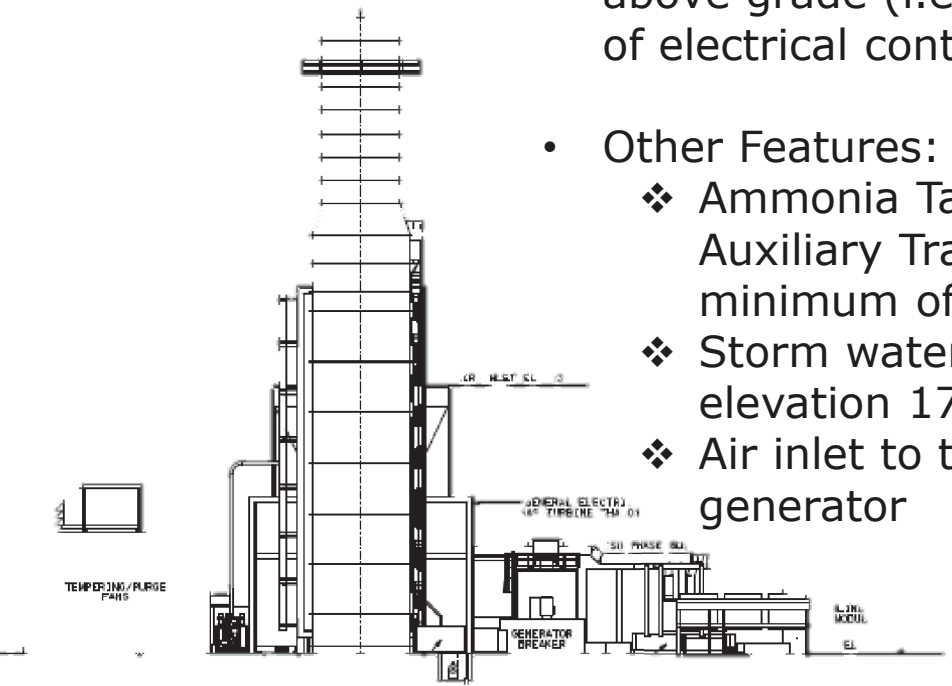

ATTACHMENT B

Application for Certification (15-AFC-01)

Puente Power Project

Oxnard, California

Supplemental Coastal Hazards Analysis Summary Report

Prepared For:

NRG Energy Center Oxnard LLC

June 2017

Table of Contents

List of Tables

List of Figures

Appendices

Attachments

List of Acronyms

AFC	Application for Certification
Cal-EMA	California Emergency Management Agency
CEC	California Energy Commission
CoSMoS	Coastal Storm Modeling System
cm	centimeters
FSA	Final Staff Assessment
MGS	Mandalay Generating Station
NAVD88	North American Vertical Datum of 1988
OPC	Ocean Protection Council
P3	Puente Power Project
PTHA	probabilistic tsunami hazard analyses
RCP	representative concentration pathways
SAFRR	Science Application for Risk Reduction
SLR	sea-level rise
TNC	The Nature Conservancy
USGS	United States Geological Survey

Executive Summary

The Application for Certification for the proposed Puente Power Project (P3 or Project) was submitted to the California Energy Commission (CEC) in April 2015. Since that time, there have been numerous studies performed and documents prepared on the likelihood and potential magnitude of coastal hazards by the Applicant, CEC Staff, the Project intervenors (primarily the City of Oxnard), the United States Geological Survey (USGS), and others. In the March 10, 2017, "Committee Orders for Additional Evidence and Briefing Following Evidentiary Hearings" (TN #216505), the Committee requested additional information regarding coastal hazards, and directed CEC Staff to hold a workshop to discuss coastal hazards. As a follow-up to the Committee's request and the workshop that was held on March 28, 2017, Applicant provides this summary related to the following six key topics related to coastal hazards.

1.0 **Historical Accretion at Mandalay Beach** – Several studies conducted by the Applicant, CEC Staff, and USGS Staff have shown that the beach fronting the P3 site has been historically accretional. A review of historical aerial photographs indicates that the beach has widened by approximately 300 feet since construction of the Mandalay Generating Station (MGS) in 1959. For reasons explained below, this trend is expected to continue over the life of the Project and beyond.

2.0 **Sea-Level Rise –** Since construction of the MGS in 1959, sea levels have risen about 3 inches, yet the beach has accreted about 300 feet. Predictions of sea-level rise (SLR) indicate that the rate of SLR could exceed the average rate of beach accretion sometime in the future. If SLR exceeds the rate of beach accretion, the beach would begin to narrow. The USGS' Coastal Storm Modeling System (CoSMoS) predicts that by 2050 the beach could accrete further and then erode back to a width similar to what exists today, if an extreme rate of SLR is assumed; however, if more likely estimates of SLR are assumed, as presented in the Ocean Protection Council's (OPC's) recently released document, "Rising Seas in California: An Update on Sea-Level Rise Science," then the beach would be expected to continue to grow, though at a slower rate. The predicted 2 feet of SLR that CEC Staff used in the Final Staff Assessment (TN #s 214712 and 214713—Exhibit Nos. 2000 and 2001) is considered a conservative estimate. The probability analysis presented in the OPC document suggests that 2 feet of SLR by 2050 is not very likely (less than 0.5 percent of occurrence), and a more likely range would be approximately 0.7 to 1.2 feet by 2050.

3.0 **Dredging at Ventura Harbor –** Intervenors have repeatedly claimed that the dredging of Ventura Harbor is a major contributor to the accretion of Mandalay Beach, and if the dredging were to cease (e.g., due to funding limitations by the United States Army Corps of Engineers), Mandalay Beach would narrow and potentially disappear. Ventura Harbor has about 1,500 boat slips; dozens of shops, restaurants, and hotels; a commercial fishery; and hundreds of waterfront homes. The likelihood that Ventura County and City would abandon Ventura Harbor seems remote. Furthermore, even if dredging were to cease, sediment would eventually bypass the harbor naturally as it did before the harbor was constructed.

4.0 **Flooding Predicted by The Nature Conservancy Model –** The Nature Conservancy (TNC) model, which is the City of Oxnard's preferred model for predicting coastal impacts to P3, is overly conservative and provides unrealistic results. The TNC model inaccurately predicts that an El Niño-type storm event, such as the one that occurred in January 1983, would flood the MGS site by waves and storm surge under current sea-level conditions; however, the January 1983 El Niño storm and other large coastal storm events (i.e., large waves, high tides, and storm surge) that have occurred since construction of the site have had no impact on the MGS site. The CoSMoS 3.0 model correctly predicted that the MGS facility would not flood under a similar event.

5.0 **Dune Erosion –** The City of Oxnard has suggested that the dunes fronting the MGS are susceptible to erosion and not sufficient to protect the site from flooding due to coastal hazards. The City's erosion analysis, which is based on TNC model results, is unrealistic and overly conservative. The City also claims that significant dune erosion occurred during the 1982-83 El Niño event. No data have been found to substantiate this claim; in fact, data show that that the dunes are growing and expanding seaward, and now provide more protection then they did when MGS was constructed. Furthermore, the City contends that the dunes could be eroded by multiple severe storm events; however the likelihood of multiple storm events large enough to impact the dunes occurring over the life of the Project is considered negligible.

6.0 **Tsunami Hazard –** Recent studies on potential tsunami hazards show that inundation of the Project site would be unlikely. For return periods less than 1,000 years, the predicted tsunami wave height would be about 6 feet and would not inundate the project site. Even for the 2,500-year return period (2 percent probability of exceedance in 50 years or 1.2 percent probability in 30 years), the predicted inundation for a potential tsunami does not reach the project site.

In the March 10, 2017, Committee Order (TN #216505), the Committee also asked about "utility and applicability of using CoSMoS 1.0 instead of, or as a supplement to, the analysis conducted using CoSMoS 3.0." As explained at the workshop by representatives from the USGS (USGS being the author of the CoSMoS model), the CoSMoS 3.0 version supersedes CoSMoS version 1.0. Therefore, CoSMoS 3.0 is the version that should be used.

1 Historical Accretion at Mandalay Beach

Accretion has been occurring along Mandalay Beach adjacent to the Project site for a long time. Supporting evidence that the beach has been growing and not eroding is presented in the following paragraphs.

- Aerial photographs of the beach, taken between 1947 and 2014 and shown on Figure 1-1, show significant accretion. Analysis of the photographs indicates that the beach was approximately 300 feet wider in 2014 than it was in 1947. For the analysis in Figure 1-1, the width of the beach was defined as the distance from the Mandalay Generating Station (MGS) outfall headwall to the waterline shown in the photograph. Applicant recognizes that there would be some change in beach width over time due to tides and seasonal changes; however, this approach is considered reasonable to show overall trends in changes to beach width (see TN #204220-14—Exhibit No. 1042, Application for Certification [AFC] Appendix N-2; TN #206310—Exhibit No. 1059, Applicant's Responses to Oxnard Data Requests Set 2, Response to Data Request 64; and TN #213625—Exhibit No. 1087, Comments on California Coastal Commission Report to California Energy Commission on AFC 15-AFC-01 – NRG Puente Power Project).

- In the 1950s and 1960s, a paved road ran along the beach just above the MGS outfall headwall. The road is currently buried about 3 to 4 feet beneath the sand (based on an exploratory excavation done in 2014) (see TN #213625—Exhibit No. 1087, Comments on California Coastal Commission Report to California Energy Commission on AFC 15-AFC-01 – NRG Puente Power Project).

- The United States Geological Survey (USGS) (Barnard et al. 2009) studied beach erosion and accretion along the coasts of Santa Barbara and Ventura Counties. Beach profiles from 1987 through 2007 were collected at several locations along the coast, including along the Mandalay Beach area. The sections showed a general trend of accretion south of the Santa Clara River. The study identified the Santa Clara River as a large source of sediment that caused accretion south of the river mouth. This was attributed to large pulses of sediment from the river after large storm events (e.g., January 2005) (Barnard et al. 2009).

- The USGS National Assessment of Shoreline Change (Hapke et al. 2006) shows the shoreline back near the present toe of the dunes in the mid-19th century, indicating a growth of 300 to 500 feet in beach width since then.

- Elwany and Diener (2000) evaluated changes in nearshore bathymetry at Mandalay Beach. They reviewed bathymetry data from 1933 to 1987, reporting slight erosion from 1933 to 1977 and stable or modest advancement since 1987. This increase in beach width may also be a consequence of the jetties and breakwater constructed at the mouth of Channel Islands Harbor, which may be trapping sediment and causing accretion.

- Other studies acknowledge that the beach between the Santa Clara River and the Channel Islands Harbor has been accreting (Patsch and Griggs 2007). Barnard et al. (2009) stated that:

  – the shoreline adjacent to the Santa Clara River prograded as much as 129 meters (approximately 400 feet) as a result of the winter flood in 2004-2005;

  – the shoreline south of the Santa Clara River mouth accreted an average of 34 meters (approximately 100 feet) from 1987 to 2007; and

  – From 2005 to 2008, despite rapid shoreline-retreat rates, the beach south of the Santa Clara River gained more than 200,000 cubic meters (approximately 260,000 cubic yards) of sediment.

Conclusion: Substantial evidence, including review of historical aerial photographs, site observations, and studies conducted by the USGS and others, clearly demonstrates that Mandalay Beach fronting the MGS property has grown substantially over a sustained period of time. Since 1947, the beach fronting the MGS site has increased in width by up to 300 feet. The phenomena, including natural and human-induced, that have led to this growth are expected to continue. Therefore, accretion of the beach is expected to continue for the life of the Project and beyond.

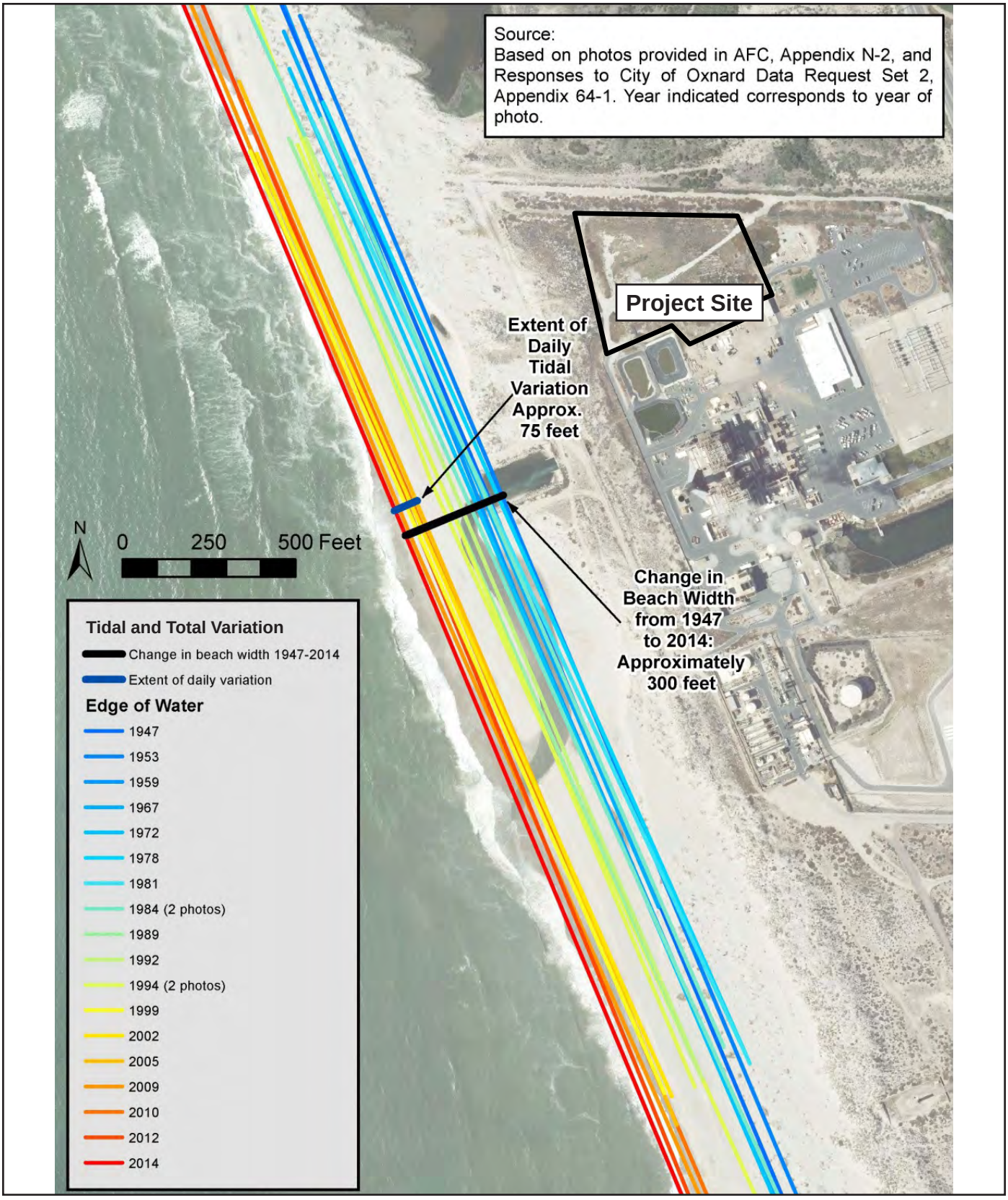

06/02/17 hk \\172.26.108.16\Data\GIS\Netshare\GIs\Graphics\NRG Puente Power Project\Coastal Hazards Summary\Figs_CHSR_June2017.indd

CHANGE IN BEACH WIDTH 1947-2014

NRG
Puente Power Project
June 2017 Oxnard, California

FIGURE 1-1

2 Sea-Level Rise

The California Energy Commission (CEC) Staff made a conservative assumption of 2 feet of sea-level rise (SLR) over the 30-year life of the proposed P3 Project. The recent studies by the Ocean Protection Council (OPC) look at probabilities of SLR predictions and indicate that the SLR prediction of 2 feet by 2050 is considered unlikely (less than 0.5 percent of occurrence). As discussed in Section 1, Historical Accretion at Mandalay Beach, the beach fronting the MGS has been growing. The amount of SLR can affect accretion rates. Even assuming conservative values for SLR by 2050, predictions indicate that Mandalay Beach would not be narrower than it is now; and using the more likely values of expected SLR by 2050, predictions indicate that the beach would continue to widen.

During the period from 1947 through 2016, SLR has been 0.0044 foot per year (1.34 millimeters per year), as measured at the Santa Monica gage (NOAA #9410840). This amounts to about 3 inches since construction of the MGS approximately 60 years ago. Although the historical rate of SLR is less than the predicted future rate, the fact that the beach has grown in width notwithstanding SLR indicates that sand supply to Mandalay Beach historically has been sufficient to overcome SLR. The recent report (*Rising Seas in California, An Update on Sea-Level Rise Science*) produced by the Working Group of the California OPC Science Advisory Team provides guidance to state agencies for incorporating SLR projections into planning, design, permitting, construction, investment, and other decisions (Griggs et al. 2017). The report provides a synthesis of the state of the science on SLR and provides the scientific foundation for the pending update to the guidance document. The OPC report is provided in Attachment 1.

An improvement to many of the previous SLR estimates is the inclusion of probabilities associated with different levels of SLR. Projections of future levels of SLR are provided for three different locations in California: Crescent City (Northern California), San Francisco (Central California), and La Jolla (Southern California). The projections for Southern California are shown in Table 2-1. The value of SLR used in the CEC Staff's Final Staff Assessment (FSA) is 2 feet by 2050 (from a baseline of year 2000). This corresponds to a SLR rate of 0.040 foot per year (10 times the historical rate). This is greater than projections reported in *Rising Seas in California*, which reports a likely range of 0.7 to 1.2 feet at 2050 (from a baseline of 2000), or 0.014 to 0.024 foot per year (three to five times the historical rate). The projected average rates of SLR in southern California have a 0.5 percent or less chance of exceeding 2 feet of SLR by 2050 (see Table 2 in Griggs et al. 2017). This indicates that the values of SLR used in the FSA are very conservative, and that actual rates are likely to be less.

An increased rate of SLR will either decrease the rate of beach accretion (see Section 1, Historical Accretion at Mandalay Beach) or, if large enough, cause the beach to erode and become narrower. The information provided in Section 1 shows that Mandalay Beach has grown by approximately 300 feet since the MGS was constructed in 1959. The information in Figure 1-1 in Section 1, Historical Accretion at Mandalay Beach, indicates a long-term average rate of accretion of about 4 feet per year. If the change in the width of the beach is assumed

Table 2-1
SLR Projections and Probabilities

Feet above 1991-2009 mean	Median	Likely Range	1-in-20 Chance	1-in-200 Chance
Year/Percentile	*50% probability SLR meets or exceeds…*	*67% probability SLR is between…*	*5% probability SLR meets or exceeds…*	*0.5% probability SLR meets or exceeds…*
2030	0.5	0.4 – 0.6	0.7	0.9
2050	0.9	0.7 – 1.2	1.4	2.0
2100 (RCP 2.6)	1.7	1.1 – 2.5	3.3	5.8
2100 (RCP 4.5)	2.0	1.3 – 2.8	3.6	6.0
2100 (RCP 8.5)	2.6	1.8 – 3.6	4.6	7.1
2100 (H++)	10			
2150 (RCP 2.6)	2.5	1.5 – 3.9	5.7	11.1
2150 (RCP 4.5)	3.1	1.9 – 4.8	6.5	11.8
2150 (RCP 8.5)	4.3	3.0 – 6.1	7.9	13.3
2150 (H++)	22			

Source: Griggs et al. 2017

H++ = extreme sea-level rise scenario. This is an unknown probability, high-consequence scenario such as would occur if high rates of Antarctic ice loss were to develop in the last half of this century.

RCP = representative concentration pathways. These are a set of four future pathways, named for the associated radiative forcing (the globally averaged heat-trapping capacity of the atmosphere, measured in watts/square meter) level in 2100 relative to pre-industrial values: RCPs 8.5, 6.0, 4.5, and 2.6. RCP 8.5 is consistent with a future in which there are no significant global efforts to limit or reduce emissions. RCP 2.6 is a stringent emissions-reduction scenario and assumes that global greenhouse gas emissions will be significantly curtailed.

SLR = sea-level rise

to be solely due to SLR, this would be equivalent to a SLR rate of -0.053 foot per year (-1.6 centimeters [cm] per year).[1] To visualize what this means, imagine standing on Mandalay Beach by the outfall from 1959 to 2016, looking toward the ocean. From your perspective, it would appear that the level of the ocean had dropped by an average of 0.053 foot per year. For the beach to narrow, the average rate of SLR would need to increase to a value greater than 0.053 foot per year. Over a 50-year period (from 2000 to 2050, to be consistent with the OPC report) this is equivalent to a total SLR of 2.6 feet (0.053 foot per year times 50 years), greater than the rate assumed in the FSA. The projections provided in Table 2-1 indicate less than a 0.5 percent chance of SLR exceeding 2 feet by 2050.

Figure 2-1 shows changes in shoreline projections for different rates of SLR from the CoSMoS 3.0 Model (see TN #217282, Presentation – Coastal Vulnerability in Ventura County using CoSMoS). Details on the CoSMoS model can be found in Erikson et al. (2017) (provided in Attachment 2). SLR was represented with a second-order polynomial curve that reached

[1] This is based on the use of the Bruun Rule with a slope of 1:75, from p. 18 of Testimony of Dr. Revell (TN #215427—Exhibit No. 3025). Deficiencies in the Bruun rule are provided in *EXPERT DECLARATION OF PHILLIP MINEART REGARDING COASTAL AND RIVERINE HAZARDS* (TN #215441—Exhibit No. 1101); however, the rule provides a simple method for comparing changes in shoreline due to different values of SLR.

1 meter (3.28 feet) or greater by the year 2100 (Erikson et al. 2017). This results in an increasing rate of SLR between the year 2000 and 2100, which is nonlinear. The six SLR scenarios ranged from 100 cm (3.28 feet) by year 2100 to 500 cm (16.4 feet) by year 2100. The CoSMoS 200 cm (6.56 feet) by year 2100 SLR scenario has 1.9 feet of SLR by the year 2050, similar to the 2 feet of SLR by 2050 assumed in the FSA. For this scenario, the CoSMoS model predicted that the beach fronting MGS would grow an additional 50 to 100 feet compared to existing conditions.

Conclusion: The latest estimates of SLR from the OPC indicate that the rate of SLR used in the FSA is conservative and that the actual rates are likely to be less (at least through 2050). The FSA assumed 2 feet of SLR by 2050. Based on the CoSMoS model results for a similar amount of SLR by 2050, the USGS predicted that Mandalay Beach would be approximately 50 to 100 feet wider than existing conditions. The recent predictions of SLR from the OPC indicate that there is a very low probability of SLR exceeding 2 feet by the year 2050.

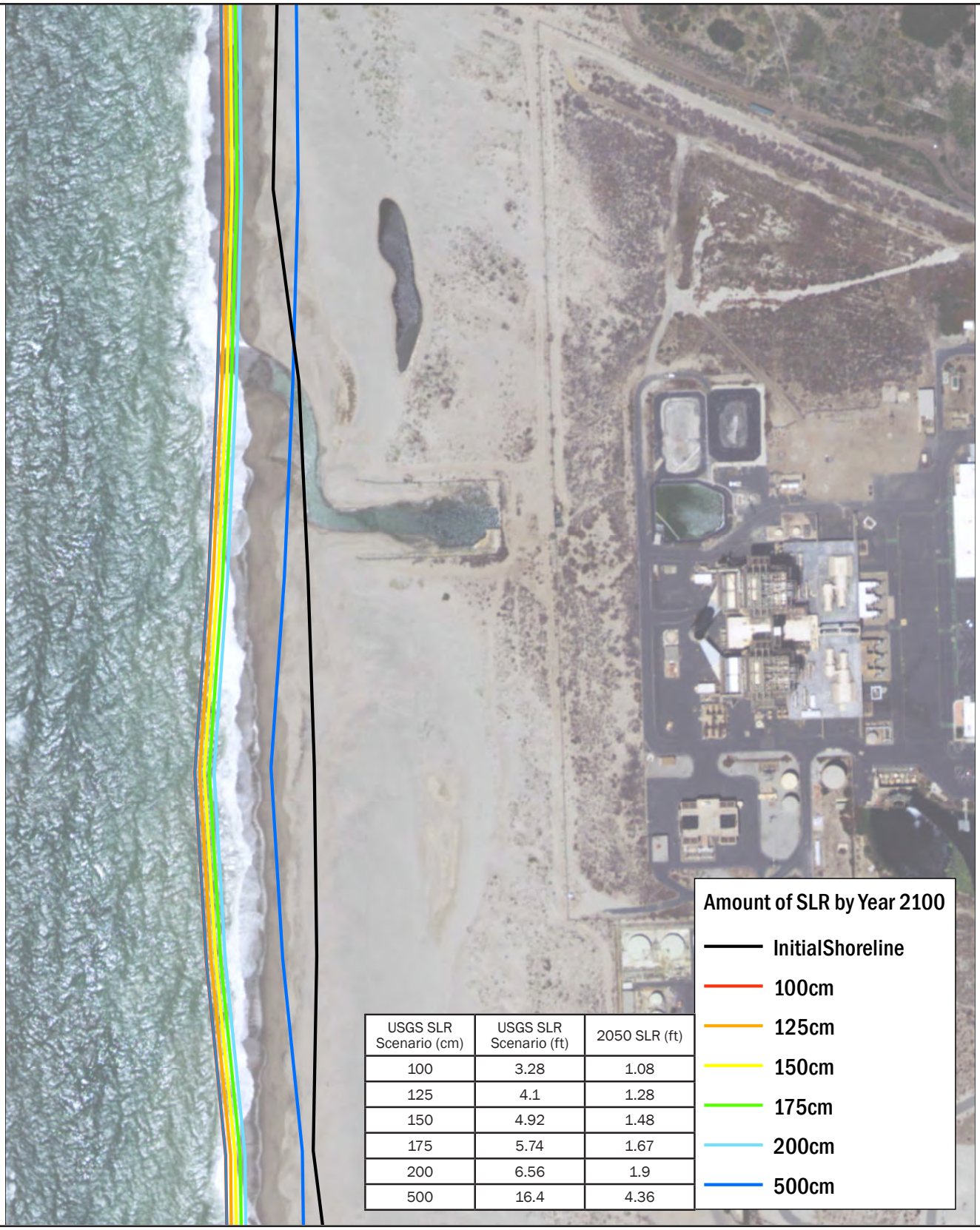

USGS SLR Scenario (cm)	USGS SLR Scenario (ft)	2050 SLR (ft)
100	3.28	1.08
125	4.1	1.28
150	4.92	1.48
175	5.74	1.67
200	6.56	1.9
500	16.4	4.36

06/02/17 hk \\172.26.108.16\Data\GIS\Netshare\Gis\Graphics\NRG Puente Power Project\Coastal Hazards Summary\Figs_CHSR_June2017.indd

CoSMoS 3.0 model results obtained at: https://www.sciencebase.gov/catalog/item/57f1d4f3e4b0bc0bebfee139
Source: USGS, 2017.

SHORELINE PROJECTIONS FROM THE COSMOS 3.0 MODEL

NRG
Puente Power Project
June 2017 Oxnard, California

FIGURE 2-1

3 Dredging at Ventura Harbor

The vulnerability of the Project site to flood hazards, now and in the future, will be determined in part by the status of the coastal dunes immediately west of the MGS. As described in Section 1, Historical Accretion at Mandalay Beach, the beach just west of MGS has a history of accretion, having expanded in size by several hundred feet since construction of the MGS in 1959. The City of Oxnard has expressed concern that insufficient dredging of Ventura Harbor would cause the beach in front of MGS to narrow due to lack of sand (see TN #215427 Exhibit No. 3025, Testimony of Dr. Revell; TN #216594, Transcript of 02/10/2017"] Evidentiary Hearing). In the FSA, CEC Staff recognized this concern but concluded that "…this contribution (*from dredging of Ventura Harbor* added) is small compared to the contribution of sediment supplied by the Santa Clara River. Although beach width could narrow if dredging of Ventura Harbor ceases, sediment loads would continue from the Santa Clara River, which comprises the majority of overall sediment supply to the littoral cell" (FSA, page 4.11-41).

The FSA acknowledged the history of beach accretion fronting the MGS site (see Section 1, Historical Accretion at Mandalay Beach) and the secondary role played by sand bypassing from the Ventura Harbor in contributing to such accretion; however, even this analysis overstates the importance of dredging in maintaining the beach at MGS. An implied assumption in the City of Oxnard's claims on the necessity of dredging Ventura Harbor to maintain Mandalay Beach, and somewhat implied in the FSA, is that the sediment that collects in Ventura Harbor is lost to the system if the harbor is not dredged. If Ventura Harbor dredging ceased, a bypass bar would likely form and sand transport past the harbor would eventually return to pre-harbor construction conditions. The sand trap updrift of Ventura Harbor usually fills within a year or two, after which sand bypasses the trap and deposits in the channel and harbor, requiring annual dredging to keep the harbor open.

In 2015-2016, a large amount of sediment bypassed the sand trap updrift of the Ventura Harbor and deposited sand into the Ventura Harbor inlet (see TN #213625—Exhibit No. 1087, Comments on California Coastal Commission Report to California Energy Commission on AFC 15-AFC-01 – NRG Puente Power Project). The January 21, 2016, Ventura County Star newspaper reported that about 900,000 cubic yards of material was deposited at Ventura Harbor during the winter, filling the sand trap and overflowing into the inlet channel to the harbor. The article also reported that the harbor entrance, which normally has a depth of 40 feet, was reduced to 14 feet; and that the harbor entrance, which normally has a navigable width of about 300 feet, was reduced to about 40 feet wide. The harbor was dredged to restore access, but if dredging had not occurred, the harbor would likely be completely blocked within a few years. Eventually, most of the sediment that normally collects in the harbor and is dredged would bypass the harbor and continue south as it did before harbor construction. Thus, if dredging was completely and permanently discontinued at Ventura Harbor, which is unlikely, there would be a short-term impact on the transport of sand past the harbor. During this period, there could be some narrowing of the beach if there was also no supply from the Santa Clara River (such as during an extended drought).

Conclusion: The contribution from dredging of Ventura Harbor to sand accumulation along Mandalay Beach is far less than the contribution of sediment supplied by the Santa Clara

River. Furthermore, sand accumulation over the long term does not depend on whether Ventura Harbor is dredged, because the sand will ultimately reach Mandalay Beach either by dredging the harbor or by natural processes, though there could be a short impact until a new equilibrium is established.

4 Flooding Predicted by The Nature Conservancy Model

The Nature Conservancy (TNC) model has been proposed by the City of Oxnard as the preferred model for predicting coastal impacts to the Puente Power Project (P3). Applicant believes that the TNC model does not accurately represent the potential flooding conditions at the P3 site, and therefore is an unreliable model for predicting site-specific coastal hazards for the P3 Project. The reasons the TNC model is inappropriate to use to predict coastal hazards at P3 are discussed in the following paragraphs:

- Figure 4-1 shows the predicted areas of inundation from the TNC model for existing conditions (i.e., without SLR). The TNC model results were obtained from Coastal Resilience California (2017). The estimated depths of the predicted inundation shown on Figure 4-1 were derived from the TNC model results, because no elevation data were included with the results (only the inundation boundary). Superimposing LiDAR data on the TNC model results for inundation boundary indicates that the inundation from the TNC model approximately follows the 13.5-foot elevation contour from Mandalay Beach Road to the MGS property.

- The TNC model has been shown to be inaccurate when applied to the Project site. The model predicted that an El Niño-type storm event, such as the one that occurred in January 1983, would flood the entire Project site under current conditions, but that prediction is contrary to what actually happened. The January 1983 El Niño storm and other large storm events that have occurred since construction of the MGS, and the resulting waves and storm surges, have had no impact on the MGS site. There was no flooding and no impact to MGS operations. (see TN #213625—Exhibit No. 1087, Comments on California Coastal Commission Report to California Energy Commission on AFC 15-AFC-01 – NRG Puente Power Project, page 10). However, The TNC model shows significant flooding of the MGS property, except for the P3 site, during this storm event; and almost complete inundation of Mandalay County Park (behind the large dunes), with flooding up to 4 to 5 feet deep (see Figure 4-1).

- The TNC model was meant as a planning-level model, not a site-specific model. The report states that "This information is intended to be used for planning purposes only. Site-specific evaluations may be needed to confirm/verify information presented in these data" (see TN #215428 1— Exhibit No. 3026, Coastal Resilience Ventura Technical Report for Coastal Hazards Mapping, page 8).

- No information has been provided to indicate that the TNC model was ever verified at the P3 site. Under cross-examination during the California Public Utilities Commission proceedings, the City of Oxnard's consultant, Dr. David Revell, admitted that he did not consider what actually happened (or did not happen) at Mandalay during the 1983 storm event that he modeled. Revell also admitted that he did not validate his model to actual events at the Mandalay site (which would have shown him that the model's predictions are wrong), and he did not try to calibrate the model with data regarding historical events to improve its accuracy (see TN #213625—Exhibit No. 1087,

Comments on California Coastal Commission Report to California Energy Commission on AFC 15-AFC-01 – NRG Puente Power Project, Attachment B, page 11).

- The TNC model inundation mapping uses an overly conservative approach to show areas that could be flooded under coastal storm and wave conditions. Mapping is described as: "Flooded areas with connectivity to the ocean (either overland or through culverts) were mapped, as well as any pools (greater than 3 m^2) within 3 meters of areas connected to the ocean to conservatively account for seepage and potential errors in the DEM. For the same reason, donut holes smaller than 1 acre (208 feet x 208 feet) were assumed flooded." This method is reasonably conservative in areas such as Oxnard Shores where wave runup and storm surge can inundate areas behind the beach, but unreasonable for areas behind dunes. The TNC model showed flooding of Mandalay Beach Road in Oxnard Shores under existing conditions for Coastal Storm and Coastal Wave hazards. Mandalay Beach Road[2] ends at West 5th Street, approximately 0.6 mile south of the MGS property. For water to reach the MGS property and P3 site, it would need to travel perpendicular to the direction of wave runup. Storm surge or waves are not large or persistent enough to drive flow more than 3,000 feet from Oxnard Shores through Mandalay County Park past the Edison Canal onto the MGS property (see Figure 4-1). It is unreasonable to assume that because Mandalay Beach Road in Oxnard Shores is inundated, the MGS property would also be inundated.

Conclusion: The TNC model has been proposed by the City as providing a reasonable estimate of coastal hazards at the MGS property, including the P3 site. Although the TNC model may provide an estimate of potential coastal hazards along the Ventura County Coast when viewed at a large scale, it does not provide an accurate representation of potential flooding from coastal hazards when applied at a site-specific scale such as at the MGS property, as discussed above. The TNC model is too conservative when applied at the site-specific scale to be a useful tool for analysis.

[2] Mandalay Beach Road referenced herein is a paved road in the Oxnard Shores residential area, and is not to be confused with the "Beach Road" that runs along Mandalay Beach in front of the MGS property.

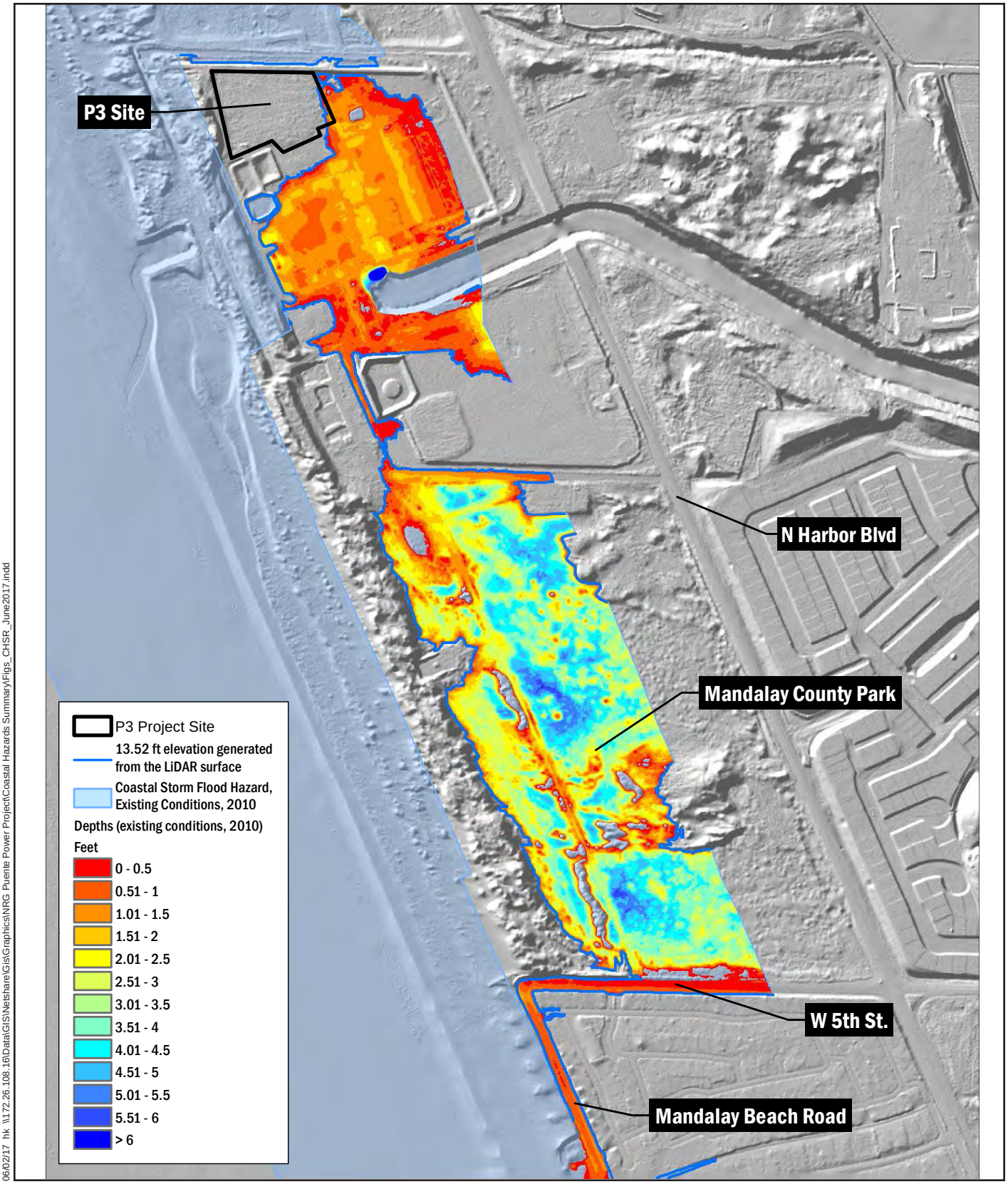

06/02/17 hk \\172.26.108.16\Data\GIS\Netshare\Gis\Graphics\NRG Puente Power Project\Coastal Hazards Summary\Figs_CHSR_June2017.indd

Topographic surface: 2013 NOAA Coastal California TopoBathy Merge Project (data collected between 2009 - 2011)
Model data: Coastal Resilience Ventura: Coastal Hazards Mapping
Environmental Science Associates - Philip Williams and Associates (ESA PWA), San Francisco and The Nature Conservancy

N

0 500 1,000
Feet

FLOODING PREDICTED BY TNC MODEL

NRG
Puente Power Project
Oxnard, California

June 2017

FIGURE 4-1

5 Dune Erosion

The City of Oxnard has suggested that the dunes fronting the MGS are susceptible to erosion and not sufficient to protect the site from flooding due to coastal hazards. The City's description of the potential dune erosion is unreasonable and does not accurately represent the potential dune erosion at the P3 site. The reasons that the City's erosion analysis is unrealistic and overly conservative are discussed in the following paragraphs.

- The TNC model should be considered a worst-case analysis that predicts results that may not be physically possible. The City relies on the TNC model for estimates of dune erosion; however, this model uses an extremely conservative (worst-case) dune erosion algorithm. The method is purely a geometric model (that is, the amount of dune erosion is primarily based on the geometry of the dune and beach without regard to any physical process). It does not account for storm characteristics. "Instead of predicting storm-specific characteristics and response, this potential erosion projection assumes that the coast would erode or retreat to a maximum storm wave event with unlimited duration" (see TN #215428-1— Exhibit No. 3026, Coastal Resilience Ventura Technical Report for Coastal Hazards Mapping, prepared by ESA/ PWA for TNC, page 20). In reality, storms have a limited duration; even during large storm events, wave runup may only reach the dunes during a limited portion of the storm. Unlike the TNC model, the CoSMoS model uses reasonable assumptions and a physically based model to predict erosion; the CoSMoS model does not predict flooding of the site during an extreme event (see TN #217282, Presentation – Coastal Vulnerability in Ventura County using CoSMoS).

- In the January 1983 El Niño storm and other large storm events that have occurred in the past, the resulting waves and storm surges have had no identifiable impact on the MGS site—there was no flooding and no impact to MGS operations (see TN #215441—Exhibit No. 1101, Applicant's Opening Testimony, Testimony of Phillip Mineart, page 6). The City claims, however, that significant erosion of the dunes fronting the P3 site occurred during the 1982-83 El Niño event (see TN #215427— Exhibit No. 3025, Testimony of Dr. Revell, page 16; TN #215541— Exhibit No. 3054, Rebuttal Testimony of Dr. David Revell to Testimony of Phillip Mineart, page 2). This is apparently based on a review of a 1984 infrared aerial photograph (see Figure 5-1 for photograph). Applicant researched its records for any mention of dune erosion during this period (MGS staff conduct frequent beach inspections because of its outfall) and could not find any mention of dune erosion. Applicant also researched historical aerial photographs for evidence of erosion (see TN #204220-14—Exhibit No. 1042, AFC Appendix N-2; TN #206310—Exhibit No. 1059, Applicant's Responses to Oxnard Data Requests Set 2, Response to Data Request 64). Figure 5-2a is a photograph from October 1979, 3 years before the El Niño event, and Figure 5-2b is from June 1987, 5 years after the supposed large erosion event (Figures 5-2a and 5-2b are from the California Coastal Record Project). Figure 5-2b shows an intact vegetated dune; the vegetation implies that the dune has been stable for a number of years. There is a clear area with no visible vegetation in the 1984 photograph in the dune fronting the P3 site,

which could possibly be interpreted as an area of erosion. Although the two photographs comprising Figure 5-3 were taken at different angles and scales, the same area can be seen in the 1979 photograph (Figure 5-2a) and the 1987 photograph (Figure 5-2b), showing that this area is not a result of erosion during the 1982-82 El Niño event, as claimed by the City.

- The main dunes that provide protection of the site from coastal hazards have expanded instead of eroding (see Section 1, Historical Accretion at Mandalay Beach, for details). Since the 1983 event, the beach fronting the MGS site has accreted and is now wider than it was in 1983. In addition, foredunes have formed and stabilized farther out toward the ocean. Thus, under "current conditions," the Project site is not more vulnerable to coastal hazards than it was in 1983, but is actually less vulnerable (see TN #213625—Exhibit No. 1087, Comments on California Coastal Commission Report to California Energy Commission on AFC 15-AFC-01 – NRG Puente Power Project).

- Based on an analysis of 50 years of wave data, the likelihood of multiple large storm events that could erode the dunes is small (see Appendix A for a detailed discussion of the probability of multiple large events). The probability of three or more events large enough to run up the dunes is less the 1 percent over the 30-year life of the Project. Even assuming that large events are more likely during strong El Niño years, the probability of three or more large events remains less than 5 percent during the 30-year life of the Project.

Conclusion: The City has expressed a concern that the dunes fronting the P3 Project site may not provide adequate protection from coastal hazards such as storms and waves. This opinion is at least partially based on the results of the TNC erosion model, which is a worst-case condition model based primarily on geometry and not physical processes, and assumes a storm of unlimited duration. The City also appears to base its opinion on significant dune erosion it claims occurred during the 1982-83 El Niño event. No data have been found to substantiate this claim; in fact, the data that have been found contradict the claim of significant dune erosion (see Figure 5-2). Furthermore, a comparison between an aerial photograph taken just after plant construction (1959) to a present day aerial photograph shows that that the dunes are growing and have expanded seaward and now provide more protection then they did when the plant was constructed. In addition, the City claims that waves from multiple large storm events could erode the dunes; however, this type of combined event is highly unlikely.

Source:
TN #215427, Testimony of Dr. Revell, page 16; TN #215541, Rebuttal Testimony of Dr. David Revell to Testimony of Phillip Mineart, page 2.

1984 INFRARED AERIAL PHOTOGRAPH

NRG
Puente Power Project
June 2017 Oxnard, California

FIGURE 5-1

AERIAL PHOTOGRAPH OF MANDALAY BEACH IN 1979

NRG
Puente Power Project
June 2017 Oxnard, California

FIGURE 5-2a

AERIAL PHOTOGRAPH OF MANDALAY BEACH IN 1987

NRG
Puente Power Project
June 2017 Oxnard, California

FIGURE 5-2b

06/02/17 lhk \\172.26.108.16\Data\GIS\Netshare\Gis\Graphics\NRG Puente Power Project\Coastal Hazards Summary\Figs_CHSR_June2017.indd

Source:
1959 Photo: TN #204220 14—Exhibit No. 1042, Application for Certification [AFC] Appendix N-2

2016 Photo: Topographic surface: 2013 NOAA Coastal California TopoBathy Merge Project (data collected between 2009 - 2011); Imagery: Google Earth

DUNES COMPARISON

NRG
Puente Power Project
June 2017 Oxnard, California

FIGURE 5-3

6 Inundation Due to Tsunami

Previous studies analyzed both distant and local earthquake sources of tsunamis that could impact the Ventura County shoreline (see TN #207179—Exhibit No. 1070, Responses to City of Oxnard Data Requests 92 and 93; TN #206533—Exhibit No. 1061, Response to City of Oxnard Data Requests 59 and 60; and TN #206310—Exhibit No. 1059, Response to City of Oxnard Data Request 47). The studies of distant earthquakes (teletsunamis) indicate that the Project site is unlikely to be in the inundation zone. The return periods for various tsunami sources included in the studies varied between 800 and 10,000 years. In all cases, the maximum projected wave height is well below the top of the existing dunes that protect the Project site (see TN #215441—Exhibit No. 1101, Applicant's Opening Testimony, Expert Declaration of Phillip Mineart Regarding Coastal and Riverine Hazards; and TN #213625—Exhibit No. 1087, Comments on California Coastal Commission Report to California Energy Commission on AFC 15-AFC-01 – NRG Puente Power Project).

Local sources of tsunamis include:

- **Goleta landslide complex:** an area along the continental rise off Santa Barbara that shows evidence of repeated submarine landslides. Studies found runups as high as 33 feet (10 meters) in the Goleta area—the area that would be most affected. However, the expected effect at the Project site would be much less, because submarine landslides tend to have a very strong directional effect (see TN #206533—Exhibit No. 1061, Response to City of Oxnard Data Requests 59 and 60). In fact, the California Emergency Management Agency tsunami inundation maps are partly based on the Goleta landslide, and the inundation line does not reach the Project site (see TN #204220-14—Exhibit No. 1042, AFC Appendix N-2, for a copy of the inundation map).

- **Ventura-Pitas Point fold and thrust**: a fold-and-thrust system that runs through Ventura and offshore under the Santa Barbara Channel. As discussed in Applicant's response to City of Oxnard Data Request 59 (TN #206533—Exhibit No. 1061), several studies have been performed on the potential size of the tsunami and the extent of the inundation zone. With the exception of Ryan et al. (2015), modeling of the Ventura-Pitas Point complex shows no inundation of the Project site (Nicholson et al. 2015; Sorlien and Nicholson 2015; and Thio et al. 2015). Furthermore, the mapping in the Ryan study does not appear to take into consideration the presence of the dune that fronts the Project site. The maximum wave height predicted by the Ryan study is well below the height of the dune. Taking all of this into consideration, it does not appear that the Ventura-Pitas Point complex poses a significant tsunami hazard to the Project site.

- **Oak Ridge blind thrust:** an offshore blind thrust structure that is under the Santa Barbara channel, several kilometers south of the Ventura-Pitas Point complex. Although its location poses a potential tsunami hazard for the Ventura-Oxnard region, studies show that the Oak Ridge fault does not contribute significantly to the tsunami hazard at the Project site (see TN #206533—Exhibit No. 1061).

Distant sources of tsunamis, such as earthquakes around the Pacific Rim (including Alaska) were also reviewed. The source area for the 1964 Alaska earthquake (among many others) has historically had the strongest tsunami impact in central and southern California. Studies by the USGS indicate that a tsunami originating in Alaska would not result in inundation at the Project site (see TN #206533—Exhibit No. 1061, Applicant's response to City of Oxnard Data Request 59).

Several probabilistic tsunami hazard analyses have included the Project site area. Table 6-1 summarizes the results from the various studies discussed in Applicant's response to City of Oxnard Data Request 59 (TN #206533—Exhibit No. 1061). Even for the 2,500-year return period (2 percent probability of exceedance in 50 years or 1.2 percent probability in 30 years), the predicted inundation for a potential tsunami does not reach the Project site. For return periods less than 1,000 years, the predicted tsunami wave height would be about 6 feet (or 2 meters), and would not inundate the Project site.

Conclusion: Recent studies on potential tsunami hazards show that inundation of the Project site would be highly unlikely.

Table 6-1
Probabilities and Maximum Tsunami Wave Amplitudes

Source	Shoreline		Site		Analysis Resolution (feet)	Annual Return Period (years)	Reference
	Maximum Wave Height (feet)[1]	Maximum Velocity (feet per second)	Maximum Wave Height (feet)[1]	Maximum Velocity (feet per second)			
Ventura-Pitas Point	19.4	NA	12.8	NA	100	800 to 2,500	Ryan et al. (2015)
Ventura-Pitas Point	13.6	NA	—	—	33	800 to 2,500	Thio et al. (2015)
Ventura-Pitas Point	14.8	NA	—	—	33	800 to 2,500	Thio et al. (2015)
Oak Ridge	15.4	7.9	—	—	33	> 10,000	Thio et al. (2015)
PTHA	NA	NA	—	—	100	2,500	Thio et al. (2010)
SAFRR	12.1	3.8	—	—	100	500	Ross et al., 2013
Cal-EMA	NA	NA	—	—	NA	> 5,000	Cal-EMA (2009)

Source: TN #206533—Exhibit No. 1061, Response to City of Oxnard Data Requests 59 and 60, Table 59-1.

Notes:

[1] Heights are relative to NAVD88 at the shoreline and at the site for various seismic sources found in the literature. Tsunami results are expressed relative to mean high water; 4.6 feet were added to convert to NAVD88.

"— " indicates that the site is not inundated.
"NA" indicates that the data are not available.

Cal-EMA = California Emergency Management Agency
NAVD88 = North American Vertical Datum of 1988
PTHA = probabilistic tsunami hazard analyses
SAFRR = Science Application for Risk Reduction

7 References

Barnard, P.L., D.L. Revell, D. Hoover, J. Warrick, J. Brocatus, A.E. Draut, P. Dartnell, E. Elias, N. Mustain, P.E. Hart, and H.F. Ryan. 2009. Coastal processes study of Santa Barbara and Ventura Counties, California: U.S. Geological Survey Open-File Report 2009-1029, 904 pp. Available online at: http://pubs.usgs.gov/of/2009/1029/.

California Emergency Management Agency (Cal-EMA). 2009. Tsunami Inundation Map for Emergency Planning, Oxnard Quadrangle: Scale 1:24,000. February 15. Available online at: http://www.conservation.ca.gov/cgs/geologic_hazards/Tsunami/Inundation_Maps/Ventura/Documents/Tsunami_Inundation_Oxnard_Quad_Ventura.pdf.

Coastal Resilience California. 2017. Coastal Resilience Mapping Portal. Available online at: http://maps.coastalresilience.org/california/#.

Elwany, Hany, Ph.D., and Ben Diener. 2000. Evaluation of Nearshore Bathymetry, Mandalay Beach, Ventura County, California. Submitted to Southern California Edison Company by Coastal Environments. May.

Erikson, L.H., P.L. Barnard, A.C. O'Neill, S. Vitousek, P. Limber, A.C. Foxgrover, L.H. Herdman, and J. Warrick. 2017. CoSMoS 3.0 Phase 2 Southern California Bight: Summary of data and methods. U.S. Geological Survey. Available online at: http://dx.doi.org/10.5066/F7T151Q4.

Griggs, G, J. Árvai, D. Cayan, R. DeConto, J. Fox, H.A. Fricker, R.E. Kopp, C. Tebaldi, and E.A. Whiteman. 2017. California Ocean Protection Council Science Advisory Team Working Group. *Rising Seas in California: An Update on Sea-Level Rise Science*. California Ocean Science Trust. April.

Nicholson, C., C.C. Sorlien, T.E. Hopps, and A.G. Sylvester. 2015. Anomalous Uplift at Pitas Point, California: Whose fault is it anyway? 2015 annual meeting of the Southern California Earthquake Center, Palm Springs. Available online at: http://scecinfo.usc.edu/core/cis/2015am/view_abstract.php.

Hapke, C.J., D. Reid, B.M. Richmond, P. Ruggiero, and J. List. 2006. National assessment of shoreline change: Part 3: Historical shoreline changes and associated coastal land loss along the sandy shorelines of the California coast: U.S. Geological Survey Open-file Report 2006-1219.

Patsch, Kiki, and Gary Griggs. 2007. Development of Sand Budgets for California's Major Littoral Cells. January. Available online at: http://www.researchgate.net/publication/240635473_LITTORAL_CELLS_AND_SAND_BUDGETS_ALONG_THE_COAST_OF_CALIFORNIA_Proposal_to_the_California_Coastal_Sediment_Management_Working_Group_And_California_Department_of_Boating_and_Waterways.

Ross, S.L., L.M. Jones, K. Miller, K.A. Porter, A. Wein, R.I. Wilson, B. Bahng, A. Barberopoulou, J.C. Borrero, D.M. Brosnan, J.T. Bwarie, E.L. Geist, L.A. Johnson, S.H. Kirby, W.R. Knight, K. Long, P. Lynett, C.E. Mortensen, D.J. Nicolsky, S.C. Perry,

G.S. Plumlee, C.R. Real, K. Ryan, E. Suleimani, H.K. Thio, V.V. Titov, P.M. Whitmore, and N.J. Wood. 2013. The SAFRR tsunami scenario—Improving resilience for California: U.S. Geological Survey Fact Sheet 2013–3081, 4 pp. Available online at: http://pubs.usgs.gov/fs/2013/3081/.

Ryan, K.J., E.L. Geist, M. Barall, and D.D. Oglesby. 2015. Dynamic models of an earthquake and tsunami offshore Ventura, California, Geophysical Research Letters, 42, 6599-6606, doi:10.1002/2015GL064507. Available online at: http://onlinelibrary.wiley.com/doi/10.1002/2015GL064507/full.

Sorlien, C.C., and C. Nicholson. 2015. Post-1 Ma deformation history of the Pitas Point-North Channel-Red Mountain fault system and associated folds in the Santa Barbara Channel, California. Final Report to U.S. Geological Survey NEHRP, contract USDI/USGS G14AP00012, 24 pages. Available online at: http://earthquake.usgs.gov/research/external/reports/G14AP00012.pdf.

Thio, H.K., P.G. Somerville, and J. Polet. 2010. Probabilistic tsunami hazard in California, *Pacific Earthquake Engineering Research Center Report*, 108, 331. Available online at: http://peer.berkeley.edu/publications/peer_reports/reports_2010/web_PEER2010_108_THIOetal.pdf.

Thio, H.K., K. Ryan, R. Wilson, A. Plesch, D. Oglesby, and J. Shaw. 2015. Tsunami hazard from earthquakes on the Ventura-Pitas Point fault and adjacent structures, 2015 annual meeting of the Southern California Earthquake Center, Palm Springs. Available online at: http://scecinfo.usc.edu/core/cis/2015am/view_abstract.php.

United States Geological Survey (USGS). 2017. Presentation – Coastal Vulnerability in Ventura County using CoSMoS. USGS Presentation at March 28, 2017, Staff Workshop. TN #217282. Docketed on April 24, 2017.

Appendix A
Probability of Multiple Storms Eroding Dunes Fronting Mandalay Generating Station

Appendix A
Probability of Multiple Storms Eroding Dunes Fronting Mandalay Generating Station

For the dunes in front of the Mandalay Generating Station (MGS) property to be eroded, it would be necessary for waves to run up the face of the dune. The wave runup elevation is based on beach slope, still water elevation, and wave height. This analysis estimates the wave runup that would be necessary to erode the dunes and assesses the likelihood of this occurring over the life of the Puente Power Project (P3).

A.1. Beach Slope

For dune erosion in California, the critical waves are the large waves that occur during winter storm events. The slope generally used to calculate wave runup is the foreshore slope, which is the slope of the beach generally between low water and high water. Large slopes (steep foreshores) have large runup values and small slopes (shallow foreshore slopes) have smaller runup values.

Wave runup calculations provide an estimate of the potential wave runup if the slope of the beach continued at the foreshore slope. Figure A-1 is an example beach profile from in front of the P3 site. On this profile, the foreshore slope is 7.95 percent. Wave runup calculations provide the elevation of potential wave runup based mainly on the foreshore slope (the blue dashed line on Figure A-1shows the extension of the foreshore). If the foreshore does not extend to the elevation of wave runup, its energy will be dissipated on the flatter section of the profile behind the foreshore. Therefore, the calculated runup elevation on beaches with foreshore slopes greater than the slope of the beach landward of the foreshore (for example, distances greater than 1,440 feet on Figure A-1) may be overestimated and the actual runup elevation may be closer to the maximum elevation in the foreshore (for example, elevations between 9.5 and 13 feet on Figure A-1).

Slopes of the foreshore are not constant. Beaches undergo seasonal changes in the shape of their beach profile as a way to adapt to changes in the incoming wave energy. A beach that is subject to mild (summer) wave conditions will generally display a wide beach with a fronting berm and steep foreshore slope. In the winter months, when multiple large storms are hitting the beach, the berm will erode, the beach will narrow, and the foreshore slope will be milder than the slope observed in the summer, because the steep face of the summer foreshore berm is eroded away by the winter storms. The eroded sediment will move offshore to create a sand bar. However, this sediment is not lost from the system; in the summer, the smaller waves “push” the sediment back on shore to recreate the wide beach, fronting berm, and steep foreshore slope typically observed in the summer. This process has been well documented by Shepard (1950), Bascom (1953), Shih and Komar (1994), and summarized in Komar (1998).

The profile data collected for Mandalay Beach show a naturally occurring sand berm on the foreshore area of the beach, which is most likely due to the accretion of sand over the years (see Figure A-2 for example). The berm creates a steep foreshore slope of approximately

24 percent for the profile shown on Figure A-2 (24 percent is considered an extremely steep foreshore slope, and the slope shown in the example on Figure A-2 is likely affected by the presence of the outfall; foreshore slopes are generally much shallower).

As described above, if the berm were to erode due to multiple large storms, the sand would be moved offshore, creating a sand bar. The slope would then decrease and the waves would flatten out the foreshore area. Figure A-2 shows potential foreshore slopes given various stages of beach morphology. In the current configuration (No. 1), the slope is steep. Although high calculated runup values are possible for this slope, the water overtops the berm and dissipates its energy in the pooled area behind, limiting the extent of runup (see Figure A-1 for an example of a calculated path of potential wave runup). If multiple large storms occur, it is possible for the fronting berm to erode, as is shown in configuration No. 2. This would create a mild slope and narrow beach typical of beaches exposed to winter storms. The mild slope would reduce the runup elevation, because wave runup is proportional to beach slope. For the beach to progress to configuration No. 3 (beach slopes up to the toe of the dune), it would require multiple large events greater than the dune toe (approximately 14 feet NAVD88) to occur. This is highly unlikely to occur with such a mild slope as shown in configuration No. 2 (i.e., severe winter slope). In the summer, the sand that eroded away during the winter storm events would migrate onshore and build the beach back up.

Six beach profiles of the beach fronting MGS were reviewed to select a reasonable estimate of the beach slope that would extend from the surf zone (where the waves are breaking) to the dunes (see TN #207179—Exhibit No. 1070, Applicant's Responses to City of Oxnard Data Requests Set 4, Response to Data Request 87). The beach slopes were generally very shallow, less than 5 percent (the foreshore slopes were steeper). One profile taken near McGrath Lake had the steepest profile observed, 6.3 percent. For purposes of calculating runup, the analysis presented below assumes a slope of 6.3 percent.

A.2. Still Water Elevation

Still water elevation is the water elevation in the absence of waves. It includes the elevation of the tides and storm surge. For this analysis, the still water elevations corresponding to the available wave data were used in the calculations described below.

A.3. Wave Runup Calculation

Several methods are available to calculate wave runup, all empirically based. For the Draft Federal Emergency Management Agency (FEMA) Flood Insurance Rate Maps (FIRMs) for Mandalay Beach, FEMA used a method referred to as the Stockdon Equation (BakerAECOM 2015). This equation calculates potential runup based on the beach slope, deep water wave height, and wave length. Fifty years of hourly wave heights and period and corresponding still water levels were obtained from FEMA. The wave lengths needed by the Stockdon Equation were calculated for each hour from the wave period data. For each hour in the dataset, the potential wave runup was calculated using a slope of 6.3 percent, based on the discussion above. As shown in the example Figure A-1, the use of the foreshore slope provides a reasonable estimate of the runup elevation on the foreshore, but may overestimate the runup

on the beach if the beach has a much shallower slope landward of the foreshore, which is the case at Mandalay. Because the foreshore is several hundred feet from the toe of the dunes, the use of a relatively steep foreshore slope may result in an unreasonable estimate of wave runup.

A.4. Total Water Level

For waves to erode the dunes, the total water level (TWL) would need to exceed the elevation of the toe of the dunes. TWL is the elevation of wave runup plus the still water elevation.

To calculate TWL, 50 years of hourly wave height and period and still water data were used. TWL was calculated using the assumed slope of 6.3 percent for the 50 years of hourly wave data to estimate how often the wave runup would exceed the elevation of the toe of the dunes. The elevation of the toe of the dunes was assumed to be 14.5 feet. In the 50 years of data, the TWL elevation exceeded the toe of the dune elevation five times (or 0.10 events per year on average), with a maximum elevation of 16.8 feet. Note that for beach slopes less than 4 percent, no TWL elevations would exceed the elevation of the toe of the dunes in the 50 years of data.

Note that the analysis above differs from the FEMA analysis used to calculate the Special Flood Hazard Area subject to coastal high hazard flooding (i.e., Zone VE) shown on the draft FIRM. For wave runup calculations used to generate the VE zone, FEMA used a foreshore slope of 10 percent and assumed that the 10 percent slope extended all the way to the dunes, similar to Slope 3 shown on Figure A-2. This may be a reasonable approach for planning and determining insurance ratings, but does not represent what could actually happen (Slope 3 on Figure A-2 is extremely unlikely to ever exist).

A.5. Storm Probability

The TWL calculation above provides a method to estimate how often storms large enough to potentially erode the dunes could occur. The TWL elevation was calculated for the 50 years of hourly data mentioned above. Each time the TWL elevation exceeded the elevation of the toe of the dune was counted as a storm event. By counting all the storms that occurred during the period of analysis (50 years), it is possible to estimate how often storms could impact the dunes and whether such impacts could happen multiple times a year.

To calculate the probability of storms impacting the dunes, the following assumptions were made:

- The average number of storms that exceed the elevation of the dune toe is 0.1 storm/ year (five storm events in 50 years);
- The probability of a storm occurring in a year is independent of whether a storm has occurred previously in that year or in a preceding year (storms are independent); and
- The number of large storms that occur will be sufficient to erode the beach berm and reduce the slope to a winter storm slope (assumed to be 6.3 percent) before any large storms that impact the dunes occur. This is assumed to have a probability of 100 percent, though there are no data available to indicate that this has ever

happened since the plant was constructed. Therefore, the result shown below should be considered very conservative.

Given these assumptions, the probability of storms occurring that could impact the dunes are shown in the Table A-1.

Table A-1
Probability of Storms Occurring at Mandalay Beach that Could Potentially Impact the Dunes[1]

Number of Storms per Year	Probability (%) in a single year	Probability of Occurring in 30 Years (%)
1	10	96
2	0.45	13
3	0.015	0.45
4	0.00015	0.0046

Note:
[1] A storm that could potentially impact the dune was assumed to be a storm in which the wave runup elevation exceeded the dune toe.

A review of the potential runup elevations calculated from the 50 years of wave data indicates that multiple large storms are more likely to occur during very strong El Niño years. During the 50 years of data (1960 through 2010), two very strong El Niño years occurred, in 1982-83 and 1997-1998, or 4 percent per year of a strong El Niño event. Of the five storm events that were predicted to have a TWL elevation higher than the toe of the dunes, three occurred during very strong El Niño years. The probability of multiple storms occurring during a single year was recalculated assuming that storm events are more likely to occur during an El Niño year then a non-El Niño year. To calculate the probability of multiple storms occurring in any year with an increased probability during an El Niño year, the following assumptions were made:

- The probability of a strong El Niño year is 0.04 (two strong El Niño years in 50 years);
- The probability of a runup event large enough to reach the toe of the dunes during a strong El Niño year is 0.6 (three of the five storm events occurred during a strong El Niño year);
- The probability of a storm occurring in a year is independent of whether a storm has occurred previously in that year or in a preceding year (storms are independent); and
- The number of large storms that occur will be sufficient to erode the beach berm and reduce the slope to a winter storm slope (assumed to be 6.3 percent) before any large storms that impact the dunes occur. This is assumed to have a probability of 100 percent, though there are no data available to indicate that this has ever happened since the plant was constructed. Therefore, the result shown below should be considered very conservative.

Given these assumptions, the probability of multiple storms occurring in any year, assuming an increased probability during a strong El Niño year, is shown in the Table A-2.

Table A-2
Probability of Storms Occurring at Mandalay Beach that Could Potentially Impact the Dunes with Increased Probability During Strong El Niño Years

Number of Storms per Year	Probability (%)	Probability of Occurring in 30 years (%)
1	11	97
2	0.85	22
3	0.094	2.8
4	0.012	0.36

The results provided in Tables A-1 and A-2 are based on the assumption that the beach has eroded to a profile that allows the waves to run up the dune face. However, there is no evidence that this has occurred since construction of the MGS in 1959. In fact, the evidence indicates growth of the dunes since 1959. If the waves do not erode the beach berm and create a shallow winter profile (as shown on Figure A-2, profile #2), then waves are unlikely to run up and erode the dunes, because wave energy will be dissipated on the flatter sections of the beach. Therefore, the results shown above should be considered very conservative and the actual probabilities much less. Also, the analysis above calculates probabilities for wave runup that exceed the elevation of the toe of the dunes whether the runup exceeds the toe elevation by 1 inch, 1 foot, or 10 feet. Most of the predictions of wave runup are only slightly higher than the toe of the dune and would not result in any significant erosion. The probability that the wave runup would be high enough to cause significant erosion of the dune is much less than the probabilities shown in Tables A-1 and A-2 (the highest estimated elevation from the 50 years of data was 16.8 feet, 2.3 feet above the toe of the dune and more than 10 feet below the top of the dune).

A.6. References

BakerAECOM. 2015. Intermediate Data Submittal #2. Offshore Waves and Water Levels. Southern California. California Coastal Analysis and Mapping Project/Open Pacific Coast Study. Submitted to FEMA Region IX. January 6.

Bascom, W.H. 1953. Characteristics of Natural Beaches. *Proceedings of the 4th Coastal Engineering Conference, American Society of Civil Engineers*., pp. 163-180.

Komar, P.D. 1998. *Beach Processes and Sedimentation*. Upper Saddle River, New Jersey: Prentice Hall.

Shepard, F.P. 1950. *Beach Cycles in Southern California.* U.S. Army Corps of Engineers, Beach Erosion Board, Technical Memo No. 20.

Shih, S.-M., and P.D. Komar 1994. Sediments, Beach Morphology and Sea Cliff Erosion within an Oregon Coast Littoral Cell. *Journal of Coastal Research* 10: 144-157.

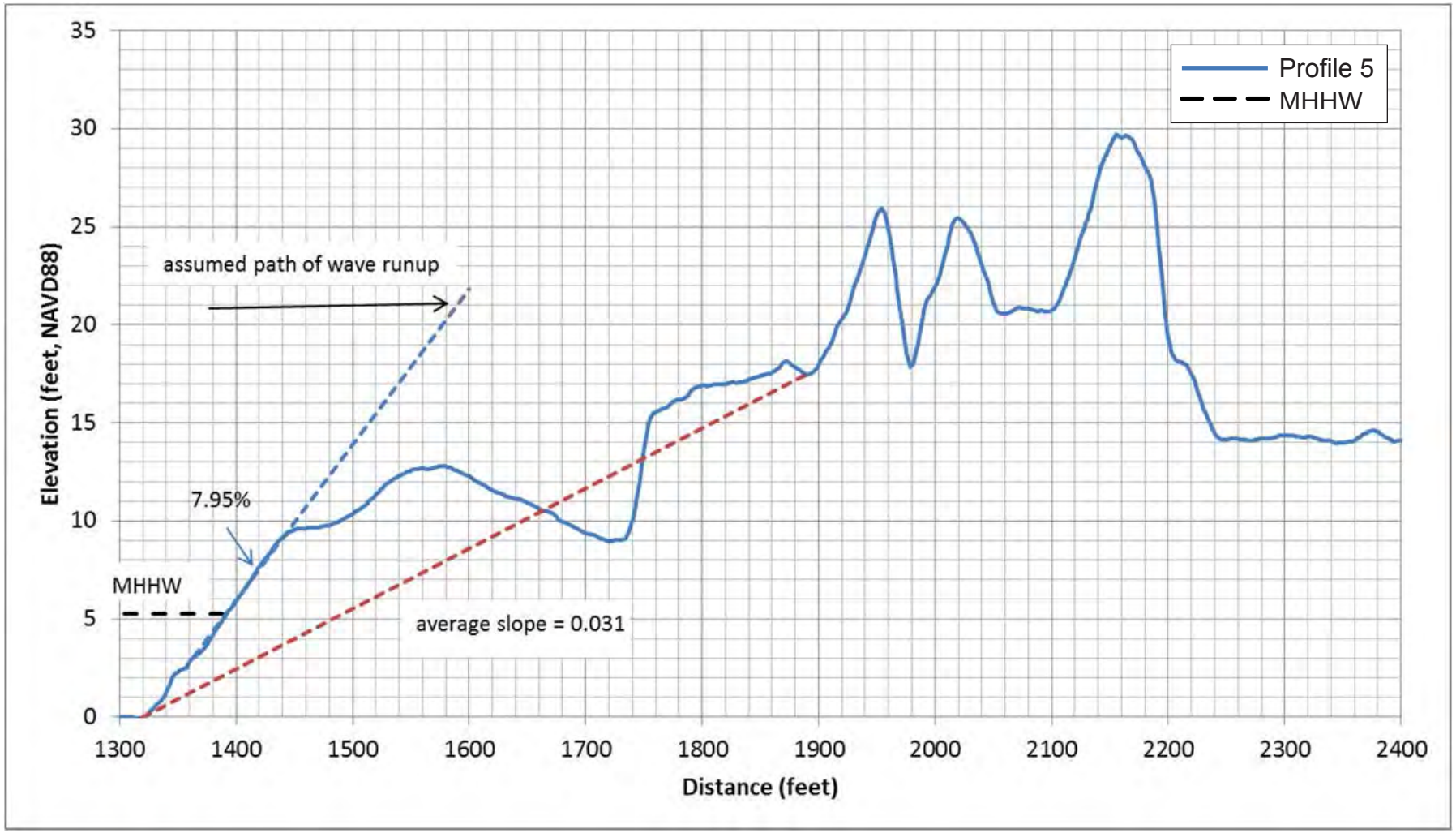

Note: See TN #207179, Response to City of Oxnard Data Request 87 for description and location of beach profile.

BEACH PROFILE ON MANDALAY BEACH SHOWING PATH OF POTENTIAL WAVE RUNUP ASSUMED IN WAVE RUNUP CALCULATIONS

NRG
Puente Power Project
June 2017 Oxnard, California

FIGURE A-1

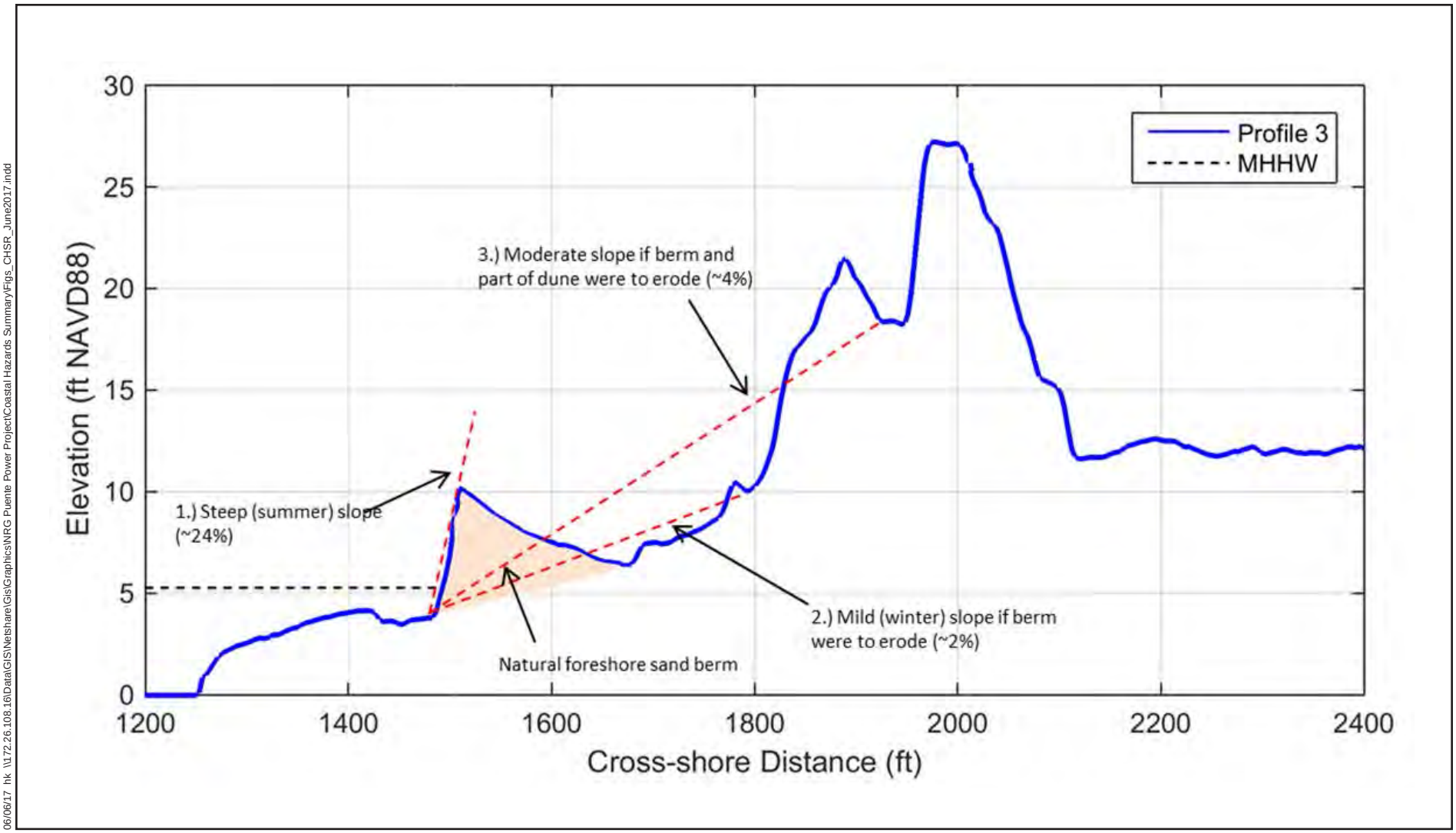

Note: See TN #207179, Response to City of Oxnard Data Request 87 for description and location of beach profile.

BEACH PROFILE AT MANDALAY BEACH SHOWING SLOPE OF BEACH UNDER OBSERVED SUMMER (SLOPE #1) AND POTENTIAL WINTER (SLOPE #2) CONDITIONS

NRG
Puente Power Project
June 2017 Oxnard, California

FIGURE A-2

Attachment 1
Rising Seas in California

Rising Seas in California

AN UPDATE ON SEA-LEVEL RISE SCIENCE

APRIL 2017

About This Document

This document was produced by a Working Group of the California Ocean Protection Council Science Advisory Team (OPC-SAT), supported and convened by the California Ocean Science Trust. *The State of California Sea-Level Rise Guidance Document,* initially adopted in 2010 and updated in 2013, provides guidance to state agencies for incorporating sea-level rise projections into planning, design, permitting, construction, investment and other decisions. Now, the California Ocean Protection Council and the California Natural Resources Agency, in collaboration with the Governor's Office of Planning and Research, the California Energy Commission, and the California Ocean Science Trust, are updating this statewide guidance to reflect recent advances in ice loss science and projections of sea-level rise. This document, requested by the California Ocean Protection Council and guided by a set of questions from the state Sea-Level Rise Policy Advisory Committee, provides a synthesis of the state of the science on sea-level rise. It provides the scientific foundation for the pending update to the guidance document.

CALIFORNIA OCEAN SCIENCE TRUST

California Ocean Protection Council OPC-SAT Science Advisory Team

CONTRIBUTORS

Working Group Members

Gary Griggs
University of California Santa Cruz, OPC-SAT (Working Group Chair)

Dan Cayan
Scripps Institution of Oceanography, OPC-SAT

Claudia Tebaldi
National Center for Atmospheric Research & Climate Central

Helen Amanda Fricker
Scripps Institution of Oceanography

Joseph Árvai
University of Michigan

Robert DeConto
University of Massachusetts

Robert E. Kopp
Rutgers University

Project Team

Liz Whiteman
California Ocean Science Trust

Susi Moser
Susanne Moser Research & Consulting

Jenn Fox
Consultant

SUGGESTED CITATION

Griggs, G, Árvai, J, Cayan, D, DeConto, R, Fox, J, Fricker, HA, Kopp, RE, Tebaldi, C, Whiteman, EA (California Ocean Protection Council Science Advisory Team Working Group). Rising Seas in California: An Update on Sea-Level Rise Science. California Ocean Science Trust, April 2017.

FUNDING

Funding was provided by the California Ocean Protection Council.

CALIFORNIA OCEAN PROTECTION COUNCIL

Key Findings

1 **Scientific understanding of sea-level rise is advancing at a rapid pace.** Projections of future sea-level rise, especially under high emissions scenarios, have increased substantially over the last few years, primarily due to new and improved understanding of mass loss from continental ice sheets. These sea-level rise projections will continue to change as scientific understanding increases and as the impacts of local, state, national and global policy choices become manifest. New processes that allow for rapid incorporation of new scientific data and results into policy will enable state and local agencies to proactively prepare.

2 **The direction of sea level change is clear.** Coastal California is already experiencing the early impacts of a rising sea level, including more extensive coastal flooding during storms, periodic tidal flooding, and increased coastal erosion.

3 **The rate of ice loss from the Greenland and Antarctic Ice Sheets is increasing.** These ice sheets will soon become the primary contributor to global sea-level rise, overtaking the contributions from ocean thermal expansion and melting mountain glaciers and ice caps. Ice loss from Antarctica, and especially from West Antarctica, causes higher sea-level rise in California than the global average: for example, if the loss of West Antarctic ice were to cause global sea-level to rise by 1 foot, the associated sea-level rise in California would be about 1.25 feet.

4 **New scientific evidence has highlighted the potential for extreme sea-level rise.** If greenhouse gas emissions continue unabated, key glaciological processes could cross thresholds that lead to rapidly accelerating and effectively irreversible ice loss. Aggressive reductions in greenhouse gas emissions may substantially reduce but do not eliminate the risk to California of extreme sea-level rise from Antarctic ice loss. Moreover, current observations of Antarctic melt rates cannot rule out the potential for extreme sea-level rise in the future, because the processes that could drive extreme Antarctic Ice Sheet retreat later in the century are different from the processes driving loss now.

5 **Probabilities of specific sea-level increases can inform decisions.** A probabilistic approach to sea-level rise projections, combined with a clear articulation of the implications of uncertainty and the decision-support needs of affected stakeholders, is the most appropriate approach for use in a policy setting. This report employs the framework of Kopp et al. (2014) to project sea-level rise for three representative tide gauge locations along the Pacific coastline: Crescent City in northern California, San Francisco in the Bay area, and La Jolla in southern California. These projections may underestimate the likelihood of extreme sea-level rise, particularly under high emissions scenarios, so this report also includes an extreme scenario called the H++ scenario. The probability of this scenario is currently unknown, but its consideration is important, particularly for high-stakes, long-term decisions.

6 **Current policy decisions are shaping our coastal future.** Before 2050, differences in sea-level rise projections under different emissions scenarios are minor but they diverge significantly past mid-century. After 2050, sea-level rise projections increasingly depend on the trajectory of greenhouse gas emissions. For example, under the extreme H++ scenario rapid ice sheet loss on Antarctica could drive rates of sea-level rise in California above 50 mm/year (2 inches/year) by the end of the century, leading to potential sea-level rise exceeding 10 feet. This rate of sea-level rise would be about 30-40 times faster than the sea-level rise experienced over the last century.

7 **Waiting for scientific certainty is neither a safe nor prudent option.** High confidence in projections of sea-level rise over the next three decades can inform preparedness efforts, adaptation actions and hazard mitigation undertaken today, and prevent much greater losses than will occur if action is not taken. Consideration of high and even extreme sea levels in decisions with implications past 2050 is needed to safeguard the people and resources of coastal California.

Report Outline

1. Introduction

Global sea-level rise is the most obvious manifestation of climate change in the ocean. It is an issue that will have far-reaching consequences for California, given its 1100-mile open coastline and many additional miles of estuarine shoreline, as well as high concentrations of people and development along the coast. Sea-level rise will continue to threaten coastal communities and infrastructure through more frequent flooding and inundation, as well as increased cliff, bluff, dune, and beach erosion.

Human development and pressures from a rising sea threaten the already diminished coastal wetlands along the California coast. Hundreds of miles of roads and railways, harbors and airports, power plants and wastewater treatment facilities, in addition to thousands of businesses and homes, are at risk from future flooding, inundation, and coastal retreat [1]. But the total potential impact of such coastal risks is significantly larger still: not only are economic assets and households in flood zones increasingly exposed, but also people's safety, lives, daily movement patterns, and sense of community and security could be disrupted.

California also has the nation's largest ocean economy, valued at over $44 billion/year [2], with the great majority of it connected to coastal recreation and tourism, as well as ports and shipping. Many of the facilities and much of the infrastructure that support this ocean economy, as well as the State's many miles of public beaches, lie within a few feet of present high tide.

1.1. Updating California's Statewide Guidance

The State of California Sea-Level Rise Guidance Document, initially released in 2010 and first updated in 2013, has provided guidance to state agencies for incorporating sea-level rise projections into planning, design, permitting, construction, investment, and other decisions. In 2010, the Governors of Oregon and Washington, along with 10 state and federal agencies, approached the National Research Council (NRC) with a request to provide estimates and projections of future sea-level rise. The NRC Committee built upon and updated the most recent Intergovernmental Panel on Climate Change report at the time [3]. The Committee's report, Sea-Level Rise for the Coasts of California, Oregon, and Washington - Past, Present and Future was completed in 2012 [4]. The future sea-level projections from this report have guided state agencies in their sea-level rise planning in the subsequent years. Five years have elapsed since the NRC study, during which time a new Intergovernmental Panel on Climate Change (IPCC) report was published containing updated sea-level rise projections based on new scenarios, model simulations, and scientific advances [5]. New research has also been published on some of the primary drivers of sea-level change, which includes important new work on ice sheet mass loss in Antarctica, as well as on new methods for producing probabilistic projections of local sea-level change [6,7].

Now, the California Ocean Protection Council and the California Natural Resources Agency, in collaboration with the Governor's Office of Planning and Research, the California Energy Commission, and the California Ocean Science Trust, are updating this statewide guidance for a second time to reflect recent advances in ice loss science and projections of sea-level rise. The updated guidance will focus on the needs of state agencies and local governments. It will help cities and counties as they comply with a new law that requires them to incorporate climate change into their planning efforts. The updated guidance document will also assist state agencies prepare for and adapt to climate change, as directed by Governor Brown's recent Executive Order B-30-15.

This document, a synthesis of the state of the science on sea-level rise, provides the scientific foundation for the update to the existing guidance document. Because effective planning for sea-level rise involves collaboration among various departments within coastal city and county governing bodies, special districts, state agencies, federal agencies, climate researchers, non-governmental organizations, business owners and other stakeholders, a robust public engagement process has been launched and will be implemented throughout 2017 to ensure that the new policy guidance is responsive to user needs. Public input will be integrated into the final guidance document update, which is scheduled for adoption by the California Ocean Protection Council in January 2018.

1.2. How this report was developed

This report was developed by a Working Group of the Ocean Protection Council Science Advisory Team, supported and convened by California Ocean Science Trust. The Working Group was convened from January - April 2017. Working Group members met regularly via videoconference during this period and convened for a two-day in-person meeting in February 2017. The scope and content of the report was informed by a set of questions from the state sea-level rise Policy Advisory Committee (Appendix 1). All Working Group members have contributed to the development of the report, and reviewed the final product. In addition the report has been peer reviewed by experts and revised to reflect the input received.

1.3. How to use this report

This report is intended to provide the scientific foundation for updating California's statewide sea-level rise policy guidance. It is also intended to be used alongside policy recommendations to support planning, permitting, investment, and other decisions at state and local scales. Planners, land managers, consultants, and government officials can draw directly on the scientific data, graphics, and text provided herein as it offers context, explanation, and scientific foundation for planning and decisions. Scientific information is one important input into the detailed and systematic process that decision-makers undertake to evaluate options to prepare for and respond to the emerging impacts of changing coastal hazards.

We have structured this report to provide scientific information that is useful for making decisions now. Although long-range (>40-50 year) sea-level rise futures are uncertain, we explain the sources of these uncertainties, and to the extent possible offer probabilistic sea-level rise projections that can be used in decisions today and in the near future. As the Earth system enters uncharted territory due to rapid changes in the Earth's climate, resulting in sea-level rise rates unprecedented at least in human experience, scientists are attempting to understand the processes contributing to sea-level rise as quickly as possible. An update of the science underlying sea-level rise is necessary because the effects of many decisions made today will persist for decades—e.g., 50, 70 and even 100 years into the future. Just as we are still living with decisions about houses, factories, roads, and power plants—made 50 years ago on the assumption of a stable environment and without foresight about possible changes to environmental conditions—the legacy of California's current decisions in the face of continued sea-level rise will persist. However, today, we have a much-advanced scientific understanding and know that the climate and the oceans are rapidly changing; thus more defensible decisions going forward are possible. This report offers an update on this understanding and provides the best available projections of future conditions.

1.4. How often should practitioners and policy makers reassess scientific data?

Our collective scientific understanding of sea-level rise is advancing at a very rapid pace. We anticipate that new observations, new models, refinement of existing models to capture newly described sea-level rise dynamics, and updated models that are validated with observational data, will continue to be published in the peer-reviewed literature over the coming years.

Moreover, it is not just scientific understanding that is evolving and improving. Sea-level rise projections will continue to change as the impacts of local, regional, national and global policy choices are manifest. Given this dynamic environment, we encourage the creation of science-policy processes that are flexible, iterative and adaptive. At minimum, we recommend that sea-level rise projections be updated every five years, aligned with existing climate change assessment cycles, or when new data become available that are judged to significantly modify existing projections. More fundamentally, we encourage California lawmakers and policy-makers to pursue institutional arrangements and processes for dynamic and rapid incorporation of the results of new science into policy. In this report we aim to provide a robust description of the considerations in selecting approaches to project sea-level rise, and justification of the current choices. Our goal is that this scientific information can begin to make the concept of adaptive policy tractable and actionable.

2. Understanding Sea-Level Rise

Sea level is expected to rise significantly over the next century due to a changing global climate. However, change in sea level is not a new phenomenon; sea level has been rising globally since the end of the last ice age about 18,000 years ago. Driven primarily by the melting of land ice, global mean sea level rose about 120-135 m (about 400-450 feet) during this period. Much of this took place between 18,000 and 8,000 years ago at average rates of about 11 mm/year (45 in/century) and then began to slow. Sea level rose very gradually (<1 mm/year) over the past 8,000 years.

With the onset of the Industrial Revolution and the expanded use of fossil fuels, the greenhouse gas content of the atmosphere began to increase and the Earth has gradually warmed in response, accompanied by thermal expansion of a warming ocean and melting of the Earth's land ice. Estimates of the average rate of sea-level rise between 1900 and 1990, derived from the global network of tide gauges have been made but are complicated by regional land motion and ocean dynamics as well as changes in the Earth's gravitational and rotational fields. These all cause local sea level changes measured by individual tide gauges to deviate from the rate of global mean sea-level rise. Several different approaches have been used to analyze the global tide gauge records in order to accommodate the spatial and temporal variations, and these efforts have yielded sea-level rise rates ranging from about 1.2 mm/year to 1.7 mm/year (about 0.5 to 0.7 inches/decade) for the 20th century, but since 1990 the rate has more than doubled, and the rise continues to accelerate [8–12]. Since the advent of satellite altimetry in 1993, measurements of

absolute sea level from space indicate an average global rate of sea-level rise of 3.4 mm/year or 1.3 inches/decade – more than twice the average rate over the 20th century and greater than any time over the past thousand years [13,14].

2.1. What contributes to current sea-level rise?

2.1.1.Contributors to global mean sea-level rise

Over the last century, ocean thermal expansion was the single greatest contributor to global mean sea-level rise, accounting for about 50% of the signal. The remaining 50% was contributed from land ice; a mix of melting mountain glaciers and ice caps, and the loss of ice from the great polar ice sheets covering Greenland and Antarctica [10]. However, the entire global inventory of mountain glaciers contains only enough ice to raise sea levels by about a half a meter (1.5 feet). In contrast, the Greenland and Antarctic Ice Sheets contain enough ice to raise global mean sea level by 7.4 m (24 feet) and 57 m (187 feet), respectively. While these ice sheets are not expected to melt completely, even on centennial or millennial timescales, the loss of even a small of fraction of either of these huge ice sheets could raise sea level significantly, with devastating consequences for global shorelines. This is particularly concerning because satellite observations clearly show that the rate of ice loss from both the Greenland and West Antarctic Ice Sheets is accelerating. If these trends continue, the contribution from the ice sheets will soon overtake that from mountain glaciers and ocean thermal expansion as the dominant source of sea-level rise (see Appendix 2 for a more detailed discussion of this topic).

Withdrawal of groundwater, and changes in water storage behind dams also impact sea level, although over most of the 20th century the filling of reservoirs had a small negative impact on sea-level rise (i.e., reduced the rate of sea-level rise [15]). In recent decades, increasing groundwater depletion has begun contributing positively to sea-level rise by about 0.4 mm/year (0.15 inches per decade; [10]), because about 80% of the groundwater that is withdrawn and then utilized for domestic, agricultural or industrial purposes ultimately flows to the ocean. However, ongoing contributions to global sea levels from this source will likely be small relative to other potential sources.

2.1.2. Contributors to regional and local relative sea-level rise

While global mean sea level is rising, it is relative sea level, the local difference in elevation between the height of the sea surface and the height of the land surface at any particular location, which directly impacts coastal communities and ecosystems at risk from coastal flooding. Changes in relative sea level arise from 1) vertical land motion, 2) changes in the height of the geoid (the gravitationally determined surface of the ocean in the absence of tides and ocean currents), and 3) changes in the height of the sea surface relative to the geoid. In sum, future changes in relative sea level will not be the same across the globe and will even vary along the length of the California coastline.

Vertical land motion can be caused by tectonics (see Box 2), sediment compaction, withdrawal of groundwater and hydrocarbons, and isostatic adjustments which describe the Earth's deformation associated with redistributions of ice and ocean mass [16,17]. For example, the Earth's surface, and relative sea level, is still adjusting to the retreat of the massive ice sheets that covered much of the Northern Hemisphere during the Last Glacial Maximum about 18,000 years ago. Locally, this post-glacial isostatic adjustment can either produce a long-term rise or fall of sea level, depending on the proximity to the past ice load. In the case of California, relatively far from the Last Glacial Maximum ice sheets, this effect is small [18]. Persistent changes in winds and ocean currents can also have local to regional scale impacts on relative sea level, although these effects are not projected to be as consequential for the U.S. West Coast as they are for the U.S. Northeast.

Of particular relevance for California will be future redistributions of ice and water caused by the retreat of the polar ice sheets, especially on Antarctica. These mass redistributions affect the Earth's gravitational field and the orientation and rate of Earth's rotation, and deform the Earth's crust and mantle [16,19]. While the mantle responds on millennial timescales, the gravitational, rotational and crustal effects are essentially instantaneous. As a retreating ice sheet loses mass to the ocean, its gravitational pull on the surrounding ocean is reduced. Within about a thousand miles of a retreating ice sheet, the reduced gravitational pull on the ocean causes the sea-surface (and relative sea level) to drop, even though the ocean has gained volume overall. Further from the ice sheet (~4000 miles), the change in relative sea level is comparable to that expected from the increase in ocean volume contributed by the melting ice sheet. Beyond that distance, the change in

relative sea level is greater than expected from the extra water added to the ocean by the melting ice sheet. Consequently, Northern Hemisphere coastlines generally experience enhanced sea-level rise from the loss of Antarctic ice, while coastlines in the Southern Hemisphere experience enhanced sea-level rise from loss of Greenland ice. Changing distributions of ice and water also shift the Earth's pole of rotation (the physical North and South Poles) and rate of rotation, which modifies the main gravitational response.

Calculations of the spatial distribution of sea-level rise that take into account these gravitational and rotational effects, sometimes called sea level "fingerprints" (Figure 1, [16]), show that North America experiences more sea-level rise from a given meltwater contribution from Antarctica than from Greenland, and if the ice loss is from West Antarctica, the impacts are exaggerated even further. In fact, these calculations show that for California, there is no worse place for land ice to be lost than from the West Antarctic Ice Sheet. For every foot of global sea-level rise caused by the loss of ice on West Antarctica, sea-level will rise approximately 1.25 feet along the California coast, not including the additional local factors mentioned above. In addition, the West Antarctic Ice Sheet is considered the most vulnerable major ice sheet in a warming global climate, and serious irreversible changes are already underway (see discussion below and Appendix 2, [20–22]).

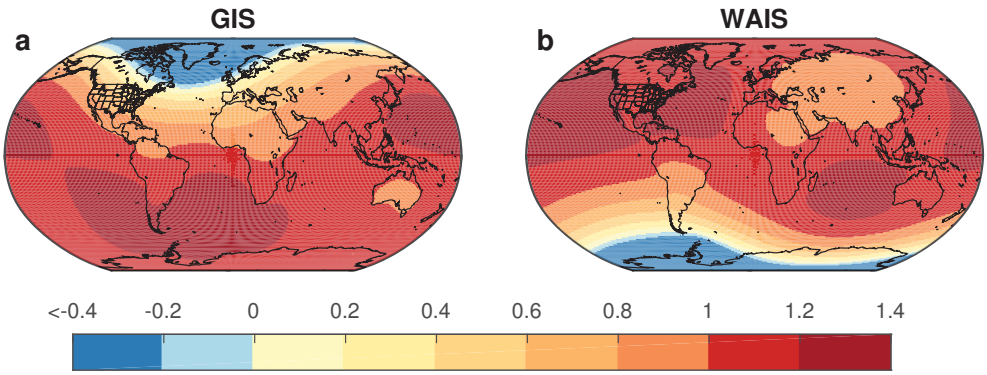

Figure 1. Sea-level 'fingerprints' resulting from the distribution of ice and water around the Earth and ensuing gravitational and rotational effects.

The maps depict the relative response of sea-level to the loss of ice mass from (a) Greenland Ice Sheet (GIS) and (b) West Antarctic Ice Sheet (WAIS). The color bar represents the fractional departure of relative sea level rise from that expected given the ice contribution to global mean sea level. For example, when ice is lost from the Greenland Ice Sheet the relative effect on the US West Coast is 75% of the sea-level rise expected from the water volume added to the ocean. By comparison, when ice is lost from the West Antarctic Ice Sheet the US West Coast experiences 125% of sea-level rise from that expected from the water volume added.

2.2. What are recent scientific advances in understanding sea-level rise?

2.2.1. New observations and understanding of climate changes

During the last five years, the atmospheric greenhouse gas concentration has continued to increase. Since late 2015, measurements of the atmospheric CO_2 concentration have consistently exceeded 400ppm.[i] Recent concentrations are approximately 45% higher than the pre-industrial level, and about 2.5% higher than in 2012. Increases in CO_2 and other greenhouse gases have resulted in the Earth's climate system absorbing more energy than it is emitting back to space, an imbalance estimated to be greater than 0.5 Watts/m^2. More than 90% of this excess heat is being captured by the global ocean [23]. Heat gain in the deep ocean has occurred unabated at least since 2006, with temperature increases extending from the surface to depths exceeding 1500m in all ocean basins [24].

The Earth's surface has also continued to warm. Sixteen of the 17 warmest years in the 136-year period of global temperature measurements have all occurred since 2001.[ii] 2016 was the warmest year on record, and it was the 3rd year in a row that the record was broken. Arctic sea ice at the peak of the summer melt season now typically covers 40% less area than it did in the early 1980s. Arctic sea ice extent in September, the seasonal low point in the annual cycle, has been declining at a rate of about 13% per decade.[iii]

2.2.2. Advances in observing and modeling sea-level rise

Of the major contributors to global sea-level rise, the loss of ice from the Greenland and Antarctic Ice Sheets has the greatest potential to increase sea levels. Contributions from ice sheet losses also present the greatest uncertainty in the rate and amount of sea-level rise at time horizons beyond the next few decades. In the past five years (since the existing State guidance document was developed), new models and observations have highlighted this possibility and advanced our understanding of the dynamics of ice loss, and the atmospheric and ocean conditions that can drive significant loss. A more comprehensive discussion of this topic is provided in Appendix 2.

Observational data from the GRACE (Gravity Recovery and Climate Experiment) satellites, which measure the Earth's gravitational field, have revealed increased loss of land ice from Greenland and West Antarctica [13], and confirmed previous observations. Satellite altimeter data show increased loss of grounded land ice from West Antarctica, and evidence of accelerated volume loss of ice shelves in West Antarctica, which buttress grounded ice [22].

[i] https://www.esrl.noaa.gov/gmd/ccgg/trends/monthly.html
[ii] https://www.nasa.gov/press-release/nasa-noaa-data-show-2016-warmest-year-on-record-globally
[iii] https://www.nasa.gov/feature/goddard/2017/sea-ice-extent-sinks-to-record-lows-at-both-poles

New radar sounding observations have also revealed that the very different climates and underlying bedrock topography of Greenland and Antarctica will result in markedly different contributions to global sea-level rise. The bedrock beneath the Greenland Ice Sheet is above sea level around most of its margin, and below sea level only in the interior, which limits its rate of outflow to the ocean [25]. By contrast, much of the West Antarctic Ice Sheet and parts of the East Antarctic Ice Sheet lie on bedrock that is below sea level and deepens toward the continental interior [26]. Model results indicate that, while low rates of loss are possible, much higher rates of ice loss and sea-level rise could occur if oceanic and atmospheric warming is great enough to erode the floating ice that buttresses grounded ice. Ice flow mechanics responding to a high warming scenario could result in an escalating, effectively irreversible discharge of ice into the ocean as the grounded ice front recedes inland. Importantly, the change in the Earth's gravitational field and rotation that would result from the loss of ice from West Antarctica would result in a higher sea-level rise along the coast of California than the overall global average, an amplification that becomes increasingly consequential as Antarctic ice loss grows larger (see above and Appendix 2).

New studies have also examined historical periods of high sea levels, and rapid rates of sea-level rise, to better understand the potential for specific levels of future sea-level rise [27]. Extremely high sea levels during the Last Interglacial Period (about 125,000 years ago) and Pliocene (about 3 million years ago) indicate that the polar ice sheets are sensitive to relatively modest climate warming. During the Last Interglacial Period, global mean temperatures were similar to today, but sea level was 20 - 30 feet (6 - 9 m) higher. Most of this sea-level rise is thought to have originated from Antarctic ice loss. The Pliocene was approximately 2°C - 3°C warmer than today, and sea levels may have been higher by 30 - 90 feet (10 - 30 m) than today, requiring a substantial contribution from East Antarctica in addition to Greenland and West Antarctica (Appendix 2). Using the reconstructed atmospheric and oceanic climate, new models have been applied to test mechanisms of ice loss (and resulting sea level rise) during those periods to better understand how those high sea levels could have occurred and also to inform future sea-level rise projections [27,28].

While there has been much progress in recent years in observing and modeling the Antarctic Ice Sheet, the precise magnitude and timing of when it will begin to contribute substantially to rising sea levels remains highly uncertain. This is partly due to insufficient knowledge of the physics of Antarctic ice loss processes, such that they cannot be faithfully represented in models. More importantly, however, we do not know what future greenhouse gas emissions

will be; so even if the physics were perfectly captured in the models, there would still be major uncertainty about which processes will become important as the ice sheet evolves. That said, the recent work does allow for some important new conclusions (see also Appendix 2):

- Previously underappreciated glaciological processes, examined in the research of the last five years, have the potential to greatly increase the probability of extreme global sea-level rise (6 feet or more) within this century if emissions continue unabated.

- The processes that could drive extreme Antarctic Ice Sheet retreat later in this century are different from those driving Antarctic Ice Sheet changes now, so the fact that the current rise in global sea level is not consistent with the most extreme projections does not rule out extreme behavior in the future.

- An aggressive reduction in greenhouse gas emissions substantially reduces but does not eliminate the risk of extreme global sea-level rise driven by Antarctic ice loss.

- Once marine-based ice is lost, the resulting global sea-level rise will last for thousands of years.

BOX 1

Short-term increases in sea level

Although long-term mean sea-level rise by itself will provoke increasing occurrences of nuisance flooding, over the next several decades it is highly likely that short-term increases in sea level will continue to be the driver of most of the strongest impacts to infrastructure and coastal development along the coast of California. Short-term processes, including Pacific Basin climate fluctuations (Pacific Decadal Oscillation, El Niño Southern Oscillation, and North Pacific Gyre Oscillation), King tides (perigean high tides), seasonal cycles, and winter storms, will produce significantly higher water levels than sea-level rise alone, and will present greater risks to coastal development.

El Niño associated flooding

Over the recorded era of the 20th and early 21st centuries, most of the significant storm damage to California's coastline has occurred during major El Niño events, when elevated sea levels coincided with storm waves and high tides [29]. The record from the San Francisco tide gauge, the longest continuously running gauge along California's coast, reveals several years when seasonal anomalies rose above the long-term trend of 1.9 mm/year (0.07 inches/year). The most prominent of those cases were major El Niño events, for example, 1940-41, 1982-83, and 1997-98, when sea levels were elevated 8-12 inches (20-30 cm) for several months at a time (Figure 2).

Adding these weather and short-period climate events to the more gradual, incremental global rise in mean sea level will present increasing risks for low-lying coastal infrastructure and development. The latest generation of climate model simulations suggests that North Pacific storminess will remain at about the same level of activity as seen in the 20th and early 21st century but that the frequency of extreme El Niño events may increase under a warmer climate [30]. Given the strong association between El Niño, large winter North Pacific storms, and anomalously high sea levels and storm surge [31], occasional large sea level events in future decades must be considered in future scenario planning.

King tides

High tides along the California coast occur twice daily, typically of uneven amplitude, and are caused predominantly by the gravitational attraction of the moon and the sun on the Earth's oceans. Extreme tides, called spring tides, occur in multi-day clusters twice monthly at times of the full and new moon. Additionally, even higher tides occur several times a year and are designated as perigean high tides, or more popularly "King tides". These events are now recognized as producing significant coastal flooding in some well-known areas such as the Embarcadero in San Francisco, where King tides are already washing onto the sidewalks. The Earth-moon-sun orbital cycles also amplify tidal ranges every 4.4 and 18.6 years, producing peaks in the monthly high tide that are about 6 inches (15 cm) and 3 inches (8 cm) respectively, higher than in the intervening years.

Storm surges

Storm surges, created when strong onshore winds combined with low barometric pressure force seawater onto the shoreline, also temporarily elevate sea levels. While storm surge along the coast of California is considerably less than that experienced during severe hurricanes and nor'easters along the Gulf and Atlantic Coasts of the United States, the storm surge during major winter storms here can reach as much as 3 feet above predicted sea levels.

Wave-driven water level increase

Large ocean waves can transport significant volumes of water up onto the shoreline as they break, causing temporary increases in sea level through two related processes. Wave run-up describes the process of an individual breaking wave washing up the beach face to an elevation as much as 6 feet above sea level. Wave set-up results from a set of large waves breaking in rapid succession, which can elevate the overall water level along the shoreline as much as 4 or 5 feet for a few minutes at a time. Because many beaches have shallow slopes, extremely high waves and resulting set-up and run-up events can have enormous impacts in causing erosion and damage to coastal infrastructure. Short-term elevated sea levels from any of these processes can not only cause flooding in low-lying coastal areas but can also exacerbate flooding along stream or river courses when runoff is temporarily obstructed by an elevated ocean or high tides, thereby leading to enhanced inland flooding.

Implications of short-term increases in sea level

The historic records and measurements (from tide gauges) of short-term elevated sea levels, whether due to El Niño events, King tides, storm surges, or a combination of these (as dramatically occurred during the 1982-83 El Niño), provide useful indicators for understanding future total water levels. These short-term elevated sea levels need to be added to projected future sea levels to obtain future total water levels.

3. Sea-Level Rise Projections

3.1. Approach, definitions, and limitations

3.1.1. Emissions scenarios

The Intergovernmental Panel on Climate Change (IPCC) adopted a set of emissions scenarios known as 'representative concentration pathways', or RCPs. These are a set of four future pathways, named for the associated radiative forcing (the globally averaged heat trapping capacity of the atmosphere measured in watts/square meter) level in 2100 relative to pre-industrial values: RCP 8.5, 6.0, 4.5 and 2.6 [32]. RCP 8.5 is consistent with a future in which there are no significant global efforts to limit or reduce emissions. RCP 2.6 is a stringent emissions reduction scenario and assumes that global greenhouse gas emissions will be significantly curtailed. Under this scenario, global CO_2 emissions decline by about 70% between 2015 and 2050, to zero by 2080, and below zero thereafter [33].

RCP 2.6 most closely corresponds to the aspirational goals of the United Nations Framework Convention on Climate Change's 2015 Paris Agreement, which calls for limiting global mean warming to less than 2°C and achieving net-zero greenhouse gas emissions in the second half of this century. This pathway will be very challenging to achieve, and most simulations of such stringent targets require widespread deployment of nascent carbon-negative technologies, such as sustainable bioenergy coupled to carbon capture and storage, or direct air capture of CO_2.

Three of these pathways are used here to project sea-level rise: RCP 8.5, RCP 4.5 and RCP 2.6. We do not include RCP 6.0 because it yields 21st century sea level projections that are nearly identical to those of RCP 4.5 [10], and few climate models have run RCP 6.0 beyond 2100.

3.1.2. Approach to projections

The scientific literature offers several distinct approaches to generating future sea-level rise projections. One set focuses on providing scenarios that span a range of possible futures, while making little or no attempt to assess the relative likelihood of different scenarios. Another set focuses on estimating the probability of different levels of future sea-level change, either by estimating a central projection with an associated range or by attempting to estimate a comprehensive probability distribution that also estimates the likelihood of extreme 'tail' outcomes. These approaches also differ in whether they explicitly represent the dependence of future sea-level change on specific greenhouse gas emission pathways (with the implied storyline about future economic and social development attached to them) or present results with no explicit connection to them, for example as a function of global average temperatures, independently of the emission pathways that would produce them, or as a set of low/medium/high projections with no explicit description of what would be driving them (see also Box 3).

For the Third National Climate Assessment, Parris et al. (2012) [34] constructed four discrete scenarios, spanning a range of global mean sea-level change in 2100 from 20 cm to 200 cm. They did not discuss the likelihood of these scenarios, nor did they tie them to specific emissions scenarios. They also did not make explicit geographic projections. However, the U.S. Army Corps of Engineers' sea-level rise calculator does combine these discrete scenarios with tide-gauge-based estimates of local background processes to produce partially localized sea-level rise projections.[iv]

The National Research Council effort in 2012 [4] produced a set of three scenarios (low, central, and high), with greater weight given to the central scenario. The dependence of ocean thermal expansion and ocean dynamics on emissions was explicitly considered in producing these projections, but the emissions dependence was combined with other sources of uncertainty in producing the low and high values. The IPCC's Fifth Assessment Report [5,10] did not produce local projections for California, but their global mean sea level projections served as a touchstone for all the work that has followed. They produced estimates of the 'likely' range of global sea-level rise under each of four RCPs, where 'likely' covers the central 66% of the probability distribution (i.e., the sea levels that fall within the range created by the value that is 17% likely to occur and the value that is 83% likely to occur). They did not, however, attempt to estimate sea-level rise outside these central 66% probability ranges.

[iv] http://www.corpsclimate.us/ccaceslcurves.cfm

Both the absence of local projections and the incompleteness of their estimated probabilities led Kopp et al. (2014) [6] to synthesize several lines of evidence to estimate comprehensive probability distributions for global mean sea level and local relative sea level changes under the four RCPs, with a focus on RCP 2.6, 4.5, and 8.5. In this approach, outputs from process-based models are combined with estimates of contribution from the polar ice sheets derived from an expert elicitation process [35]. The Kopp et al. (2014) framework has been employed by a range of risk analyses (e.g., [36,37]) and stakeholder groups, including the New Jersey Climate Adaptation Alliance [38], and regional groups in Washington State (e.g.,[39,40]).

Subsequent work found that the sea-level rise projections of Kopp et al. (2014) were consistent with the historical relationship between temperature and rate of global sea level change over the last two millennia [14]. Other probabilistic projections have yielded somewhat higher projections. For example, the Kopp et al., 2014 approach projects 1.2 m (almost 4 feet) global sea level rise for RCP 8.5 by 2100 (95th percentile), while Jevrejeva et al., (2014, 2016) project 1.8 m (almost 6 feet) for RCP 8.5 by 2100 (95th percentile) [41,42]. Importantly, while Kopp et al. (2014) provide comprehensive probability distributions conditional upon emissions scenarios, they emphasize the tentative nature of these distributions and highlight the 99.9th percentile of their RCP 8.5 projections (about 8 feet or 2.5 m) as being consistent with estimates of 'maximum physically plausible' global mean sea level estimates derived through other methods. An expert panel convened to provide guidance in New Jersey [38] included a narrative recommendation to give this outcome greater weight in decisions involving facilities or structures with a low tolerance for risk (e.g. international airports, large power plants or sewage treatment facilities).

Since 2014, new work on Antarctic Ice Sheet modeling (Appendix 2) has identified various modes of marine ice-sheet instability that could make extreme sea-level outcomes more likely than indicated by the IPCC Fifth Assessment Report or the Kopp et al. (2014) framework, particularly under high-emissions scenarios. To address this possibility, the City of Boston [43] and the Fourth California Climate Change Assessment [44] employed modified versions of the Kopp et al. (2014) framework, in which the Antarctic projections of Kopp et al. (2014) were replaced with ensembles of simulations from DeConto and Pollard (2016). This ad hoc approach highlights the sensitivity of global and local sea-level projections to Antarctic ice sheet instability. However, as Kopp et al. (in review) emphasize, DeConto and Pollard's (2016) ensembles of simulations were not intended to and do not constitute probability distributions of future Antarctic changes. DeConto and Pollard (2016) explored a discrete set of ice-sheet parameterizations consistent with the geological record, but did not undertake a comprehensive assessment of the probability of different parameterizations. Therefore, these ad hoc approaches cannot be viewed as yielding probability distributions of future changes in the same manner as Kopp et al. (2014).

For the Fourth National Climate Assessment, Sweet et al. (2017) [45] maintained the scenario-based approach of Parris et al. (2012), but drew upon the framework of Kopp et al. (2014) to localize their projections and to discuss the relative likelihood of different scenarios under different emissions pathways. Notably, in light of various assessments of the 'maximum physically plausible' global mean sea-level rise and new work such as that of DeConto and Pollard (2016), they added an extreme scenario reaching 8 feet (2.5 m) of global mean sea-level rise in 2100, a level that requires the invocation of the marine ice-sheet instability mechanisms discussed in Appendix 2. In this assessment, ice sheet mass changes were projected based on combining the IPCC expert assessment of likely ranges with information about the broader probability distribution from the expert elicitation of Bamber and Aspinall (2013).

After considering the comprehensive probabilistic approach of Kopp et al. (2014), the ad hoc modification of this approach in the California 4th Climate Change Assessment, and the scenario-based approach of the recent Fourth National Climate Assessment, the Working Group concluded that the comprehensive probabilistic approach was most appropriate for use in a policy setting in California. Probabilistic approaches can be used in a range of decision frameworks, including the sea-level rise allowance framework, which is focused on maintaining expected flood risk at a target level over the lifetime of a decision [46,47]. The scenarios-based approach in the Fourth National Climate Assessment does not provide as rich a source of information for risk management and does not highlight the dependence of future sea-level change on greenhouse gas emissions as clearly. The approach of the California 4th Climate Change Assessment depends heavily on a single recent modeling study in a rapidly developing field and does not provide truly probabilistic information. However,

recognizing that the Kopp et al. (2014) projections may underestimate the likelihood of extreme sea-level rise, particularly under high-emissions scenarios, the Working Group concluded that the extreme sea-level rise scenario in the Fourth National Climate Assessment (here called the H++ scenario) should be considered alongside the Kopp et al. (2014) probability distributions for RCPs 2.6, 4.5 and 8.5. At this point, it is scientifically premature to estimate the probability that the H++ scenario will come to pass, and, if so, when the world will move onto the H++ trajectory.

One important point that is underscored by the ad hoc approaches is that the mechanisms driving Antarctic ice mass loss today are different than those that may drive future ice sheet collapse. Although sea-level rise is not following the H++ scenario at this moment, this scenario cannot be excluded for the second half of this century on these grounds.

3.1.3. Timeframes and planning horizons

The projections of sea-level rise provided here are averages across an interval of 19 contiguous years, centered on 2030, 2050, 2100 and 2150. Although the planning horizons of most infrastructure decisions fall within the near-term end of this range, we believe that it is essential to place all decisions within a longer-term context to foster choices that - to the extent possible - do not eliminate or reduce future options.

3.1.4. Starting in 2000

The baseline for the projections in this report is the year 2000, or more specifically, average relative sea level over 1991-2009. Due to a combination of atmosphere and ocean dynamics, the decadal average sea level in San Francisco can change up to 2 inches around the mean, which is equivalent to about 15 years of present-day global sea-level rise.

3.1.5. California tide gauges

There are 12 active NOAA tide gauges along the outer coast of California[v], which range in their periods of record from 39 years (Point Arena) to 162 years (San Francisco). Considerable local variability is evident in rates of sea-level rise recorded across these tide gauges, simply because they are all anchored on some land mass or structure that may be experiencing long-term uplift or subsidence (Box 2).

We selected three of these gauges to use as the basis for sea-level rise projections: Crescent City, San Francisco Golden Gate, and La Jolla. Although there is considerable local variation that they do not represent, these gauges span the broad scale geographic extent of the California coastline taking into account the changing tectonic context along the coastline, the gradient of storm and wave climate from north to south, and in consideration of centers of human population and development.

[v] http://www.corpsclimate.us/ccaceslcurves.cfm

BOX 2

Local sea-level rise rates along the coastline of California

For the shoreline of Southern and Central California (San Diego to Point Reyes) sea-level rise rates recorded at NOAA tide gauges range from just under 1 mm/year to just over 2 mm/year (a little less than 4 inches to just over 8 inches/century). By comparison, the state's three northernmost tide gages lie in tectonic environments that modify global sea-level rise rates. Point Arena, which lies virtually on the San Andreas Fault, has recorded 0.4 mm/year of relative sea-level rise for the past 39 years. At Cape Mendocino, one hundred miles to the north, a major tectonic boundary occurs as the strike slip or transform boundary marked by the San Andreas Fault transitions to the Cascadia Subduction Zone, which continues northward to Vancouver Island. From Cape Mendocino north for the next 120 miles to the Oregon border, the shoreline is being arched upward due to the collision and subduction of the Gorda Plate beneath northern California, although there are local settings, for example Humboldt Spit, where subsidence is occurring. The general pattern of uplift is evidenced by the Crescent City tide gauge, which has recorded relative sea-level change averaging -0.8 mm/year over the past 84 years, or a drop in sea level relative to the coast, illustrating that the coastline here is rising faster than sea level (Figure 2, [4]).

The pattern of coastal uplift north of Point Arena is subject to major periodic interruptions. A wide range of evidence indicates that the Cascadia Subduction Zone periodically generates great earthquakes of magnitude 8 to over 9 that cause sudden shifts and reset rates of vertical motion. Fieldwork along the coasts of northern California, Oregon and Washington indicates that these great earthquakes are accompanied by shoreline subsidence on the order of three feet or more, as well as major tsunami flooding. The last great earthquake occurred in January 1700 and caused a large segment of coastline to subside and be suddenly inundated. The geologic evidence revealing a long series of these events, which occur every 300 to 500 years on average, strongly suggests that the present regime of relatively quiescent sea-level rise along the California coast north of Cape Mendocino will change virtually instantaneously when the next great earthquake occurs.

While the timing of such an event is impossible to predict, the fact that this phenomena has repeatedly occurred over thousands of years means that it must be taken as a serious threat.

Figure 2. NOAA tide gauge records for Crescent City, San Francisco, and La Jolla stations.

Long-term change is listed on top of each record in mm/year. Short-term increases in sea level (such as 1982-93 and 1997-98 El Niños) are clear in the records for all three stations.

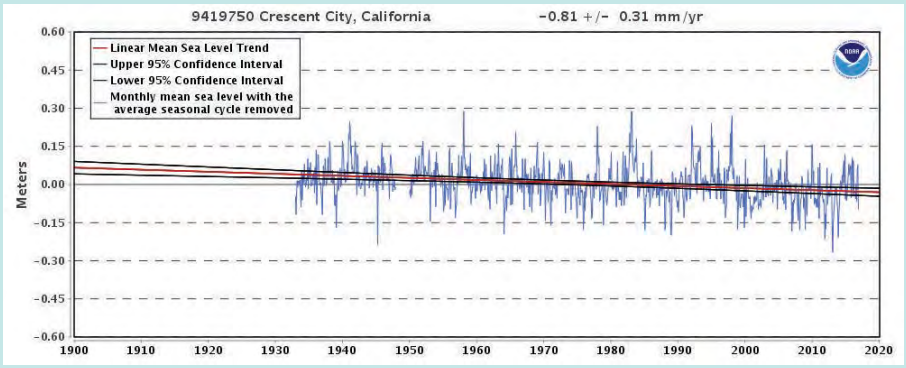

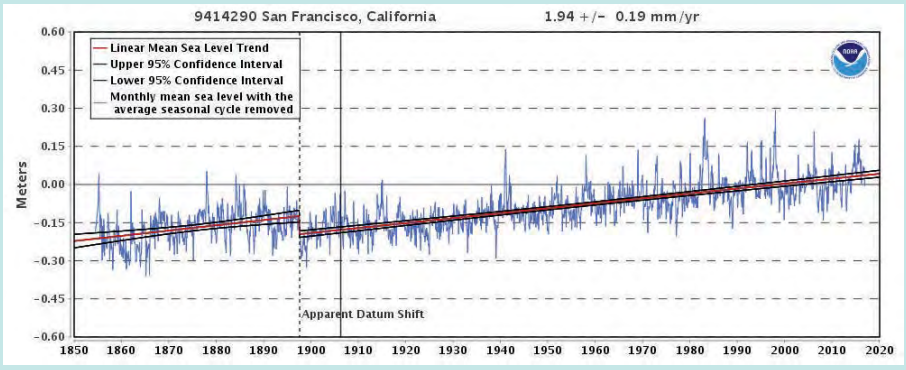

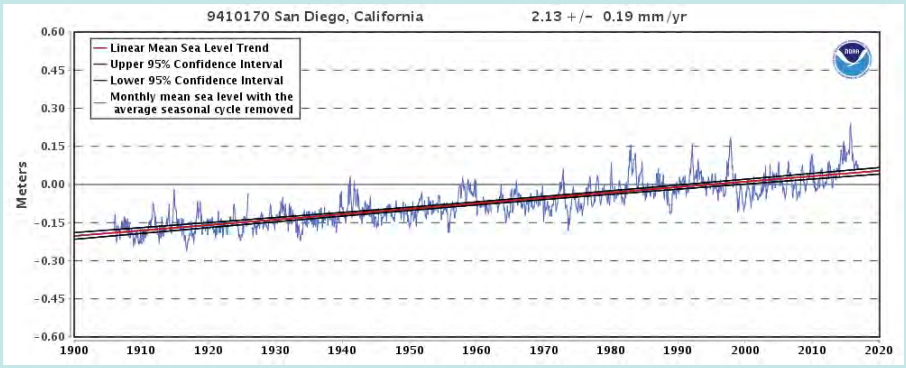

3.2. How much sea-level rise will California experience?

Using the methodology of Kopp et al. (2014), we provide projections of sea-level rise that are based on the data from tide gauges in Crescent City, San Francisco and La Jolla (Figure 3, Table 1). As described above (Section 3.1.1), these projections may underestimate the probability of extreme Antarctic ice loss, an outcome that is highly uncertain but, given recent observations and model results, cannot be ignored. Accordingly, we have also included an extreme sea-level rise scenario, which we call the H++ scenario. This is an unknown probability, high consequence scenario such as would occur if high rates of Antarctic ice loss were to develop in the last half of this century. When decisions involve consequential infrastructure, facilities or assets, we advise that extra consideration be given to this upper end of potential sea-level rise outcomes.

We note that the differences in projections under different emissions scenarios before 2050 are minor. By comparison, after 2050, projections increasingly depend on greenhouse gas emissions. Accordingly, we present only projections for RCP 8.5 through 2050, and distinguish between emissions pathways for 2100 and 2150.

Figure 3: Projections of: (a) Global mean sea level, and; (b) Relative sea level in San Francisco, California.

Sea-level rise projections for RCP 8.5 and RCP 2.6 are calculated using the methodology of Kopp et al., 2014. The shaded areas bounded by the dashed lines denote the 5th and 95th percentiles. The H++ scenario corresponds to the Extreme scenario of Sweet et al. (2017) and represents a world consistent with rapid Antarctic ice sheet mass loss. Note that the behavior of the Antarctic ice sheet early in this century is governed by different processes than those which would drive rapid mass loss; although the world is not presently following the H++ scenario, this does not exclude the possibility of getting onto this path later in the century. The historical global mean sea level curve in (a) is from Hay et al. (2015).

(a) Global mean sea level

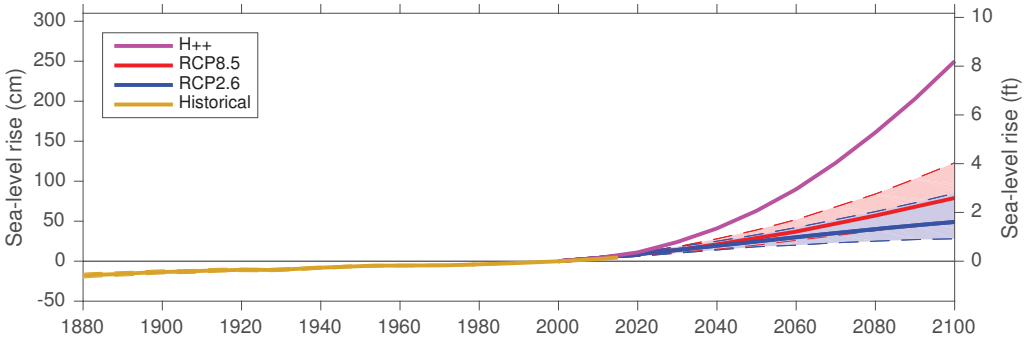

(b) Relative sea level in San Francisco, California

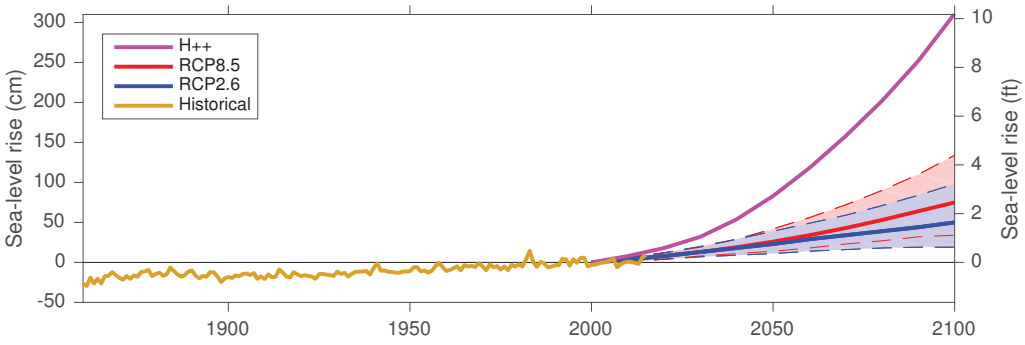

Table 1. Projected sea-level rise (measured in feet) for three tide gauge locations in California: (a) Crescent City (b) San Francisco, Golden Gate, and (c) La Jolla.

Projections are based on the methodology of Kopp et al., 2014 with the exception of the H++ scenario. The 'likely range' is consistent with the terms used by the IPCC meaning that it has about a 2-in-3 chance of containing the correct value. All values are with respect to a 1991-2009 baseline. The H++ scenario is a single scenario, not a probabilistic projection, and does not have an associated distribution in the same sense as the other projections; it is presented in the same column for ease of comparison.

(a) Crescent City

Feet above 1991-2009 mean	MEDIAN	LIKELY RANGE	1-IN-20 CHANCE	1-IN-200 CHANCE
Year / Percentile	*50% probability SLR meets or exceeds...*	*67% probability SLR is between...*	*5% probability SLR meets or exceeds...*	*0.5% probability SLR meets or exceeds...*
2030	0.1	0.0 — 0.3	0.4	0.5
2050	0.4	0.2 — 0.7	0.9	1.5
2100 (RCP 2.6)	0.7	0.1 — 1.5	2.3	4.8
2100 (RCP 4.5)	1.0	0.3 — 1.8	2.6	5.0
2100 (RCP 8.5)	1.5	0.7 — 2.5	3.4	5.9
2100 (H++)	9.3			
2150 (RCP 2.6)	1.0	0.0 — 2.4	4.2	9.6
2150 (RCP 4.5)	1.6	0.3 — 3.2	5.0	10.4
2150 (RCP 8.5)	2.6	1.3 — 4.4	6.2	11.6
2150 (H++)	21			

(b) San Francisco, Golden Gate

Feet above 1991-2009 mean	MEDIAN	LIKELY RANGE	1-IN-20 CHANCE	1-IN-200 CHANCE
Year / Percentile	*50% probability SLR meets or exceeds...*	*67% probability SLR is between...*	*5% probability SLR meets or exceeds...*	*0.5% probability SLR meets or exceeds...*
2030	0.4	0.3 — 0.5	0.6	0.8
2050	0.9	0.6 — 1.1	1.4	1.9
2100 (RCP 2.6)	1.6	1.0 — 2.4	3.2	5.7
2100 (RCP 4.5)	1.9	1.2 — 2.7	3.5	5.9
2100 (RCP 8.5)	2.5	1.6 — 3.4	4.4	6.9
2100 (H++)	10			
2150 (RCP 2.6)	2.4	1.3 — 3.8	5.5	11.0
2150 (RCP 4.5)	3.0	1.7 — 4.6	6.4	11.7
2150 (RCP 8.5)	4.1	2.8 — 5.8	7.7	13.0
2150 (H++)	22			

(c) La Jolla

Feet above 1991-2009 mean	MEDIAN	LIKELY RANGE	1-IN-20 CHANCE	1-IN-200 CHANCE
Year / Percentile	*50% probability SLR meets or exceeds...*	*67% probability SLR is between...*	*5% probability SLR meets or exceeds...*	*0.5% probability SLR meets or exceeds...*
2030	0.5	0.4 — 0.6	0.7	0.9
2050	0.9	0.7 — 1.2	1.4	2.0
2100 (RCP 2.6)	1.7	1.1 — 2.5	3.3	5.8
2100 (RCP 4.5)	2.0	1.3 — 2.8	3.6	6.0
2100 (RCP 8.5)	2.6	1.8 — 3.6	4.6	7.1
2100 (H++)	10			
2150 (RCP 2.6)	2.5	1.5 — 3.9	5.7	11.1
2150 (RCP 4.5)	3.1	1.9 — 4.8	6.5	11.8
2150 (RCP 8.5)	4.3	3.0 — 6.1	7.9	13.3
2150 (H++)	22			

3.3. How fast will sea levels rise?

We recognize that planning decisions are often informed by estimates of rates of sea-level rise and estimates of when a particular level of sea-level rise is projected to occur. Rates of sea-level rise provide important context for the time needed to plan and implement adaptation options. They are also an important consideration in evaluating when and where natural infrastructure is a feasible and prudent choice for helping to mitigate the effects of sea-level rise. In some locations, rates of sea-level rise may exceed the rate at which habitats (e.g., seagrass beds, coastal marshes) can migrate and adapt. It is also important to keep in mind that while these natural habitats may provide some buffer to future sea-level rise in estuarine environments (San Francisco Bay, for example), on the exposed, high-energy, open coast, there are very few locations where biological buffers or habitats exist to provide any significant reduction to the impacts of coastal flooding and erosion from future sea-level rise.

Employing the methodology of Kopp et al. (2014), and consistent with the projections above, we provide probabilistic estimates of the rates of sea-level rise at each of the three selected tide gauges: Crescent City, San Francisco and La Jolla (Table 2). We also provide tables of probabilities that sea-level rise will meet or exceed a given height for RCP 8.5 and RCP 2.6 at each of the three tide gauges (Tables 3, 4 and 5). Under the H++ scenario, with rapid ice-sheet loss in the Antarctic, average rates of sea-level rise in California would exceed 50 mm/year (2 inches/year) by the end of the century.

Table 2. Projected average rates (mm/year) of sea-level rise in: (a) Crescent City (b) San Francisco, and (c) La Jolla.

Projections are based on the methodology of Kopp et al., 2014 with the exception of the H++ scenario. For example, there is a 50% probability that sea-level rise rates in San Francisco between 2030-2050 will be at least 3.8 mm/year. The 'likely-range' is consistent with the terms used by the IPCC meaning that it has about a 2-in-3 chance of containing the correct value. The H++ scenario is a single scenario, not a probabilistic projection, and does not have an associated distribution in the same sense as the other projections; it is presented in the same column for ease of comparison.

(a) Crescent City

mm / yr	MEDIAN	LIKELY RANGE	1-IN-20 CHANCE	1-IN-200 CHANCE
Year / Percentile	*50% probability SLR meets or exceeds...*	*67% probability SLR is between...*	*5% probability SLR meets or exceeds...*	*0.5% probability SLR meets or exceeds...*
2010-2030	1.9	1.0 — 2.9	3.8	5.7
2030-2050 (RCP 2.6)	2.4	0.4 — 4.7	6.8	12
2030-2050 (RCP 4.5)	3.1	1.3 — 5.1	6.9	12
2030-2050 (RCP 8.5)	3.8	1.6 — 6.4	9	14
2030-2050 (H++)	23			
2080-2100 (RCP 2.6)	2.6	-0.2 — 6.4	11	25
2080-2100 (RCP 4.5)	3.9	0.7 — 8	12	26
2080-2100 (RCP 8.5)	8	3.4 — 13	19	34
2080-2100 (H++)	51			

(b) San Francisco, Golden Gate

mm / yr	MEDIAN	LIKELY RANGE	1-IN-20 CHANCE	1-IN-200 CHANCE
Year / Percentile	*50% probability SLR meets or exceeds...*	*67% probability SLR is between...*	*5% probability SLR meets or exceeds...*	*0.5% probability SLR meets or exceeds...*
2010-2030	4.7	3.8 — 5.7	6.5	8.4
2030-2050 (RCP 2.6)	5.1	3.1 — 7.4	9.6	15
2030-2050 (RCP 4.5)	5.8	4.2 — 7.7	9.5	14
2030-2050 (RCP 8.5)	6.7	4.5 — 9.3	12	17
2030-2050 (H++)	26			
2080-2100 (RCP 2.6)	5.2	2.3 — 9.1	14	28
2080-2100 (RCP 4.5)	6.5	3.1 — 11	15	29
2080-2100 (RCP 8.5)	11	6.0 — 16	22	37
2080-2100 (H++)	55			

(c) La Jolla

mm / yr	MEDIAN	LIKELY RANGE	1-IN-20 CHANCE	1-IN-200 CHANCE
Year / Percentile	*50% probability SLR meets or exceeds...*	*67% probability SLR is between...*	*5% probability SLR meets or exceeds...*	*0.5% probability SLR meets or exceeds...*
2010-2030	5.1	4.1 — 6.2	7.1	9.1
2030-2050 (RCP 2.6)	5.4	3.6 — 7.6	9.7	16
2030-2050 (RCP 4.5)	6.2	4.5 — 8.3	10.2	15
2030-2050 (RCP 8.5)	7.2	5.1 — 9.6	12	18
2030-2050 (H++)	26			
2080-2100 (RCP 2.6)	5.3	2.4 — 9.2	14	28
2080-2100 (RCP 4.5)	6.7	3.3 — 11	16	29
2080-2100 (RCP 8.5)	11	6.5 — 17	22	38
2080-2100 (H++)	54			

Table 3. Probability that sea-level rise at Crescent City will meet or exceed a particular height (feet) in a given year under: (a) RCP 8.5, and (b) RCP 2.6.

Estimates are based on Kopp et al., 2014. All heights are with respect to a 1991-2009 baseline; values refer to a 19-year average centered on the specified year. Grey shaded areas have less than a 0.1% probability of occurrence.

(a) RCP 8.5

	1 FT.	2 FT.	3 FT.	4 FT.	5 FT.	6 FT.	7 FT.	8 FT.	9 FT.	10 FT.
2020										
2030										
2040	0.3%									
2050	3%	0.1%								
2060	13%	1%	0.1%							
2070	31%	2%	0.4%	0.1%	0.1%					
2080	49%	8%	1%	0.4%	0.2%	0.1%				
2090	63%	17%	4%	1%	0.4%	0.2%	0.1%	0.1%		
2100	72%	30%	9%	3%	1%	1%	0.3%	0.2%	0.1%	0.1%
2150	90%	67%	40%	21%	11%	6%	3%	2%	1%	1%
2200	92%	81%	67%	51%	37%	26%	18%	13%	9%	6%

(b) RCP 2.6

	1 FT.	2 FT.	3 FT.	4 FT.	5 FT.	6 FT.	7 FT.	8 FT.	9 FT.	10 FT.
2020										
2030										
2040	0.3%									
2050	2%	0.1%								
2060	6%	0.3%	0.1%							
2070	13%	1%	0.2%	0.1%						
2080	20%	2%	1%	0.2%	0.1%	0.1%				
2090	28%	5%	1%	0.4%	0.2%	0.1%	0.1%			
2100	36%	8%	2%	1%	0.4%	0.2%	0.1%	0.1%	0.1%	
2150	52%	23%	11%	6%	3%	2%	1%	1%	1%	1%
2200	58%	39%	24%	16%	11%	7%	5%	4%	3%	2%

Table 4. Probability that sea-level rise at San Francisco, Golden Gate, will meet or exceed a particular height (feet) in a given year under: (a) RCP 8.5, and (b) RCP 2.6.

Estimates are based on Kopp et al., 2014. All heights are with respect to a 1991-2009 baseline; values refer to a 19-year average centered on the specified year. Grey shaded areas have less than a 0.1% probability of occurrence.

(a) RCP 8.5

	1 FT.	2 FT.	3 FT.	4 FT.	5 FT.	6 FT.	7 FT.	8 FT.	9 FT.	10 FT.
2020										
2030	0.1%									
2040	3.3%									
2050	31%	0.4%								
2060	65%	3%	0.2%	0.1%						
2070	84%	13%	1.2%	0.2%	0.1%					
2080	93%	34%	5%	0.9%	0.3%	0.1%	0.1%			
2090	96%	55%	14%	3%	0.9%	0.3%	0.2%	0.1%	0.1%	
2100	96%	70%	28%	8%	3%	1%	0.5%	0.3%	0.2%	0.1%
2150	100%	96%	79%	52%	28%	15%	8%	4%	3%	2%
2200	100%	97%	91%	80%	65%	50%	36%	25%	18%	13%

(b) RCP 2.6

	1 FT.	2 FT.	3 FT.	4 FT.	5 FT.	6 FT.	7 FT.	8 FT.	9 FT.	10 FT.
2020										
2030										
2040	3.1%									
2050	19%	0.3%								
2060	43%	1.4%	0.2%							
2070	62%	4%	0.6%	0.2%						
2080	74%	11%	2%	0.4%	0.2%	0.1%				
2090	80%	20%	3%	1.0%	0.4%	0.2%	0.1%	0.1%		
2100	84%	31%	7%	2%	0.8%	0.4%	0.2%	0.1%	0.1%	
2150	93%	62%	31%	14%	7%	4%	2%	2%	1%	1%
2200	93%	68%	42%	22%	12%	7%	5%	3%	2%	1%

Table 5. Probability that sea-level rise at La Jolla will meet or exceed a particular height (feet) in a given year under: (a) RCP 8.5, and (b) RCP 2.6.

Estimates are based on Kopp et al., 2014. All heights are with respect to a 1991-2009 baseline; values refer to a 19-year average centered on the specified year. Grey shaded areas have less than a 0.1% probability of occurrence.

(a) RCP 8.5

	1 FT.	2 FT.	3 FT.	4 FT.	5 FT.	6 FT.	7 FT.	8 FT.	9 FT.	10 FT.
2020										
2030	0.1%									
2040	5.5%									
2050	40%	0.5%								
2060	74%	4%	0.3%	0.1%						
2070	89%	17%	1.5%	0.3%	0.1%					
2080	95%	41%	6%	1.1%	0.3%	0.1%	0.1%			
2090	97%	62%	17%	4%	1.0%	0.4%	0.2%	0.1%	0.1%	
2100	98%	75%	33%	10%	3%	1%	0.5%	0.3%	0.2%	0.1%
2150	100%	97%	83%	58%	33%	17%	9%	5%	3%	2%
2200	100%	98%	93%	83%	70%	55%	40%	28%	20%	14%

(b) RCP 2.6

	1 FT.	2 FT.	3 FT.	4 FT.	5 FT.	6 FT.	7 FT.	8 FT.	9 FT.	10 FT.
2020										
2030										
2040	4.4%									
2050	25%	0.3%								
2060	52%	1.7%	0.2%							
2070	70%	6%	0.7%	0.2%						
2080	80%	14%	2%	0.4%	0.2%	0.1%				
2090	85%	24%	4%	1.1%	0.4%	0.2%	0.1%	0.1%		
2100	88%	36%	8%	2%	0.9%	0.4%	0.2%	0.1%	0.1%	
2150	96%	68%	35%	16%	8%	4%	3%	2%	1%	1%
2200	96%	72%	47%	26%	14%	8%	5%	3%	2%	2%

BOX 3

Sources of, and approach to, uncertainties

Depending on the time horizon being considered, different sources of uncertainty play smaller or larger roles in projections of sea-level rise [48]. For long-term changes (second half of this century and beyond), the choice of model and scenario of anthropogenic greenhouse gas emissions significantly affect the outcome. By comparison, for short- to mid-term projections (within the next two or three decades), variability in the Earth's climate system, which would exist even in the absence of human-driven changes, is the predominant source of uncertainty.

Emissions scenarios

Emissions of the last decade position us along the highest scenario considered by the last IPCC report, RCP 8.5, and greenhouse gas emissions will continue through this century. However, exactly how large emissions will be depends on policy and societal choices, as well as technological progress, at local to global scales. Greenhouse gas emissions scenarios, which serve as inputs into climate models, are not predictions but rather the outcomes of a set of internally consistent assumptions about the evolution of population, GDP, technology, and, in some cases, mitigation policies. As such, the scientific community that develops and uses them has generally resisted attaching relative likelihoods to different scenarios, and future climate change projections are usually provided specific to - and conditional upon - a given scenario, as is the case in this report.

Model uncertainty

The uncertainty in model projections stems from the unavoidable approximations involved in the modeling of complex and interacting processes of the Earth system: any type of process model needs to adopt a grid resolution, and choose which processes to either represent explicitly, approximate through parameter selection, or not include at all [49]. These choices introduce unavoidable imprecision in the representation of the real world by any model, and differences among any ensemble of models. The diversity of existing models, each of which relies on a defensible set of parameter choices and computational approaches, translates into differences and uncertainties in sea-level rise projections.

In this report we adopt an approach (that of Kopp et al., 2014) in which model uncertainties are quantified for thermal expansion of seawater, ocean dynamics, and glaciers. These are the model components that are derived (directly for thermal expansion and ocean dynamics, and indirectly via a surface mass-balance model for glaciers) from climate model simulations. For these types of models, a large multi-model ensemble is available [50] that is used to calibrate the probability distributions in the model. By comparison, there is not yet an equivalent model ensemble that would enable us to develop probabilities of other sources of sea-level rise, including ice loss from ice sheets. As a result, we are forced to make approximations or use single-model estimates. In the case of the Antarctic or Greenland Ice Sheets, recent scientific advances reveal deep uncertainties, with different modeling approaches changing our understanding and projections (see also Appendix 2). Even with additional observations, it will not be straightforward to characterize model structural dependencies, limitations, and uncertainties, hence the need for a special treatment of the ice-sheet component in sea-level rise projections (see further below).

Variability in the Earth system

Natural variability in the Earth's climate system occurs alongside variability caused by anthropogenic influences. Variability in the Earth's system occurs on daily to centennial timescales and affects both mean water levels and the amplitude of extreme

BOX 3

storm surges. Long-term tide gauge records give us observational data to use in validating models of sea-level rise.

Statistical models of decadal amplitude changes (driven by natural modes of variability in the ocean, like ENSO or other oscillations) and of storm surges (driven by short-term weather phenomena, like storms) can be estimated on the basis of observed or modeled records, thus isolating these components from mean sea level changes and - when needed - superimposing them on projected mean sea-level rise [51]. The underlying assumption here is that the interplay of the two sources of variability is additive rather than non-linear. We note that locations may be identified where changes in mean sea level can indeed affect the size of surges, in which case ad-hoc process models of storm surges driven by scenarios of sea-level rise can be deployed.

As for climate system drivers at large (e.g., ENSO, storms), the question boils down to assessing possible future changes and their statistical characteristics. At the moment, uncertainties in modeling outcomes are large and there is not robust evidence that the internal variability of these phenomena will change significantly under future scenarios [52]. As mentioned, the interplay of these different sources of uncertainty is not unique as we move from short- to mid- to long-term horizons for our projections. Estimated probabilities of particular outcomes are increasingly less robust -- in the sense of comprehensively covering the range of expected outcomes and firmly quantifying their relative probability -- as we lengthen those horizons, and we move into climate scenarios of unprecedented nature as far as anthropogenic forcing is concerned.

Accounting for uncertainty

For projections over the next few decades, we do not expect the role of models and scenarios to be as crucial to pin down. However, as we move into the more distant future, our ability to guess what society will do diminishes, different models will be more or less dependable, and the processes generating our extreme scenario will unfold. As a result, our ability to quantify uncertainty through formal probability distributions decreases. We therefore include a qualitatively different scenario (H++) whose likelihood we cannot characterize at this time, and note that quantified probabilistic projections need to be taken as an evolving representation of our understanding, open to updates and modifications especially in the tails of probability distributions. In this context of likely continued and unquantifiable uncertainties, incorporating long-range planning for sea-level rise in decisions is increasingly urgent.

3.4. How do these projections compare with other regional and national projections?

Figure 4. Projections of sea level rise in California and U.S. national reports and assessments of the last decade.

Projections are provided for 2100 according to the approach described in each report. The different approaches reflect the evolution of modeling techniques to project sea-level rise including new approaches to provide greater geographic resolution in projections and probabilistic projections, as well as the different intended purposes of the assessments (i.e., state and national). In brief, the figure depicts: CA 1st, 2nd, 3rd Assessments: range of projections for South Cape Mendocino, NOAA 2012 – range of projections of global mean sea level rise, NRC 2012 – range of projections for South Cape Mendocino, IPCC 2013 – projections of global mean sea-level rise under RCP2.6 and RCP 8.5, NOAA 2017 – range projections for U.S. sea level rise, California 4th Assessment – 5th-95th percentile probabilistic projections for San Francisco under RCP 4.5 and RCP 8.5, California Science Update (this report) – 5th -95th percentile for San Francisco using the Kopp et al., 2014 framework and H++ scenario from NOAA 2017.

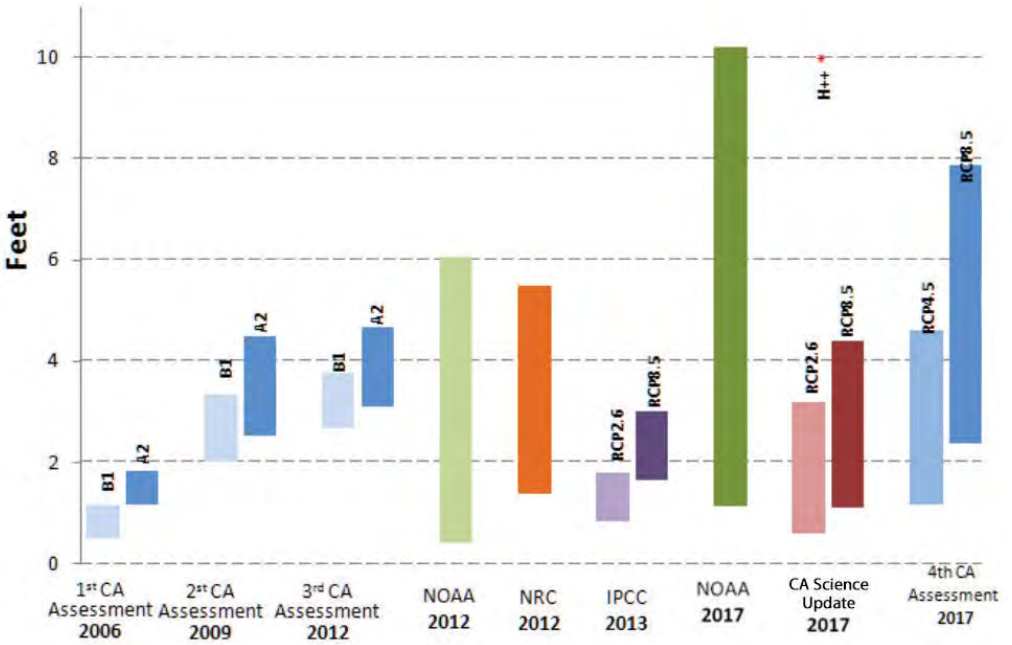

Over the last decade, projections of sea-level change in California have evolved considerably (Figure 4).

The common threads across these evolving projections are the recognition that the magnitude and timing of future sea-level rise is uncertain, and that emissions in the near- and mid-term 21st century will have long-lasting consequences that will become increasingly clear in the decades after 2050.

In particular, the magnitudes of estimated sea-level rise have grown, especially at the upper, low probability "tail" of ranges that have been estimated. For example, sea-level rise projections for 2100 in the California 1st Climate Change Assessment (conducted in 2006) ranged from 6 - 22 inches (15 - 56 cm) above a year 2000 starting point. By comparison, the recently released estimates of the California 4th Climate Change Assessment (California 4th Assessment) range from 14 - 94 inches (36 cm - 239 cm) with an additional very low probability worst-case estimate that exceeds 9 feet (274 m).

The sea-level scenarios presented in the California 4th Assessment present a range of scenarios whose mid-to-upper level is higher than that provided in the 2012 National Research Council Report, and much higher than that published in the 4th IPCC Report. At the same time, the high end of the California 4th Assessment range is approximately comparable to that recently provided by the 2017 USGCRP Sea Level Rise and Coastal Flood Hazard Scenarios and Tools Interagency Task Force led by NOAA, as well as the 99.9th percentile of Kopp et al. (2014)'s projections.

The strongest driver of this shift toward higher distributions of possible future sea levels is the possibility of high rates of ice loss from the West Antarctic Ice Sheet under scenarios of continued increases in greenhouse gas emissions. The California 4th Assessment includes recent estimates by DeConto and Pollard (2016) of Antarctic Ice Sheet losses from a model that introduces new physical processes that invoke high rates of ice discharge into the Antarctic Ocean. The Working Group's assessment for the purposes of developing updated sea-level rise projections for California was that the DeConto and Pollard (2016) results are compelling enough to include an extreme SLR scenario (called the H++ scenario), based on the highest scenario developed by Sweet et al. (2017). However, since these results are very fresh, and the processes are not yet actually observed in Antarctica, they await further modeling and observational evidence. Consequently, we rely upon the earlier model presented in Kopp et al. (2014) for the emissions scenario-dependent probabilistic projections presented in this report.

BOX 4

Integrating Sea-Level Rise with Coastal Storm and Wave Impacts

There are several different sea-level rise visualization tools available; the NOAA Sea Level Rise Viewer and Climate Central's Surging Seas are the two most commonly used examples. These allow a user to develop an inundation map for virtually any coastal area in California that will project a range of future sea levels onto the specific area of concern or interest. These viewers have been referred to as a "bathtub approach" simply because, while they use accurate elevation and tide data, inundation is determined by uniformly raising water levels by various selected future sea level values in combination with the average daily high tide. This passive approach is a reasonable approximation of the future everyday impacts of sea-level rise. However, it does not consider potential flooding driven by the dynamic processes that affect coastal water levels daily (e.g., tidal variability, waves), seasonally (e.g., elevated water levels during El Niño events) or during storm events (e.g., storm surge, wave run-up, and river discharge) and the hydrodynamic complexity associated with bathymetry, built structures and the natural coastline configuration.

The Coastal Storm Modeling System (CoSMoS)[vi] is a dynamic modeling approach that has been developed by the United States Geological Survey in order to allow more detailed predictions of coastal flooding due to both future sea-level rise and storms integrated with long-term coastal evolution (i.e., beach changes and cliff/bluff retreat) over large geographic areas. This model simulates a reasonable range of plausible 21st century sea-level rise and storm scenarios to provide coastal planners and decision makers with more accurate information than sea-level rise alone in order to predict areas of coastal flooding and impacts. The model incorporates wave projections, tides and regional atmospheric forcing to generate sea and surge levels that can then be dynamically downscaled to depict local changes. CoSMoS has now been applied to most of the urbanized California coast (e.g., Southern California and the San Francisco Bay Area) and will soon cover the state's shoreline. Considerable opportunity exists to align the methodology for deriving sea-level rise projections in this science summary with the underlying model in CoSMoS. Doing so will not only return the greatest value on existing investments but also set the stage for efficiently incorporating updated projections into decisions as scientific understanding increases and as sea levels change.

[vi] https://walrus.wr.usgs.gov/coastal_processes/cosmos/index.html

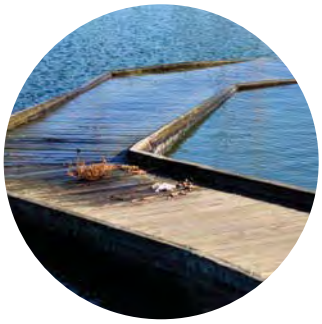

4. Conclusions

4.1. Rapidly evolving scientific understanding

Increasing the reliability of future sea-level projections will be important in decision-making for both existing and proposed development and infrastructure. This is a tractable problem, but it will require concerted action on two fronts. First, it will require improved scientific understanding of mass-loss processes from the vast polar ice sheets across all the relevant spatial and temporal scales. This can only be achieved through continued and new observations from satellites and the field (both on the ice and in the surrounding atmosphere and ocean), combined with modeling to investigate key processes such as ice-ocean interactions, surface melting, and fracture mechanics of ice. This will require substantial international and interagency investment to support collaborations across the disciplines of glaciology, meteorology, oceanography, and computational science. Second, it will require tighter integration between the scientific and decision-making communities such that feedbacks from the latter can inform, via recursive process of scientific analysis and stakeholder deliberations [53,54], future sea-level rise studies and projections.

Advances in our understanding of global, regional, and local sea-level rise are already occurring and substantial advances are expected within the next decade. In the meantime, research currently underway and expected in the next one to five years includes improved understanding of the warming thresholds capable of driving substantial retreat in the West Antarctic Ice Sheet. Given these expected rapid developments, the approach taken here allows for relatively frequent updates of location-specific sea-level rise projections. Updating of the science underpinning California's statewide guidance will be important as our understanding of these ice-

sheet contributions to sea-level rise increases, and/or the range of likely future emissions scenarios begins to narrow. In addition, the explicit consideration of an extreme H++ scenario of indeterminate probability flags for decision-makers the potential for extreme outcomes. Based on some modeling studies the possibility of such extreme sea-level rise is now supported and may come to be viewed as either more or less likely as scientific understanding evolves.

4.2. Informing near-term decisions

These projections of future sea level and changing coastal hazards can and should be used along with a comprehensive assessment of what is at risk (i.e., exposed to future coastal hazards) and what is at stake (i.e., the monetized and non-monetary values attached to what is exposed) to weigh the different types of costs, and potential losses and benefits of taking action now to prevent future harm against the wide-ranging risks of inaction [55].

However, doing so will require the development of decision-support systems that help California decision-makers and stakeholders to decompose what will be complex, uncertain, and inter-temporal decisions into more manageable parts. Various approaches are available for decision analysis and decision-making under uncertainty that aim to go beyond economic efficiency in determining the best possible way forward in the face of multiple objectives and criteria for making difficult choices [55,56]. At their core, these approaches help stakeholders and decision-makers to identify, define, and bound management problems and opportunities; they help these same groups to identify, characterize, and operationalize a shared set of objectives to guide management choices; these approaches emphasize the importance of characterizing the anticipated consequences, based on scientific assessments, of a broad array of different development and management alternatives; and they support the need for tradeoffs when objectives across alternatives inevitably conflict [57–59].

These decision-support approaches, together with numerous studies on the cost of inaction, generally suggest that uncertainty about the exact amount of future sea-level rise should not be a deterrent to taking action now [60–62]. Adaptation and hazard mitigation decisions and investments in the near-term can prevent much greater losses (many times the initial cost) than would incur if such action were not taken (e.g., [63,64]).

The forthcoming, updated sea-level rise policy guidance will thus provide a decision-centric approach to using sea-level rise projections that is informed by a clear understanding of the decision-makers and the decision contexts. It will guide decision-makers through a systematic and defensible process that assists them in framing and structuring the decisions at hand, explicitly laying out objectives and decision criteria, laying out distinct solution options and assessing them in the context of sea-level rise projections and key uncertainties, directly confronting trade-offs, and setting up an adaptive management process going forward [56,65]. In addition, providing recommendations for how to effectively communicate sea-level rise risks and meaningfully engage stakeholders in these challenging planning and decision processes can make the use of uncertain sea-level rise projections in decision making easier and ultimately lead to decisions that reflect decision-makers' risk tolerances and desired outcomes.

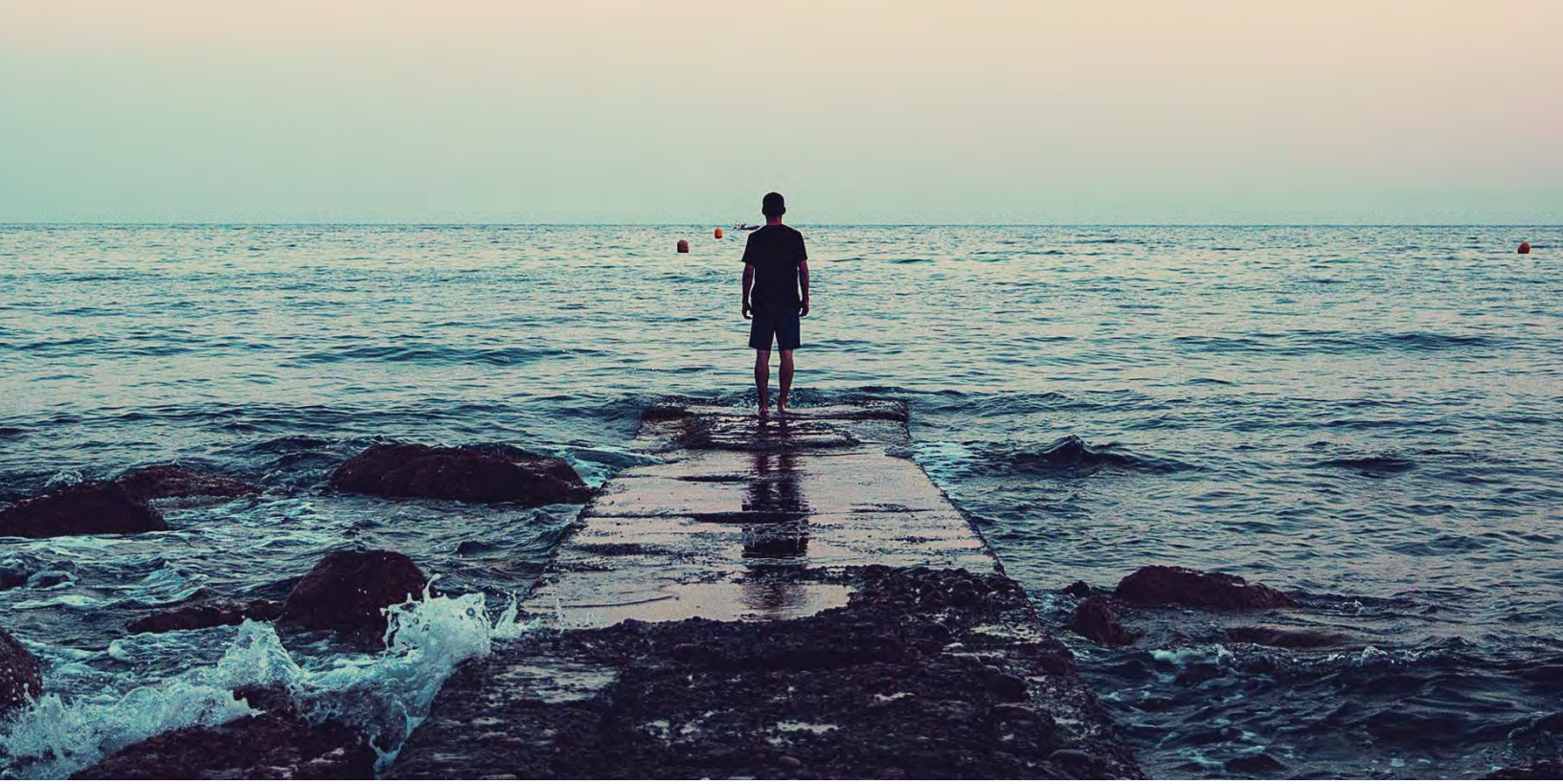

5. References

1. Griggs GB. Introduction to California's beaches and coast. University of California Press. 2010.
2. Kildow J, Colgan C, Scorse J, Johnston P, Nichols M. State of the U.S. Ocean and Coastal Economies 2014. 2014.
3. IPCC. Climate Change 2007: Synthesis Report. Contribution of Working Groups I, II and III to the Fourth Assessment Report of the Intergovernmental Panel on Climate Change [Core Writing Team, Pachauri, R.K and Reisinger, A. (eds.)]. Geneva, Switzerland. 2007.
4. National Research Council. Sea-Level Rise for the Coasts of California, Oregon, and Washington. Washington, D.C.: National Academies Press. 2012.
5. IPCC. Climate Change 2014: Synthesis Report. Contribution of Working Groups I, II and III to the Fifth Assessment Report of the Intergovernmental Panel on Climate Change [Core Writing Team, R.K. Pachauri and L.A. Meyer (eds.)]. Geneva, Switzerland. 2014.
6. Kopp RE, Horton RM, Little CM, Mitrovica JX, Oppenheimer M, Rasmussen DJ, et al. Probabilistic 21st and 22nd century sea-level projections at a global network of tide-gauge sites. Earth's Future. 2014; 2:383–406.
7. New York City Panel on Climate Change. Climate Risk Information 2013: Observations, Climate Change Projections, and Maps. C. Rosenzweig and W. Solecki (Editors). New York, New York. 2013.
8. Thompson PR, Hamlington BD, Landerer FW, Adhikari S. Are long tide gauge records in the wrong place to measure global mean sea level rise? Geophys Res Lett. 2016; 43:10,403-10,411.
9. Hay CC, Morrow E, Kopp RE, Mitrovica JX. Probabilistic reanalysis of twentieth-century sea-level rise. Nature. 2015; 517:481–4.
10. Church, J.A., P.U. Clark, A. Cazenave, J.M. Gregory, S. Jevrejeva, A. Levermann, M.A. Merrifield, G.A. Milne, R.S. Nerem, P.D. Nunn, A.J. Payne, W.T. Pfeffer DS and ASU. Sea Level Change. In: Stocker, T.F., D. Qin, G.-K. Plattner, M. Tignor, S.K. Allen, J. Boschung, A. Nauels, Y. Xia, VB (Editors). Climate Change 2013: The Physical Science Basis Contribution of Working Group I to the Fifth Assessment Report of the Intergovernmental Panel on Climate Change. Cambridge University Press, Cambridge, United Kingdom and New York, NY, USA. 2013.

11. Ray RD, Douglas BC. Experiments in reconstructing twentieth-century sea levels. Prog. Oceanogr. 2011; 91:496–515.

12. Church JA, White NJ. Sea-Level Rise from the Late 19th to the Early 21st Century. Surv Geophys. 2011; 32:585–602.

13. Leuliette E, Nerem S. Contributions of Greenland and Antarctica to Global and Regional Sea Level Change. Oceanography. 2016; 29:154–159.

14. Kopp RE, Kemp AC, Bittermann K, Horton BP, Donnelly JP, Gehrels WR, et al. Temperature-driven global sea-level variability in the Common Era. Proc Natl Acad Sci. 2016; 113:E1434-41.

15. Reager JT, Gardner AS, Famiglietti JS, Wiese DN, Eicker A, Lo M-H. A decade of sea level rise slowed by climate-driven hydrology. Science. 2016; 351.

16. Mitrovica JX, Gomez N, Morrow E, Hay C, Latychev K, Tamisiea ME. On the robustness of predictions of sea level fingerprints. Geophys J Int. 2011; 187:729–742.

17. Kopp RE, Hay CC, Little CM, Mitrovica JX. Geographic Variability of Sea-Level Change. Curr Clim Chang Reports. 2015; 1:192–204.

18. Sella GF, Stein S, Dixon TH, Craymer M, James TS, Mazzotti S, et al. Observation of glacial isostatic adjustment in "stable" North America with GPS. Geophys Res Lett. 2007; 34:L02306.

19. Peltier WR. Globsl Glacial Isostacy and the Surface of the Ice-Age Earth: The ICE-5G (VM2) Model and GRACE. Annu Rev Earth Planet Sci. 2004; 32:111–149.

20. Joughin I, Smith BE, Medley B. Marine Ice Sheet Collapse Potentially Under Way for the Thwaites Glacier Basin, West Antarctica. Science. 2014; 344.

21. Mouginot J, Rignot E, Scheuchl B. Sustained increase in ice discharge from the Amundsen Sea Embayment, West Antarctica, from 1973 to 2013. Geophys Res Lett. 2014; 41:1576–1584.

22. Paolo FS, Fricker HA, Padman L. Volume loss from Antarctic ice shelves is accelerating. Science. 2015; 348.

23. Trenberth KE, Fasullo JT, Balmaseda MA, Trenberth KE, Fasullo JT, Balmaseda MA. Earth's Energy Imbalance. J Clim. 2014; 27:3129–3144.

24. Roemmich D, Church J, Gilson J, Monselesan D, Sutton P, Wijffels S. Unabated planetary warming and its ocean structure since 2006. Nat Clim Chang. 2015; 5:240–245.

25. Bamber JL, Griggs JA, Hurkmans RTWL, Dowdeswell JA, Gogineni SP, Howat I, et al. A new bed elevation dataset for Greenland. Cryosph. 2013; 7:499–510.

26. Fretwell P, Pritchard HD, Vaughan DG, Bamber JL, Barrand NE, Bell R, et al. Bedmap2: improved ice bed, surface and thickness datasets for Antarctica. Cryosph. 2013; 7:375–393.

27. Dutton A, Carlson AE, Long AJ, Milne GA, Clark PU, DeConto R, et al. Sea-level rise due to polar ice-sheet mass loss during past warm periods. Science. 2015; 349:aaa4019.

28. DeConto RM, Pollard D. Contribution of Antarctica to past and future sea-level rise. Nature. 2016; 531:591–597.

29. Storlazzi CD, Griggs GB. Influence of El Nino-Southern Oscillation (ENSO) events on the evolution of central California's shoreline. Geol Soc Am Bull. Geological Society of America. 2000; 112:236–249.

30. Cai W, Borlace S, Lengaigne M, van Rensch P, Collins M, Vecchi G, et al. Increasing frequency of extreme El Nino events due to greenhouse warming. Nat Clim Chang. 2014; 4:111–116.

31. Bromirski PD, Flick RE, Miller AJ. Storm surge along the Pacific coast of North America. J Geophys Res Ocean. 2017; 122:441–457.

32. Moss RH, Edmonds JA, Hibbard KA, Manning MR, Rose SK, van Vuuren DP, et al. The next generation of scenarios for climate change research and assessment. Nature. 2010; 463:747–756.

33. van Vuuren DP, Stehfest E, den Elzen MGJ, Kram T, van Vliet J, Deetman S, et al. RCP2.6: exploring the possibility to keep global mean temperature increase below 2°C. Clim Change. 2011; 109:95–116.

34. Parris, A., P. Bromirski, V. Burkett, D. Cayan, M. Culver, J. Hall, R. Horton, K. Knuuti, R. Moss, J. Obeysekera, A. Sallenger. Global Sea Level Rise Scenarios for the US National Climate Assessment. 2012.

35. Bamber JL, Aspinall WP. An expert judgement assessment of future sea level rise from the ice sheets. Nat Clim Chang. 2013; 3:424–427.

36. Houser T. Economic risks of climate change: an American prospectus. Columbia University Press. 2015.

37. Congressional Budget Office. Potential Increases in Hurricane Damage in the United States: Implications for the Federal Budget. 2016.

38. Kopp, R.E., A. Broccoli, B. Horton, D. Kreeger, R. Leichenko, J.A. Miller, J.K. Miller, P. Orton, A. Parris, D. Robinson, C.P.Weaver, M. Campo, M. Kaplan, M. Buchanan, J. Herb LA and CA. Assessing New Jersey's Exposure to Sea-Level Rise and Coastal Storms: Report of the New Jersey Climate Adaptation Alliance Science and Technical Advisory Panel. New Brunswick, New Jersey. 2016.

39. Petersen, S., Bell, J., Miller, I., Jayne, C., Dean, K., Fougerat M. Climate Change Preparedness Plan for the North Olympic Peninsula. A Project of the North Olympic Peninsula Resource Conservation & Development Council and the Washington Department of Commerce, funded by the Environmental Protection Agency. 2015.

40. Miller, I, Petersen, S, Pucci, D, Clark, L, Wood B. Sea Level Rise and Coastal Flood Risk Assessment: Island County, Washington. 2016.

41. Jevrejeva S, Jackson LP, Riva REM, Grinsted A, Moore JC. Coastal sea level rise with warming above 2 °C. Proc Natl Acad Sci. 2016; 113:13342–13347.

42. Jevrejeva S, Grinsted A, Moore JC. Upper limit for sea level projections by 2100. Environ Res Lett. 2014; 9:104008.

43. Douglas, E, Kirshen, P, Hannigan, R, Herst, R, Palardy A. Climate Ready Boston: Climate Change and Sea-Level Rise Projections for Boston. 2016.

44. Cayan, DR, Kalansky, J, Iacobellis, S, Pierce D. Creating Probabalistic Sea Level Rise Projections to support the 4th California Climate Assessment. La Jolla, California. 2016.

45. Sweet, W.V., R.E. Kopp, C.P. Weaver, J. Obeysekera, R.M. Horton, E.R. Thieler and CZ. Global and Regional Sea Level Rise Scenarios for the United States. 2017.

46. Hunter J. A simple technique for estimating an allowance for uncertain sea-level rise. Clim Change. 2012; 113:239–252.

47. Buchanan MK, Kopp RE, Oppenheimer M, Tebaldi C. Allowances for evolving coastal flood risk under uncertain local sea-level rise. Clim Change. 2016; 137:347–362.

48. Hawkins E, Sutton R, Hawkins E, Sutton R. The Potential to Narrow Uncertainty in Regional Climate Predictions. Bull Am Meteorol Soc. 2009; 90:1095–1107.

49. Knutti R. Should we believe model predictions of future climate change? Philos Trans R Soc London A. 2008; 366.

50. Taylor KE, Stouffer RJ, Meehl GA, Taylor KE, Stouffer RJ, Meehl GA. An Overview of CMIP5 and the Experiment Design. Bull Am Meteorol Soc. 2012; 93:485–498.

51. Tebaldi C, Strauss BH, Zervas CE. Modelling sea level rise impacts on storm surges along US coasts. Environ Res Lett. 2012; 7:14032.

52. Christensen, J.H., K. Krishna Kumar, E. Aldrian, S.-I. An, I.F.A. Cavalcanti, M. de Castro, W. Dong, P. Goswami, A. Hall, J.K. Kanyanga, A. Kitoh, J. Kossin, N.-C. Lau, J. Renwick, D.B. Stephenson S-PX and TZ. Climate Phenomena and their Relevance for Future Regional Climate Change. Climate Change 2013: The Physical Science Basis Contribution of Working Group I to the Fifth Assessment Report of the Intergovernmental Panel on Climate Change. Cambridge, United Kingdom and New York, NY, USA: Cambridge University Press. 2013.

53. Arvai, J, Rivers L. Effective Risk Communication: Learning from the Past, Charting a Course for the Future. Taylor & Francis, London, UK. 2013.

54. National Research Council. Understanding Risk: Informing Decisions in a Democratic Society. Washington, D.C.: National Academy Press. 1996.

55. Chambwera, M., G. Heal, C. Dubeux, S. Hallegatte, L. Leclerc, A. Markandya, B.A. McCarl, R. Mechler A, Neumann JE. Economics of adaptation. In: Field, C.B., V.R. Barros, D.J. Dokken KJM, M.D. Mastrandrea, T.E. Bilir, M. Chatterjee, K.L. Ebi, Y.O. Estrada, R.C. Genova, B. Girma, E.S. Kissel ANL, S. MacCracken, P.R. Mastrandrea (Editors). Climate Change 2014: Impacts, Adaptation, and Vulnerability Part A: Global and Sectoral Aspects Contribution of Working Group II to the Fifth Assessment Report of the Intergovernmental Panel on Climate Change. Cambridge, United Kingdom and New York, NY, USA: Cambridge University Press. 2014. pp. 945–977.

56. Arvai J, Bridge G, Dolsak N, Franzese R, Koontz T, Luginbuhl A, et al. Adaptive Management of the Global Climate Problem: Bridging the Gap Between Climate Research and Climate Policy. Clim Change. 2006; 78:217–225.

57. Bessette DL, Campbell-Arvai V, Arvai J. Expanding the Reach of Participatory Risk Management: Testing an Online Decision-Aiding Framework for Informing Internally Consistent Choices. Risk Anal. 2016; 36:992–1005.

58. Arvai J. An appeal for smarter decisions. Policy Options. 2014; 35:40–43.

59. Arvai, J., Campbell-Arvai V. Risk communication: Insights from the decision sciences. In: Arvai, J., Rivers L, editor. Effective Risk Communication: Learning from the Past, Charting a Course for the Future. Taylor & Francis, London, UK. 2013. pp.234–257.

60. Lu Q-C, Peng Z-R, Du R. Economic Analysis of Impacts of Sea Level Rise and Adaptation Strategies in Transportation. Transportation Research Board of the National Academies. 2012; 2273:54–61.

61. Lin BB, Khoo YB, Inman M, Wang C-H, Tapsuwan S, Wang X. Assessing inundation damage and timing of adaptation: sea level rise and the complexities of land use in coastal communities. Mitig Adapt Strateg Glob Chang. 2014; 19:551–568.

62. Moser, S. C., M. A. Davidson, P. Kirshen, P. Mulvaney, J. F. Murley, J. E. Neumann, L. Petes and DR. Ch. 25: Coastal Zone Development and Ecosystems. In: Climate Change Impacts in the United States: The Third National Climate Assessment,. Washington, DC: U.S. Global Change Research Program. 2014. pp.579–618.

63. Neumann J, Hudgens D, Herter J, Martinich J. The economics of adaptation along developed coastlines. Wiley Interdiscip Rev Clim Chang. John Wiley & Sons, Inc. 2011; 2:89–98.

64. Multihazard Mitigation Council. Natural Hazard Mitigation Saves: An Independent Study to Assess the Future Savings From Mitigation Activities. Volume 2 - Study Documentation. Washington, D.C. 2005.

65. Gregory R, Ohlson D, Arvai J. Deconstructing Adaptive Management: Criteria for Applications to Environmental Management. Ecol Appl. 2006; 16:2411–2425.

Photo Credits

COVER: © Adam Sofen

PAGES 3-4: © Greg Becker

PAGE 6: © Chris Martin *(circle)*

PAGE 12: © Jay Ruzesky *(top)*

PAGE 33: © Thierry Meier *(bottom circle)*

PAGE 37: © Ant Rozetsky *(middle circle)*

PAGE 37: © Ishan Gupta *(bottom circle)*

PAGE 38: © Tom Hilton *(circle)*

PAGE 38: © Chris Leipelt *(top)*

PAGE 40: © Joshua Earle *(top)*

Appendix 1

Questions from the Policy Advisory Committee to the OPC-SAT Working Group

The questions below were developed by the State Sea-Level Rise Policy Advisory Committee. The intention of the questions is to elicit information about the current estimates of sea level rise for the California coast and how to understand the scientific context around those estimates, including the state of the science (e.g., areas of uncertainty, emerging science), the importance of each contributor to sea level rise, and sensitivity of the estimates to policy actions.

Following each question we provide a reference to the associated section of the document where the question is addressed and answered.

Estimates of Sea-level Rise

1. What is the current range of estimates of sea level rise for the California coast? *(Section 3)*

- **a.** What probabilities can be assigned to those estimates given the current state of science? *(Section 3.1)*
- **b.** Should more weight be given to certain parts of the range, and if so, why? *(Section 3.2)*

2. Across the physically plausible range of sea-level rise projections, is it possible to say which scenario(s) are more likely than others? *(Section 3.1.2)*

- **a.** What progress has been made since the existing State Sea-level Rise Guidance Document was published in 2013 on assigning probabilities to different emissions, warming and sea-level rise scenarios? *(Section 3.1.2)*
- **b.** Which contributors to sea-level rise (e.g., thermal expansion, ice loss) are currently included in developing probabilistic sea-level rise scenarios? *(Section 3.1.2)*
- **c.** What is the OPC-SAT Working Group's recommendation on how to estimate the likelihood of certain amounts of sea-level rise occurring at future dates for a given global emissions scenario? *(Section 3.1.2)*
- **d.** What other approaches is the OPC-SAT Working Group aware of, or could the Working Group recommend, for presenting uncertain sea-level rise projections? *(Section 3.1.2)*
- **e.** Is it possible to identify and characterize the degree of uncertainty in different contributors to sea-level rise? Where do the biggest uncertainties lie and what causes these uncertainties? *(Box 3)*

State of the Science

These questions are designed to elicit information on the state of sea-level rise science, including emerging issues and the treatment of ice loss in Antarctica.

3. What are the significant and notable emerging insights in sea-level rise science since the current State Sea-Level Rise Policy Guidance was issued? Why do they warrant attention? *(Section 2.2)*

- **a.** Have there been any notable changes in understanding how thermal expansion of ocean water contributes to sea-level rise? *(Section 2.1.1 and Section 2.2)*
- **b.** Have there been any notable changes in understanding of the role of ice loss from inland glaciers and major ice sheets? *(Section 2.1 and 2.2)*

   c. Have there been any notable changes in understanding of steric or dynamic ocean current changes that affect regional sea-level rise projections? *(Section 3.1.2)*

   d. Have there been any notable changes in understanding of local or regional land movement that could affect projections of relative sea level change? *(Section 2.2)*

4. Does the OPC-SAT Working Group consider the emerging science important and significant enough to warrant consideration in the current update to the State Sea-level Rise Guidance Document? If yes, why? If no, why? Please comment on the current confidence in new scientific insights or advances. *(Section 2.2, Section 3.1.1, Appendix 2)*

5. Existing models, including Kopp et al. (2014) and Cayan et al. (2016), project very different sea-level rise estimates under different emissions scenarios. However, some scientists suggest that sea levels in 2100 are determined by events in Antarctica, regardless of future GHG emission levels and trajectories. What is your scientific opinion about this issue? *(Section 2.1, Section 3.2)*

6. What are the scientific advances in best approaches to project sea-level rise since the publication of the existing State Sea-level Rise Guidance Document (2013)? What makes some modeling approaches better than others; in what way? *(Section 3.1)*

   a. What are the strengths and weaknesses of the different approaches for projecting global sea-level rise? *(Section 3.1)*

   b. Which approach or combination of approaches would the OPC-SAT Working Group recommend for estimating future global sea levels? *(Section 3.1.2)*

7. What are the best/most reliable approaches for translating global projections into regional projections? *(Section 3.1.2)*

8. What are the factors that cause sea-level rise projections to differ among locations? *(Section 2.1.2, Box 2)*

9. How are these factors considered in regional projections? *(Section 3.1.2)*

10. Is the OPC-SAT Working Group aware of additional research/modeling efforts, etc., presently underway that should inform the update to the State Sea-level Rise Guidance Document? *(Section 4.1)*

   a. How soon does the OPC-SAT Working Group expect major breakthroughs in understanding of sea-level changes? What would constitute a major breakthrough? How might these breakthroughs affect sea-level rise projections? Given current uncertainties in scientific understanding, and the anticipated rate of accumulation of new knowledge or observations, can the Working Group provide a recommended frequency for reviewing the latest available science to update guidance for state and local decision-makers? *(Section 1.4, Section 4.1, Appendix 2)*

   b. Similarly, can the Working Group provide recommendations, from a scientific perspective, on how this science could be considered in a policy setting (e.g., establishing an appropriate frequency for policy updates, establishing a scientific body to provide regular updates)? *(Section 1.4)*

Understanding the Contributors to Local Sea-Level Rise

11. In addition to projecting future sea levels, other factors may also be important.

   a. What is the state of science on identifying future (a) tidal amplitude and/or phase, and (b) frequency and intensity of extreme events (e.g., high water due to storm surges, ENSO events)? *(Box 1)*

b. What are the pros and cons of different approaches of arriving at total water level? *(Box 4)*

c. What is the OPC-SAT Working Group's recommendation on how to integrate (global or regional) sea-level rise projections with expected changes in tidal and extreme events? *(Box 4)*

d. What is the OPC-SAT Working Group's assessment of the adequacy of superimposing historical extreme event departures from mean onto projected mean sea levels to estimate future values? *(Box 4)*

Policy Sensitivity of Sea-Level Rise Projections

12. How "policy dependent" are the different contributors to sea-level rise? *(Section 2.3)*

a. Are the different contributors to sea-level rise equally sensitive to changes in global emissions/temperature? *(Section 2.1)*

b. How much sea-level rise can be avoided or how much can it be slowed down by significant emission reductions (e.g., achieving the global commitments made at COP21 in Paris or 80% GHG emissions reductions by 2050)? *(Section 2.1, Section 3.2, and Section 3.3)*

c. What new implications for planning and decision making, if any, are introduced by including ice loss scenarios in sea-level rise projections (e.g., magnitude, timing, non-linear rates, nature of the impact)? *(Section 3.1.2. Appendix 2)*

13. Sea-level rise projections typically use emissions scenarios (e.g., IPCC emissions scenarios/ Representative Concentration Pathways (RCPs)) as inputs into general circulation/sea-level rise models. The RCP 2.6 scenario (lowest IPCC emission scenario) appears out of reach, given current greenhouse gas emission trends, and the unlikely development of more ambitious emission reduction targets in the near future. Is there any physically plausible scenario under which it remains sensible to retain such low-end scenarios in the range of projections? If not, what is the lowest plausible sea-level rise scenario? *(Section 3.1.1)*

Sea-Level Rise Exposure vs. Risk-based Assessment

14. Risk (often defined as probability multiplied by consequence) is a critical input to planning and decision-making.?

a. What is the OPC-SAT Working Group's recommendation on whether and, if so, how to incorporate consideration of risk as part of the State Sea-level Rise Guidance Document to state and local decision-makers? *(Section 1.3, Section 4.2)*

b. How would this approach take account of the uncertainties in sea-level rise projections? *(Section 4.2, Box 3)*

15. What other questions should we be asking that we haven't asked? What other considerations should be brought to bear on this topic?

Appendix 2

Robert DeConto
University of Massachusetts Amherst

Helen Amanda Fricker
Scripps Institution of Oceanography

Role of Polar Ice Sheets in Future Sea-Level Rise:
IMPLICATIONS FOR CALIFORNIA

ABOUT THIS REPORT

This document was developed in response to a request from the California Ocean Science Trust to synthesize current scientific understanding of ice loss from the polar ice sheets, with particular focus on West Antarctica, and to discuss the implications for projections of sea-level rise in California. It was developed to inform an update to the science foundation of California's statewide policy guidance on sea-level rise, and an associated update in sea-level rise projections for California.

Abstract

Global mean sea level (GMSL) has risen by about 18 cm (7 inches) since 1900. Most of this rise is attributed to a combination of the thermal expansion of a warming global ocean and the loss of land ice (made up of mountain glaciers and small ice caps, and the great polar ice sheets covering Greenland and Antarctica). During the 20th-century, sea-level rise was dominated by ocean thermal expansion, but recently land-ice loss has taken over as the primary contributor. While mountain glaciers and ice caps are currently contributing more meltwater to the ocean than the ice sheets, the rate of ice loss from both Greenland and Antarctica is accelerating, and ice sheets will likely soon become the dominant component of the land-ice contribution. This is particularly concerning because the ice sheets contain enough ice to raise GMSL by about 65 meters (213 feet) if they melted completely. This report reviews emerging science that suggests ice loss from the Antarctic Ice Sheet poses the greatest potential risk to California coastlines over the next 100 years.

Sea Level is Rising, the Rate is Accelerating, and Land Ice has become the Primary Contributor.

Between ~1900 and 1990, the average rate of global mean sea level (GMSL) rise was ~1.2 ± 0.2 mm/yr (0.5 inches per decade), but the rate has risen sharply since 1990 to ~3 mm per year (1.2 inches per decade) and it continues to accelerate (Hay et al., 2015). The primary contributors to rising GMSL are ocean thermal expansion (a warmer ocean has lower density and takes up more space), increased groundwater withdrawal and diminished rates of land-water storage behind dams, shrinking mountain glaciers, and net changes in the mass of the polar ice sheets covering Greenland and Antarctica (Church et al., 2013).

Over the last century, the rise in GMSL was dominated by ocean thermal expansion, which accounted for about 50% of the increase. Land ice, collectively from mountain glaciers, ice caps, and the polar ice sheets, accounted

1 Contributions to GMSL from groundwater and land water storage were small or slightly negative over most of the 20th century. These contributions are now positive (mainly due to groundwater depletion) but are smaller than contributions from land ice or ocean thermal expansion. Together, groundwater and land water storage contributions to GMSL were 0.38 ± 0.12 mm per year (0.15 ± 0.05 inches per decade) between 1993 and 2010 (Church et al., 2013).

for most of the remaining increase, with mountain glaciers and ice caps contributing roughly 25%[1] and ice sheets the remaining 25%. However, there are vast differences in the sizes of the land ice reservoirs; losing the entire global inventory of mountain glaciers and ice caps would raise GMSL by only ~0.5 m (1.6 feet; Church et al., 2013), whereas complete loss of the Greenland and Antarctic ice sheets would raise GMSL by ~7.4m (24 feet) and ~57m (187 feet), respectively (Bamber et al., 2013; Fretwell et al., 2013). These massive ice sheets represent the greatest potential threat to the long-term sustainability of coastal populations and infrastructure.

Recently, the loss of land ice has surpassed ocean thermal expansion as the largest contributor to sea-level rise (Figure 1). Land ice contributions come from mountain glaciers and small ice caps and the polar ice sheets (Antarctica and Greenland). While glaciers and ice caps continue to contribute substantial meltwater to the oceans (Meier et al., 2009; Marzeion et al., 2012), satellite observations (Figure 2) indicate that the rate of mass loss from Greenland and Antarctica is accelerating (Harig and Simons, 2015; Rignot et al., 2011; Velicogna et al., 2014). The ice sheets have recently taken over as the dominant source of land-ice sea-level rise, with the potential to raise GMSL by several meters in future centuries (Clark et al., 2016; DeConto and Pollard, 2016; Golledge et al., 2015; Huybrechts et al., 2011; Robinson et al., 2012; Winkelmann et al., 2015).

The Greenland Ice Sheet (GIS) is currently losing mass at a faster rate than the Antarctic Ice Sheet (AIS; Figure 1), via a roughly equal combination of surface melt and dynamic thinning of its marginal outlet glaciers (Csatho et al., 2014; Moon et al., 2012). As surface melt increases, particularly around its lower elevation ice margins, the GIS will continue to lose mass at an increasing rate (Huybrechts et al., 2011; van den Broeke et al., 2009). In contrast, Antarctica's recent increase in mass loss is not through surface melt, but is instead mostly related to the increasing flow and retreat of outlet glaciers in the Amundsen Sea region of West Antarctica (Mouginot et al., 2014; Pritchard et al., 2012; Rignot et al., 2014). As discussed below, warming ocean temperatures in this region are thinning ice shelves (the floating, seaward extensions of the glaciers) triggering a dynamic response of the grounded ice upstream (Pritchard et al., 2012; Paolo et al., 2015).

NASA's Ice, Cloud and land Elevation (ICESat) mission revealed major mass loss from Antarctica's ice shelves (Pritchard et al., 2012) and grounded ice sheet (Shepherd et al., 2012) for the period 2003-2009 by estimating the change in ice height with time and converting that to mass. This Ice Sheet Mass Balance Exercise (IMBIE; Shepherd et al., 2012) also included estimates of height change from satellite radar altimetry, and results from two other mass balance techniques (gravity and mass flux) for the period 1992 to 2011. The synthesis of all three techniques showed that the grounded ice changed in mass over this period by: (1) Greenland: –142 ± 49 Gt per year, (2) East Antarctica: +14 ± 43 Gt per year, (3) West Antarctica –65 ± 26 Gt per year, and (4) Antarctic Peninsula: –20 ± 14 Gt per year. Together this contributed 0.59 ± 0.20 mm/year to GMSL (0.23 ± 0.08 inches per decade).

2 Gt (gigatonne) is a billion metric tonnes of ice, and 360 Gt of ice lost to the ocean represents about 1 mm of GMSL rise.

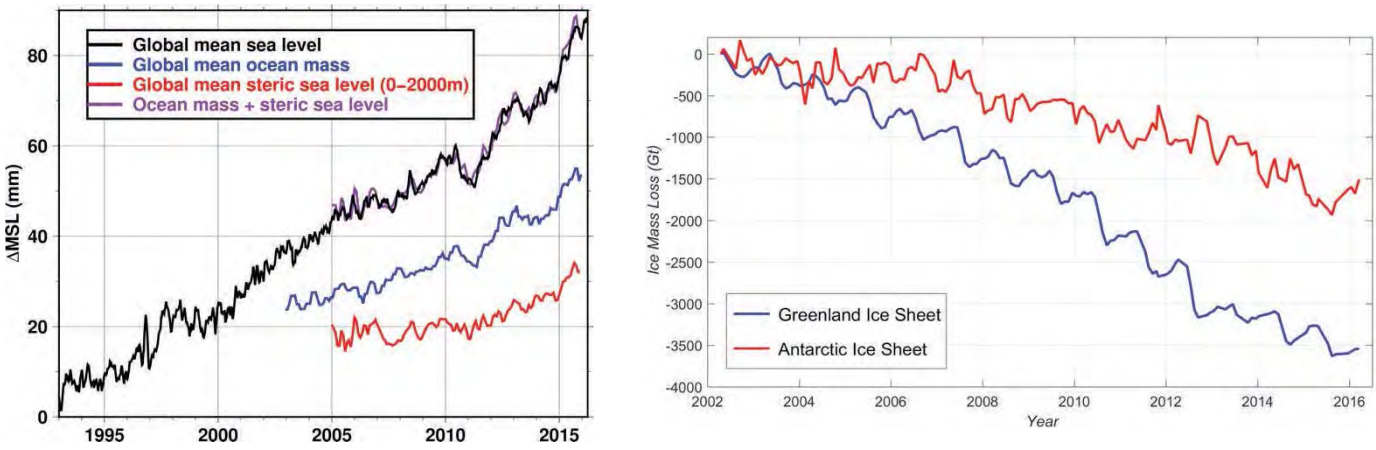

Figure 1. Left: Observations of global mean sea-level rise from satellite radar altimetry (Leuliette and Scharroo, 2010) since 1992 (black line) relative to contributions from 1) the total change in ocean mass contributed by land ice (mountain glaciers, ice caps and the polar ice sheets), and smaller contributions from groundwater and land water storage (Johnson and Chambers, 2013) (blue), and 2) the contribution from thermal (thermo-steric) expansion of the upper ocean (red) from Argo floats (Roemmich and Gilson, 2009). Note that increasing ocean mass, mostly from melting land ice, is now the dominant source of sea-level rise (Figure source: Leuliette and Nerem, 2016). Right. Estimates of ice mass loss on Greenland (blue) and Antarctica (red) from gravity measurements made by the GRACE satellites. Combined, Greenland and Antarctica have been losing an average of ~400 Gt per year since 2002 and the rate is accelerating. The ~5000 Gt of ice lost by the ice sheets since 2002 (right panel) represents a GMSL contribution of about 14 mm, more than 50% of the rise attributed to increasing ocean mass over this period (left panel). Data Source: NASA.

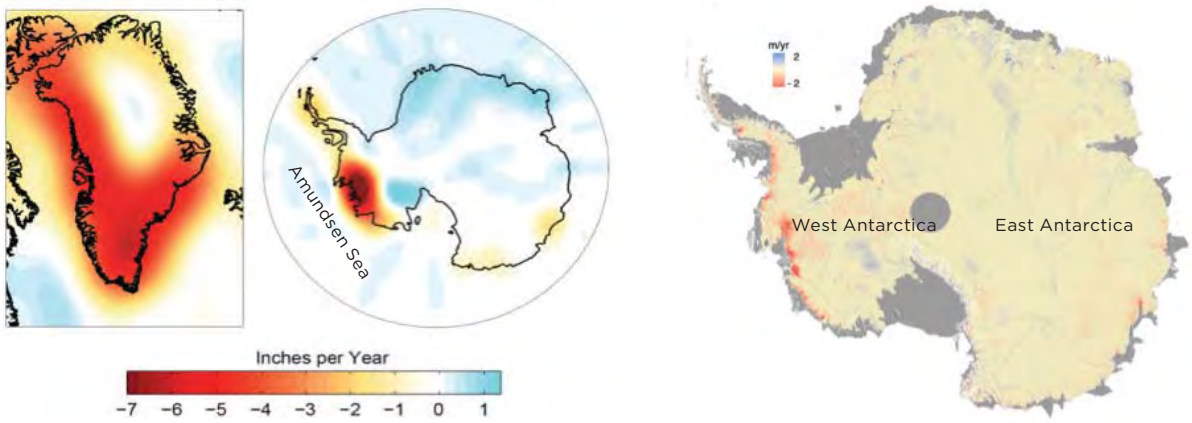

Figure 2. Spatial patterns of ice mass loss (inches of water equivalent lost per year between 2003 and 2012) over Greenland and Antarctica (left), inferred from the GRACE (Gravity Recovery and Climate Experiment) satellites' measurements of Earth's gravitational field (Velicogna et al., 2014; Velicogna and Wahr, 2013). Note the widely distributed ice loss around much of the Greenland Ice Sheet margin. In contrast, Antarctica's ice mass loss is concentrated in the Amundsen Sea sector of West Antarctica, where warming sub-surface ocean temperatures are in direct contact with the underside of ice shelves (figure source: NASA Jet Propulsion Laboratory). The image at right shows the rate of change in the surface elevation of the Antarctic ice sheet between 2010 and 2013, measured by satellite altimetry. Note the coherence between gravity and altimetry measurements, and the concentrated thinning of Amundsen Sea outlet glaciers (from McMillan et al., 2015).

Greenland's Contribution to Future Sea Level

While Greenland is currently a greater contributor to sea-level rise than Antarctica, ice sheet modeling studies spanning a range of future warming scenarios and timescales (Goelzer et al., 2012; Huybrechts et al., 2011; Seddik et al., 2012), show that the potential for the Greenland Ice Sheet (GIS) to contribute truly catastrophic sea-level rise is limited. Most projections of Greenland's contribution to GMSL by the year 2100 are below 25 cm (10 inches), even in high-end greenhouse-gas emissions scenarios (Church et al., 2013). While the balance between the rate of accumulating snowfall and the rate of meltwater and iceberg discharged to the ocean is sensitive to relatively modest warming (>2° C above 19th century temperatures), modeling studies show that the near-complete loss of the GIS will be measured in millennia (Figure 3), not decades or centuries (Robinson et al., 2012).

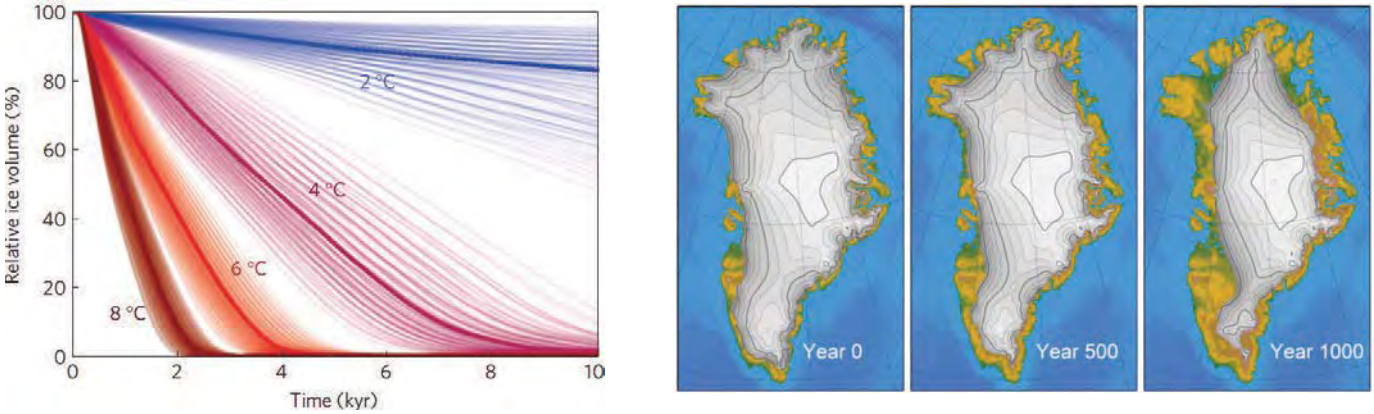

Figure 3. Future projections of the Greenland Ice Sheet. The percentage of Greenland ice volume lost in model simulations (left) using a range of melt-rate parameterizations and increasing summer temperature anomalies from 2 to 8°C (Robinson et al., 2012), whereby 100% loss is equivalent to a 7.4 m rise in global mean sea level. Note the jump in ice-sheet loss with summer temperature anomalies >2°C. Climate-ice sheet simulations (right) assuming a 4-fold increase in CO_2 concentrations over the next 200 years and maintained into the future (Huybrechts, et al., 2011). In both examples, substantial loss of the ice sheet takes centuries to millennia.

Ice Loss from Antarctica will Impact California More than an Equivalent Ice Loss from Greenland

GMSL is clearly rising (Figure 1), but it is relative sea level (RSL), the local difference in elevation between the height of the sea-surface and the height of the solid-Earth surface, that directly impacts coastal communities and ecosystems at risk from coastal flooding.[3] The rise in RSL from shrinking glaciers and ice sheets is not uniformly distributed around the Earth. Changes in the distribution of ice and water over the Earth's surface affects its gravitational field, the orientation and rate Earth's rotation, and the deformation of the Earth's crust and mantle (Mitrovica et al., 2011; Peltier, 2004). While the crust and mantle respond on long (millennial) timescales, the gravitational/rotational effects are essentially instantaneous (annual timescales) and have particular relevance for California.

[3] Changes in RSL arise from 1) vertical land motion, 2) changes in the height of the geoid (the gravitationally determined surface of the ocean in the absence of tides and ocean currents), and 3) changes in the height of the sea surface relative to the geoid. Vertical land motion can be caused by tectonics (California is tectonically active), sediment compaction, or withdrawal of groundwater and hydrocarbons, and the Earth deformation associated with redistributions of ice and ocean mass. This deformation can be separated into 1) glacial isostatic adjustment (GIA), which is the ongoing viscoelastic response of the Earth to past changes in ice volume, and 2) the elastic (gravitational/rotational) response to recent changes in land ice. Both past and current changes in ice volume also affect Earth's gravitional field and rotation, and thus the height of the geoid (Peltier, 2004; Mitrovica et al., 2011). Only the elastic, gravitational, and rotational (fast) components are shown in Figure 4.

As a retreating ice sheet loses mass to the ocean, its gravitational pull on the surrounding ocean is reduced. Within a few thousand kilometers of a retreating ice sheet, the reduced gravitational pull on the ocean causes the sea-surface and thus RSL to drop, even though the ocean has gained volume overall. At some distance further away from the ice sheet (~7000 km), the change in RSL is comparable to that expected from the increase in ocean volume contributed by the melting ice sheet. Beyond that distance, the change in RSL is greater than expected from the extra water added to the ocean by the melting ice sheet. Consequently, Northern Hemisphere coastlines generally experience enhanced relative sea-level rise from the loss of Antarctic ice, while coastlines in the Southern Hemisphere experience enhanced sea-level rise from loss of ice on Greenland. Changing distributions of ice and water also shift the Earth's pole of rotation (the physical North and South Poles) and rate of rotation, which slightly modifies the main gravitational response. The Earth's crust also flexes in response to the change in loading, affecting the height of the land; and given enough time, the Earth's viscous mantle also responds, but these are slower processes generally measured in thousands of years (Peltier, 2004).[4]

Calculations of the gravitational and rotational effects (Figure 4), sometimes called sea level "fingerprints" (Mitrovica et al., 2011), show that North America experiences more sea-level rise from a given meltwater contribution from Antarctica than Greenland, and if the ice loss is from the West Antarctic Ice Sheet (WAIS), the impacts are exaggerated even further. In fact, for California, there is no worse place for land ice to be lost than from West Antarctica (Figure 4). In the near-term, the WAIS is widely considered the most vulnerable major ice sheet to a warming ocean and atmosphere, and serious changes there are already underway, particularly in the Amundsen Sea region (Joughin et al., 2014; Mouginot et al., 2014; Paolo et al., 2015). Consequently, this report focuses on emerging science regarding the vulnerability of the polar ice sheets with a special emphasis on West Antarctica.

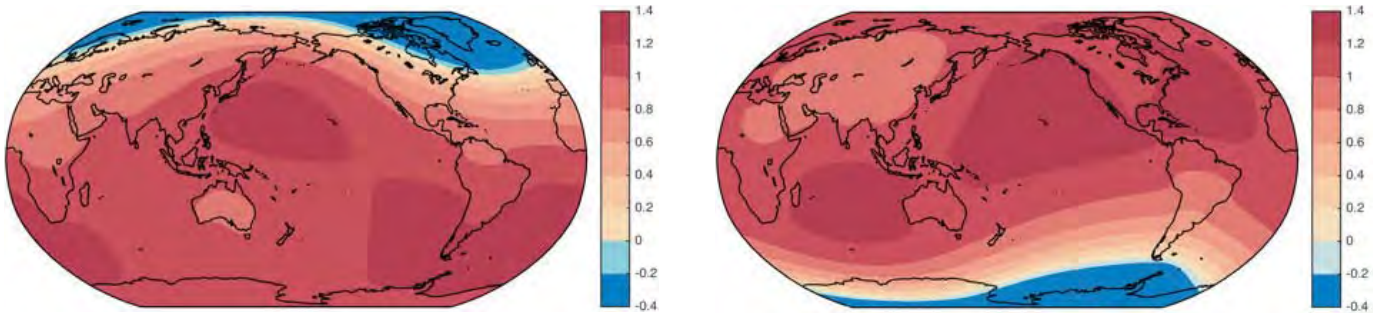

Figure 4. Sea-level "fingerprints" (Mitrovica, et al., 2011; Hay et al., 2017). The map at left shows the rapid (gravitational and rotational) response of sea level to an arbitrary unit of equivalent GMSL contributed by the Greenland Ice Sheet (GIS). The map at right shows the response from an equivalent mass loss from the the West Antarctic Ice Sheet (WAIS). The units are the fractional departure of RSL relative to a given change in GMSL. Note that the U.S. West Coast only experiences about 75% of the GMSL rise contributed by Greenland (left), but the rise in RSL is about 25% greater than expected if meltwater is added to the ocean from West Antarctica (Figure, compliments of Carling Hay).

[4] The Earth's surface is still adjusting to the retreat of the massive ice sheets that covered the Northern Hemisphere during the Last Glacial Maximum (LGM) about 18 thousand years ago. Locally, this post-glacial isostatic adjustment (GIA) can either produce a long-term rise or fall of RSL, depending on the proximity to the past ice load. In the case of California, relatively far from the LGM ice sheets, this effect is relatively small and generally on the order of <1 mm per year (Stella et al., 2007).

Greenland and Antarctic Ice Sheets are Fundamentally Different

The ice sheets covering Greenland and Antarctica behave differently, in part because of the different climate regimes they occupy (relatively warm with massive snowfall on Greenland, versus cold and dry on Antarctica), but more fundamentally, because their subglacial topographies are so different. The bedrock beneath the GIS is above sea level around most of its margin, and below sea-level only in the interior (Figure 5). As a result, much of the ice in the GIS margin is terrestrial, with fast-flowing tidewater glaciers reaching the ocean in deep fjords (Moon et al., 2012). The GIS outlet glaciers lose mass via approximately equal proportions of iceberg calving and melting at their termini.

The AIS, in contrast, contains more than seven times more grounded ice above sea level than the GIS.[5] Moreover, nearly half of the AIS sits on bedrock that is hundreds of meters (or more) below sea level (Fretwell et al., 2013). In many places around the Antarctic margin, grounded ice flows into the ocean and lifts off the bedrock to form large ice shelves; platforms of floating ice that extend over the ocean to form deep sub ice-shelf cavities. The location where the grounded, seaward flowing ice first loses contact with the bedrock to become an ice shelf is called the "grounding line" (Figure 6). Rather than surface melt, almost all of Antarctica's mass loss processes occur in the ice shelves: oceanic basal melting in the sub-ice cavities and iceberg calving from the ice fronts (Rignot et al., 2013; Paolo et al. 2015). Importantly, the ice shelves exert a back stress on the grounded ice, inhibiting its seaward flow, a process commonly called "buttressing" (Weertman, 1974; Thomas et al., 2004; Schoof, 2007). Thinning or loss of these ice-shelves reduces or eliminates this buttressing effect, allowing the grounded ice to flow faster toward the ocean (Rignot et al., 2004; Scambos et al.; 2004; Pritchard et al., 2012; Harig and Simmons, 2015, Paolo et al., 2015).

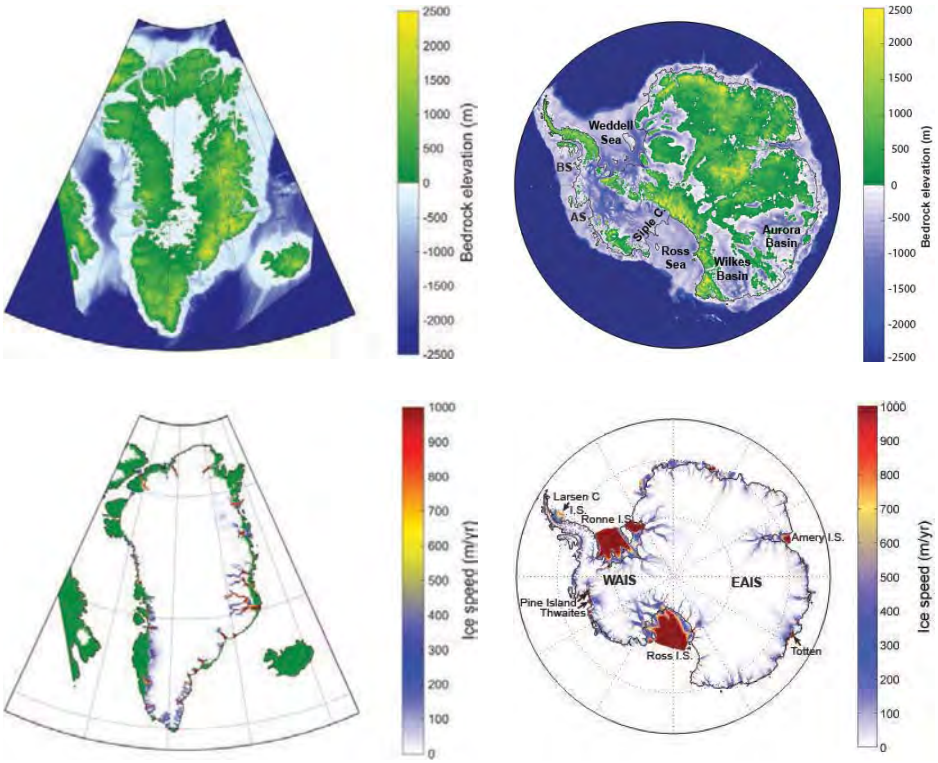

Figure 5. Greenland bedrock elevation (top left; Morlighem, et al., 2015), Antarctic bedrock elevation (top right; Fretwell, et al., 2013), and ice surface speeds from a numerical ice-sheet model (bottom; DeConto and Pollard; 2016). Most of the Greenland bedrock margin is above sea level (top left). Note the opposite configuration of Antarctica (top right), with deep sub-glacial basins adjacent to the open ocean. As a result, much of the GIS margin terminates on land, with the exception of fast flowing outlet glaciers. In contrast, almost all of the thick AIS terminates in the ocean. The location of features mentioned in the text include AS (Amundsen Sea), BS (Bellingshausen Sea), and Siple Coast. Fast ice speeds (red) show the location of major ice streams, outlet glaciers, and floating ice shelves. Major Antarctic ice shelves are labeled, as are the retreating Pine Island and Thwaites glaciers in the Amundsen Sea region.

[5] The loss of floating ice and ice below sea level have only a small direct effect on sea level.

In many places in Antarctica, especially in West Antarctica, deep troughs beneath the ice extend inland from the grounding lines, and slope downward toward the interior of the continent, eventually leading to submarine basins that can be more than 1 km deep. For example, Thwaites Glacier (Figure 5) rests on a reverse-sloped bed, leading to the deep WAIS interior (see Figures 6 and 7) where there is enough ice above floatation to raise GMSL by ~3 m (9.8 feet).[6] Vast areas of the much larger East Antarctic Ice Sheet (EAIS) also rest in deep sub-marine basins and these East Antarctic basins contain enough ice to raise GMSL by ~19 m (62 feet) if the ice they contain were lost to the ocean. With a few exceptions (e.g., Totten Glacier), the majority of the EAIS ice shelves and outlet glaciers are currently stable (Rignot et al. 2013; Paolo et al., 2015), but that situation could change with increased ocean and atmospheric warming.

Key Processes at Play in Antarctica (Marine-Based Ice)

The climate in Antarctica is colder than in Greenland, but because most of the ice sheet margin terminates in the deep ocean, its outlet glaciers, grounding lines, and the underside of buttressing ice shelves are vulnerable to even modest amounts of ocean warming. In part, this is because the melting point of ice becomes lower with increasing water depth (Holland et al., 2008; Jacobs et al., 2011; Paolo et al., 2015; Shepherd, 2004). In the Amundsen Sea sector, seasonally stronger westerly winds have driven a change in ocean circulation, favoring intrusions of warm salty deep water (upper Circumpolar Deep Water, or CDW) across the continental shelf break into the sub-ice cavities and towards the grounding zones of major ice outlets such as Thwaites Glacier, enhancing ice shelf basal melting (Pritchard et al., 2012; Steig et al., 2012). Currently, the Southern Ocean is taking up more heat and warming faster than other parts of the global ocean (Levitus et al., 2012; Masahiro et al., 2013), especially at intermediate depths (Schmidtko, et al., 2014) where CDW has the potential to flow into sub ice-shelf cavities,.

Many marine-based Antarctic outlet glaciers rest on bedrock hundreds of meters to more than 1 km below sea level (Figure 5), and many of these have reverse-sloped beds. In places with this reverse-sloped geometry, including much of WAIS and deep EAIS subglacial basins (Fricker, et al., 2015), the ice sheet is susceptible to a Marine Ice Sheet Instability (MISI; Figure 6), whereby a reduction in ice-shelf buttressing causes an initial grounding-line retreat onto a reverse-sloped bed, which triggers a non-linear acceleration of ice loss and ongoing retreat of the ice margin, because the seaward flow of ice is strongly dependent on the grounding line's thickness (Pollard and DeConto, 2009; Schoof, 2007; Weertman, 1974) which thickens upstream.

[6] Bedrock is 'reverse-sloped' if it deepens toward the continental interior. This is the reverse of the situation off the coast of most continents, including North America, where the continental shelf deepens away from the interior.

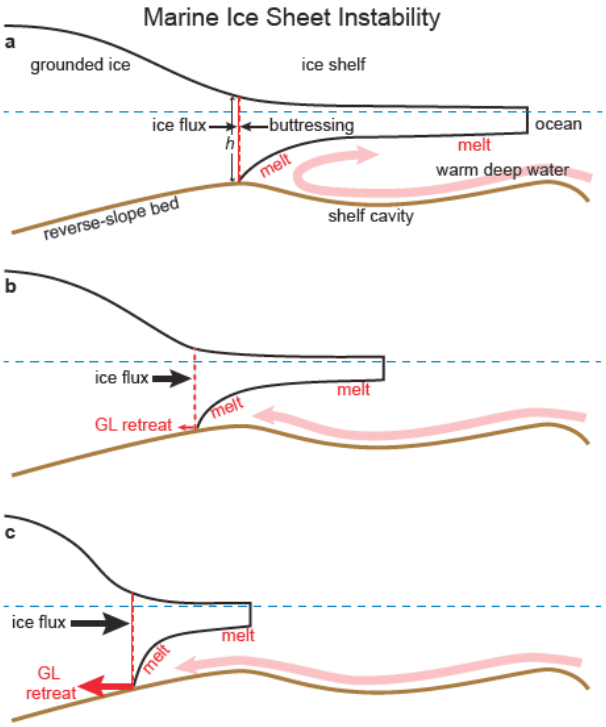

Figure 6. A time-evolving schematic sequence illustrating marine ice sheet instability (a-c), whereby a ~1-km deep, marine terminating ice-sheet margin with reverse-sloped bed is undergoing ice-shelf thinning due to oceanic warming. Note the sequentially thickening grounding lines (red dashed lines) from top to bottom and enhanced seaward ice flux as the ice margin retreats landward into a deepening basin. Once set in motion, even if the ocean forcing is removed, the retreat will continue until the grounding line meets upward sloping bedrock or a topographic bump, or if a confined ice shelf can reform to provide some buttressing against the seaward ice flow.

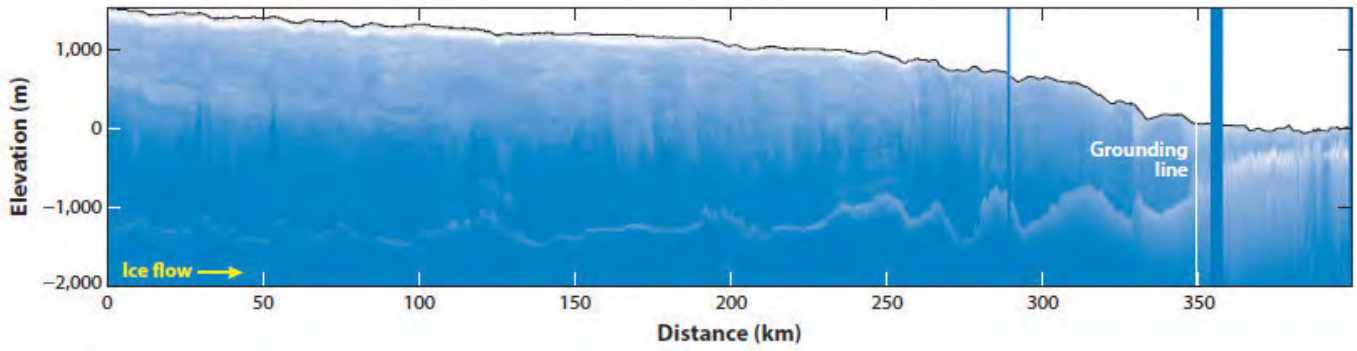

Figure 7. An ice-penetrating radar image (vertical cross section) along a flowline of Thwaites Glacier in the Amundsen Sea sector of WAIS (see Figure 5 for location). The underlying bed is clearly visible. The glacier is ~120 km wide where it reaches the ocean (right) and reaches back into a deep, ice-filled basin almost 2 km below sea level (left) under the heart of the WAIS. The grounding line (vertical white line) is currently retreating on a reverse-sloped bed and undergoing MISI at an estimated rate of ~1 km per year (Rignot, et al., 2014). Its current grounding line thickness is too thin (~600m) to trigger widespread ice-cliff instability (see below), but that situation could change if its current retreat continues (figure source: Alley et al., 2015).

The key glaciological processes associated with MISI have been known for decades, and studied with theoretical, analytical, and numerical models along flowlines or in limited-area domains (Cornford et al., 2015; Favier et al., 2014; Joughin et al., 2014; Schoof, 2007; Weertman, 1974). However, predicting what these processes mean in terms of sea-level rise requires their representation in continental-scale ice sheet models. Only recently have such models become capable of accounting for the linked dynamics of the grounded and floating ice components required to represent MISI.

There are various and well established approaches to independently model the grounded (e.g., Oerlemans, 1982; Huybrechts, 1994; Pattyn et al., 2003; Le Meur et al., 2004) and floating components of marine ice sheets (Morland, 1986; MacAyeal, 1989). However, coupling the grounded component (where vertical shear dominates ice flow) and the floating part (where horizontal stretching dominates) is a challenge, and requires either high spatial resolution at the transition between the grounded and floating ice (Goldberg et al., 2009; Cornford, et al., 2015) or a parameterization of the ice flow across the grounding zone (Schoof, 2007; Pollard and DeConto, 2012). Regardless of the approach, simplifications must be made to allow the computational efficiency needed to run a marine ice sheet model for an entire ice sheet for long time periods.

Model inter-comparisons (Pattyn et al., 2012) have tested and compared the ability of independently developed models representing a wide range of complexities and numerical approaches to capture migrating marine grounding lines (Figure 6) and the fundamental dynamics associated with MISI. These comparisons have increased our overall confidence in models' ability to capture the dynamics of retreating grounding lines on reverse-sloped bedrock, but other processes, not previously included in ice sheet models, could also be critical to Antarctica's future.

Emerging Science and Previously Underappreciated Glaciological Processes

Recently, another glaciological process: *Marine Ice Cliff Instability (MICI)*; Figure 8), not previously considered at the continental ice-sheet scale, was shown to have a profound effect on ice sheet simulations in climates warmer than today (DeConto and Pollard, 2016; Pollard et al., 2015). With summer warming sufficient to produce extensive meltwater ponding around the Antarctic margin, as expected to occur within decades if greenhouse gas emissions continue at their present rates (Trusel et al., 2015), it is possible that water-filled crevasses may 'hydrofracture' ice shelves (Banwell et al., 2013). This was witnessed during the breakup of the Larsen B ice shelf on the Antarctic Peninsula in 2002 (Scambos et al., 2000). If this were to happen to ice shelves that currently protect thick grounding lines where the bedrock has a reverse slope, this could not only trigger MISI, but could also result in tall ice cliffs, as observed at the termini of the few, ~1km thick outlet glaciers in Greenland that have recently lost their ice shelves. Such tall cliffs would be inherently unstable and fail structurally under their own weight (Bassis and Walker, 2012). Because of Antarctica's bedrock geometry and thick, marine-terminating grounding lines, if protective ice shelves were suddenly lost to hydrofracturing or a combination of hydrofracturing and ocean melt from below, then many places around the Antarctic margin would have structurally unstable ice cliffs.

Including MICI dynamics in an ice sheet model is challenging, in part because the numerical representation of fracture mechanics at an ice front is highly complex. Calving is controlled by many interacting processes. These include the stress regime at the ice front, water depth, ice thickness, flow speed, conditions at the bed of the ice, the penetration depth and spacing of crevasses, the presence of lateral shear (along the walls of a fjord for example), undercutting of the calving front by warm water, tides,

and importantly, the presence of mélange (a mix of previously calved, broken icebergs and sea ice) that can provide some support (buttressing) to the cliff face. Many of these processes are not resolved in continental-scale ice-sheet models, so the approach taken to date has been to "parameterize" (simplify) the representation of cliff-failure, to a point where retreat rates can be related to some of the basic prognostic variables (outputs) that ice sheet models can provide-like water depth at the ice terminus, ice flow speed, cliff height, buttressing, and crevassing.

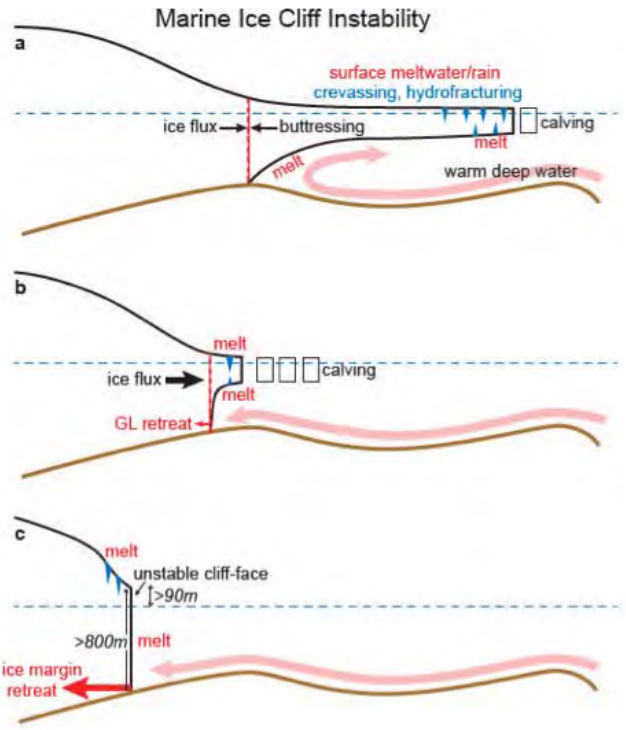

Figure 8. A similar ice sheet margin as shown in Figure 6, but feeling the effects of both sub ice-shelf oceanic warming and atmospheric warming. Meltwater and rainwater accumulating on the ice-shelf surface can fill crevasses (a), which deepens the crevasses, potentially leading to hydrofracturing (b). If the newly exposed grounding line is thick enough to have a tall subaerial ice cliff (c), the terminus would fail structurally. If the rate of structural failure outpaces the seaward flow of ice, the ice margin would back into the deep basin (after Pollard et al., 2015; DeConto and Pollard, 2016), resulting in a massive loss of ice.

The parameterization of complex processes in models usually relies on real-world observations. In the case of ice-cliff retreat, one major limitation is that marine-terminating grounding lines that are 1) thick enough to generate ~100m tall ice cliffs, and 2) have completely lost their ice shelves (like the Helheim and Jakobsavn Glaciers in Greenland; Figure 9) are few and far between today. While widespread MICI has not yet been observed in Antarctica, observations on the Antarctic Peninsula (Rignot et al, 2004; Scambos et al., 2004) and in Greenland (Joughin et al., 2008) have shown that brief episodes of ice-cliff instability lead to accelerated retreat.

Today, most places in Antarctica where ice >800m thick reaches the ocean, floating ice shelves provide buttressing and preclude exposed, tall cliffs at the 'tidewater' grounding line. In the future, given enough atmospheric and ocean warming, it is possible that wide stretches of the marine-terminating Antarctic margin, where thick ice meets the ocean, could lose their protective ice shelves and ice tongues. In that case, cliffs could begin to appear in places like the throat of the Thwaites Glacier. Thwaites Glacier is >10 times wider than the few outlet glaciers in Greenland undergoing MICI today and it is only minimally buttressed. Its grounding line is retreating on reverse-sloped bedrock via MISI (Joughin et al., 2014), but most of the grounding zone is currently resting on bedrock too shallow (Millan et al., 2017) to form a cliff face tall enough to induce MICI (Bassis and Walker, 2012). If grounding line retreat continues into the deep basin upstream, MICI could be initiated, exacerbating the rate of ice mass loss in West Antarctica.

Figure 9. The terminus of Helheim glacier in Southeast Greenland. The heavily crevassed glacier has no ice shelf and is thick enough at the calving front to produce a ~100m tall subaerial ice cliff. The cliff is failing structurally, with the calving front retreating at a rate roughly equivalent to the seaward flow of the glacier (~10 km year), despite the dense mélange trapped within the narrow, 5-km wide fjord. In Antarctica, taller and vastly wider ice cliffs could emerge if ice shelves are lost to warming ocean and atmospheric temperatures (photo: Knut Christianson).

Implications of MISI and MICI for California's Future

Accounting for MICI in an ice sheet can model dramatically increase future sea level projections, and because the epicenter of change will most likely be in WAIS, California would be especially impacted (Figure 2). After including MISI and MICI in their ice sheet model, DeConto and Pollard (2016) tested the performance of the model against the only reasonable analogue for future sea-level: times in the geologic past when GMSL was higher than today and Antarctic temperatures were known to be warmer. The benchmarks they used were the Last Interglacial (LIG, about 125 thousand years ago) and the middle Pliocene (about 3 million years ago). During the Last Interglacial, global mean temperatures were similar to today (Capron et al., 2014; Hoffman et al., 2017), but GMSL was about 6 to 9 meters (20-30 feet) higher (Dutton et al., 2015). Most of the sea-level rise is now thought to have come from Antarctica, because Greenland is believed to have remained partially to mostly intact at that time (Dahl-Jensen et al., 2013; Stone et al., 2013), although the precise magnitude of Greenland retreat continues to be re-evaluated (e.g. Yau et al., 2016). Nonetheless, Last Interglacial sea levels provide a powerful message that the polar ice sheets are sensitive to modest warming.

Global average temperatures during the middle Pliocene were warmer than the LIG, 2°-3° warmer than today. GMSL, while uncertain, is thought to have been in the range of 10-30m (30 to 90 feet) higher than present (Miller et al., 2012; Rovere et al., 2014), requiring a substantial contribution from East Antarctica in addition to Greenland and West Antarctica. Pliocene atmospheric CO_2 concentrations were comparable to today (~400 ppmv; Pagani et al., 2009), although cyclic changes in Earth's orbit (which control the seasonal distribution of solar radiation) likely contributed to periods within the Pliocene when Antarctic temperatures were amplified. It is important to note that Pollard and DeConto's models with MISI physics alone, could not come close to matching Pliocene and Last Interglacial sea level targets, even including the effects of orbital changes. (Pollard and DeConto, 2009). Only after accounting for the effects of hydrofracturing and ice-cliff failure were they able to simulate Pliocene and Last Interglacial sea levels (DeConto and Pollard, 2016), although other factors yet to be considered could have also played a contributing role.

The Pliocene and LIG sea level targets were used to explore a range of model parameters controlling 1) the sensitivity of ice-shelf melt to warming ocean temperatures, 2) the sensitivity of ice shelf hydrofracturing to surface meltwater and rain, and 3) the maximum rates of ice-cliff collapse, regardless of the height or width of the cliff face. They found 29 combinations of these model parameters capable of achieving Pliocene and LIG sea levels. Versions of the model that produced higher or lower sea levels than justified by the geological records were discarded. Hence, only the 'validated' versions of the ice model were used in future simulations, driven by a range of greenhouse gas forcing scenarios. Evolving future atmospheric conditions and ocean temperatures provided by climate model simulations were applied to the ice model, allowing the model to respond to the combined effects of both a warming ocean and a warming atmosphere.

Depending on their assumptions about the magnitude of Pliocene sea levels, which affect the choice of model physical parameters (Pliocene sea-level estimates are more uncertain than LIG estimates), DeConto and Pollard (2016) found that Antarctica has the potential to contribute between 64 ± 0.49 cm and 105 ± 0.30 cm (25 ± 0.19 inches and 41 ± 12 inches) of sea-level rise by the year 2100 in the warmest future greenhouse gas scenario (Figure 10). Another important implication of the study was the recognition that by 2100, the rate of Antarctica's contribution to sea-level rise could be in the range of 2 cm (almost an inch) per year. This finding is fundamentally different than the assessment of the IPCC AR5 (Church et al., 2013), which concluded that Antarctica would contribute little if any GMSL rise by the year 2100, even in the highest greenhouse gas forcing scenario, Representative Concentration Pathway (RCP) 8.5 (van Vuuren et al., 2011). While at the high end, the results point to the potential for much higher sea levels than previously considered, but they also demonstrate a much reduced risk of future sea-level rise from Antarctica if the lowest greenhouse gas emissions pathway (RCP2.6) is followed.[7]

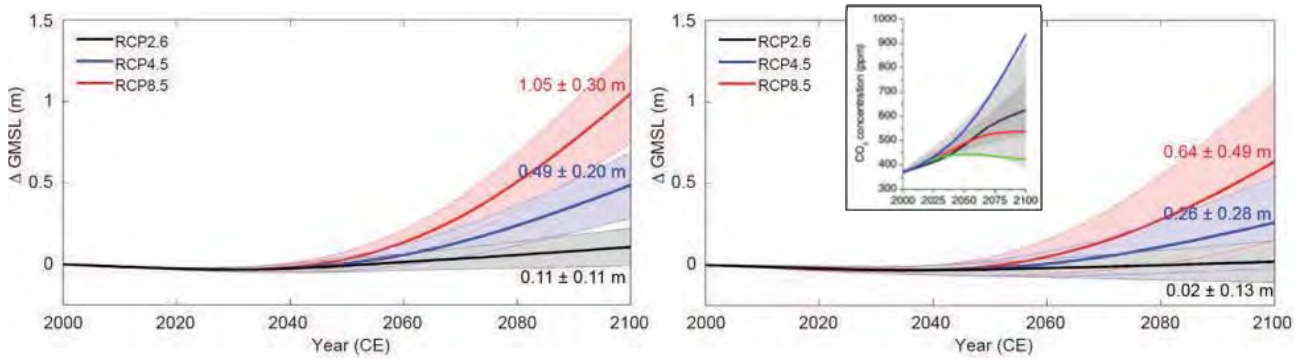

Figure 10. Ensembles of Antarctic's future contribution to sea level, using paleo-calibrated ice-model physics, high-resolution atmospheric climatologies from a regional atmospheric model, and time-evolving ocean model temperatures (from DeConto and Pollard, 2016). The inset at right shows time-evolving CO_2 concentrations (RCPs) used to force the ice sheet simulations (from van Vuuren et al., 2011). Note that different colors are used to represent the RCPs and ice sheet ensembles. The difference between the ensembles at left versus right lies in the assumptions used in the model calibration (based on geological sea-level reconstructions). These differences demonstrate the large uncertainty remaining in current projections. The timing when Antarctica begins major retreat in RCP4.5 and 8.5 (after ~2060) also remains uncertain. In addition to greenhouse-gas forcing, the onset of major retreat will be dependent on the trajectory of Antarctic warming in response to a complex combination of factors including recovery of the ozone hole, linkages with tropical dynamics, and feedbacks between the ice-sheet, solid-Earth, ocean, and sea-ice which are not accounted for here. Addressing these shortcomings and uncertainties will be the focus of future work.

[7] The RCP's refer to the extra radiative forcing (in Watts per square meter, Wm-2) added by the greenhouse gases in each scenario at the year 2100. RCP2.6 is roughly consistent with the aspirational goal of the United Nations' Framework Convention on Climate Change 2015 Paris Agreement to limit the rise in global temperature to less than 2°C. RCP8.5 is consistent with a fossil-fuel-intensive "business as usual" scenario and RCP4.5 is an intermediate scenario, closer to RCP2.6 than RCP8.5.

The Loss of Marine-Based Ice is a Multi-Millennial Commitment.

Another underappreciated consequence of the loss of marine-based ice (as in WAIS) is that it can only re-advance (regrow) if confined ice shelves can be reestablished. The shelves are required to buttress the grounding line, allowing it to migrate seaward on its reverse-sloped bed. Because ice-shelf melt rates are so sensitive to a warm ocean (Holland et al., 2008; Shepherd, 2004), the ocean will have to cool down before the ice shelves can reform. Because of the large thermal "inertia" of the ocean, this could take centuries to several thousands of years, after greenhouse gas concentrations return to their preindustrial levels (Winkelmann et al., 2015). The net result is that sea-level rise driven by the loss of marine-based ice (like WAIS) will remain elevated for thousands of years (DeConto and Pollard, 2016).

Reducing Risk of a Serious Sea Level Contribution from Antarctica

The RCP2.6 ensemble averages in Figure 10 suggest Antarctica will make only a small contribution to 21st-century sea-level rise if future greenhouse gas emissions are strictly limited. However, some of the individual RCP2.6 simulations do involve serious WAIS retreat (Figure 11), with the two highest (of 58) ensemble members exceeding a 50 cm (20 inches) contribution to GMSL by 2100. This implies that the risk of threatening sea-level rise, while much reduced, is not completely eliminated in the scenario with the lowest emissions. This finding is in general agreement with other recent modeling studies and observations of the Amundsen Sea outlet glaciers (Thwaites in particular), suggesting that MISI has commenced in that location and retreat into the heart of the WAIS could be irreversible (e.g., Rignot et al., 2014; Joughin et al., 2014). More observational and modeling work will be required, before a precise climatic threshold for unstoppable WAIS retreat can be defined. In preliminary studies, a combined atmospheric and oceanic warming in the Amundsen Sea region of 2- 3°C is found to be enough to trigger major retreat of the WAIS (Scambos et al., in press), but the timing when that much regional warming will appear in the Amundsen Sea remains difficult to predict.

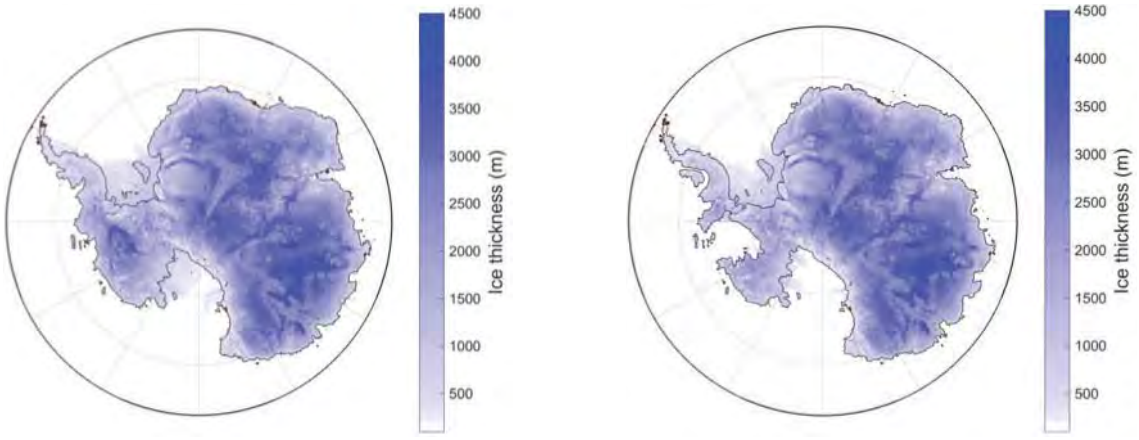

Figure 11. Two individual members of the RCP2.6 ice sheet ensembles (Figure 10) using identical future climate forcing (ocean and atmospheric temperatures), but slightly different model parameters controlling oceanic sub-ice melt rates, sensitivity of hydrofracturing to surface meltwater, and the maximum rate of ice-cliff failure. In this case, both versions of the model are equally capable of simulating realistic modern and ancient ice sheets, so both results can be considered possible future outcomes. As in most RCP2.6 simulations, the model on the left produces almost no contribution to future sea-level rise. In contrast, the model on the right undergoes dramatic retreat of Thwaites Glacier and near compete loss of the WAIS within 500 years. Despite the limited warming in the RCP2.6 scenario, the model on the right produces ~57 cm (22 inches) of GMSL rise by 2100. Reducing the range of uncertainty in future ice sheet simulations should be a top priority.

How Much Confidence Should be Placed in the New Projections?

The obvious question is: how confident can we be in the recent model projections? First, it should be emphasized that the model ensembles (Figure 10) hinge on the performance of a single ice-sheet model and a single climate model. Furthermore, the ensembles do not explore the full range of parameters in the ice sheet model. Thus, the ensembles do not provide a true probabilistic assessment of Antarctica's possible future. While much progress observing and modeling the ice sheet has been made in recent years, the precise magnitude and timing when Antarctic might begin to contribute substantial sea level should still be considered deeply uncertain. Regardless of uncertainty in model physics, one of the greatest sources of uncertainty lies in which future greenhouse gas scenario will be followed; so even if the physical model were perfect in its representation of the natural world, there would still be major uncertainty in the Antarctic ice sheet's future. With that said, the recent work does provide important, new information that should be considered at the policy level (Kopp et al., in review):

- Previously underappreciated glaciological processes have the potential to greatly increase the probability of extreme GMSL rise (2 meters or more) within this century if emissions continue unabated.
- An aggressive reduction in greenhouse gas emissions substantially reduces but does not completely eliminate the risk of extreme GMSL rise from Antarctica.
- Once marine-based ice is lost, the resulting GMSL rise will last for thousands of years.
- The processes (atmospheric dominated) that could drive extreme AIS retreat later in this century are different from those driving AIS changes now (ocean dominated), so the fact that the current rise in GMSL rise is not consistent with the most extreme projections does not rule out extreme behavior in the future.

What are the Major Model Limitations?

The model developed and used by DeConto and Pollard has a number of fundamental limitations that could lead to either an underestimate or overestimate of future ice sheet retreat. These limitations also apply to other recent studies using continental-scale ice sheet models. Perhaps the most fundamental limitation is the lack of observations in the key regions of the ice sheet, for example we do not know the ocean temperature, the ice thickness, or the bathymetry for the sub ice shelf cavities surrounding the entire Antarctic perimeter (see below). Another limitation is the interaction between the retreating ice sheet and the surrounding ocean. Massive volumes of fresh meltwater and ice volumes flowing into the Southern Ocean as the ice sheet retreats could enhance sea ice production, which might ameliorate the pace of atmospheric warming (Bintanja et al., 2013). At the same time, the resulting ocean stratification could enhance heat buildup in the subsurface, increasing ocean melt rates (Hansen et al., 2016). Interactively coupling ice and ocean models is a major challenge and accounting for these interactions at the continental scale is currently a priority of the international ice sheet modeling community.

Another missing feedback is that between the retreating ice sheet and relative sea level at the grounding line. The reduced gravitational pull on the surrounding ocean as the ice sheet retreats leads to a local relative sea level drop at the grounding line. This can have a stabilizing effect on some retreating groundling lines, particularly in places where the onset of MISI is close to a threshold (Gomez et al., 2015). While this negative feedback reduces the total amount of modeled ice sheet retreat on millennial timescales, it has only a small influence in the near-term and is not likely to substantially reduce sea level rise risk on decadal to century timescales.

In DeConto and Pollard (2016) and other recent Antarctic modeling studies (e.g., Cornford et al., 2015; Golledge et al., 2015), ice sheet retreat early in the

21st century is largely driven by sub-surface ocean warming and MISI as illustrated in Figure 6. Ocean models are well known to do a poor job simulating recent sub-surface warming trends around Antarctica (Little and Urban, 2016), making the location and magnitude of future ocean warming an important source of uncertainty, especially in the near term.

By the second half of this century, around 2060, DeConto and Pollard (2016) show that the atmosphere will likely take over as the primary driver of ice retreat, mainly though the influence of surface meltwater on hydrofracturing. This is an important new twist on our understanding of Antarctica's possible future behavior. The inclusion of hydrofracturing physics more directly links ice sheet dynamics with atmospheric conditions; the onset of major retreat is largely determined by the appearance of extensive summer meltwater and rainwater on ice shelves. Thus, the projected timing when massive sea-level rise might commence is strongly dependent on the atmospheric model forcing the ice sheet from above. Climate models currently do a poor job resolving recent changes in coastal Antarctic climate, particularly in some of the most sensitive regions of the ice sheet, like the Amundsen Sea region of West Antarctica (Bracegirdle, 2012) adding uncertainty in the predicted timing of retreat. Furthermore, in the future, the trajectory of Antarctic climate and ocean temperatures will be strongly influenced by important teleconnections to the tropical Pacific (Steig et al., 2012; Dutrieux et al., 2014) and the depletion of the Antarctic stratospheric ozone hole (Marshall et al., 2014; Turner et al., 2016), both of which remain uncertain and poorly represented in climate models.

Due to existing computational limitations, continental-scale ice sheet models, like those discussed here, need to make approximations in the mathematical representations of ice dynamics. Ice sheet models with more complete and rigorous dynamical treatments are beginning to appear, but are still too computationally expensive for the long-term, continental-scale, and parameter-exploring experiments that are required. This will likely change within the decade as greater computer power becomes available. It remains to be seen (and is an open and debated question) whether the simplifications used in the current generation of models matter to the results, and if so, by how much. This is an important issue, because key processes related to MISI are concentrated in the grounding zones, which are effectively important boundary layers between different modes of flow (grounded/shearing versus floating/stretching) that are best represented at high spatial resolution and without simplifications of the underlying physics.

A further possible complication is related to firn, old snow that is transitioning to ice and forms a layer below the newer snow. In a warming world, more snow is anticipated to fall over the EAIS, and hence the firn layer will thicken, at least in the short term. As summer air temperatures begin to exceed the freezing point, meltwater will be absorbed by the underlying firn, as long as there is remaining poor space between snow grains to allow refreezing (Figure 12). Eventually, ice lenses will begin to form, the firn will compact, and it will no longer have the ability to absorb summer melt water. At that point, meltwater will have the potential to flow into underlying crevasses where it can cause hydrofracturing. Presently, the meltwater-buffering capacity of firn is poorly represented in most ice-sheet models. Because of this limitation, the timing when hydrofracturing begins to impact ice shelves in the models could be occurring sooner (by years to a few decades) than it will in reality. With that said, in the warmest (RCP8.5) scenario, so much meltwater would begin to appear over the ice shelves by the second half of the 21st century, the firn layer would be quickly overcome regardless of its thickness or the details of the firn model. However, in more moderate warming scenarios closer to a meltwater/hydrofracturing threshold, the buffering capacity of the firn layer could be a determining factor of the timing when hydrofracturing might begin.

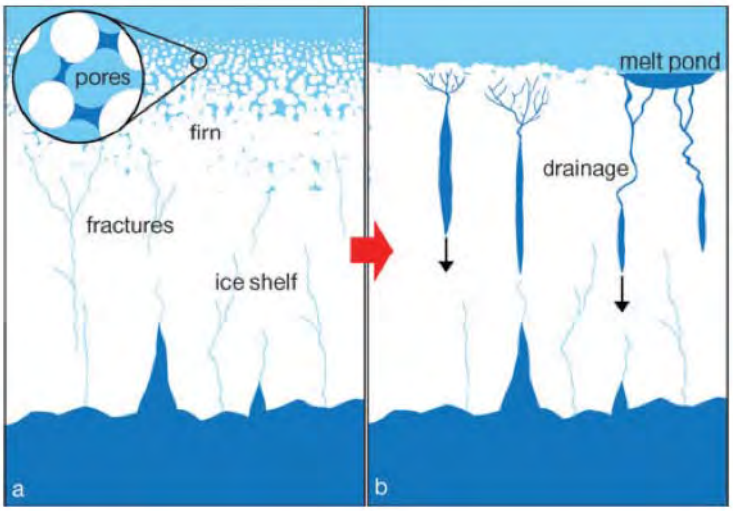

Figure 12. Porous firn (a, left) can absorb seasonal meltwater and delay water flow into underlying crevasses (b, right), delaying hydrofacturing and ice-shelf breakup. Better treatments of these processes in ice sheet models will be critical for predicting the precise timing of the ice sheet's response to a warming climate (figure source: Munneke, et al., 2014).

Could Future Sea-Level Rise be Even Worse than the new Projections?

The future ice sheet projections in DeConto and Pollard (2016) imply the potential for substantially more sea-level rise (2 m or more by 2100) than any previous model results. This is largely due to the explicit treatment of the hydrofracturing and ice-cliff physics described above. While the results remain uncertain for the reasons described here, it should be stressed that the ensemble averages in Figure 10, do not represent the model's maximum possible rates of Antarctica's contribution to sea-level rise.

In the model cliff-collapse (the horizontal rate of ice-loss at the marine "tidewater" calving terminus) only occurs where ice cliffs are tall enough to generate stresses that exceed the strength of the ice. The rate of cliff retreat ranges from near zero where this stress-strength threshold is just exceeded, to some maximum allowable rate, regardless of the cliff height. This "speed limit" imposed on the model's representation of ice-cliff retreat is meant to represent 1) the average size and frequency of individual calving events, which involve brittle fracture mechanics and modes of ice failure whose controlling factors are not well understood, and 2) the buttressing effects of mélange (icebergs and fragments of icebergs locked together by sea ice) at the ice terminus. Faster cliff collapse should generate more mélange, providing a negative feedback that dampens the rate of retreat.

In the future ice-sheet ensembles shown in Figure 10, a range of maximum cliff-failure rates are used, ranging between one and five km per year. At the tallest vertical ice cliffs observed today (e.g., Helheim and Jakobsavn glaciers in Greenland), the horizontal rate of cliff retreat is as high as 10-14km per year (Joughin et al., 2010; 2012). This is quite remarkable, considering these outlet glaciers rest in narrow fjords 5 to 12 km wide, choked with dense mélange as seen in Figure 9.

In Antarctica, the cliff faces that could appear in the future will be much taller and wider than those in Greenland, where mélange can clog seaways. For example, Thwaites Glacier is >120 km wide and its terminus ends in open ocean rather than a narrow fjord, so it might be reasonable to assume cliff collapse in open settings like Thwaites could approach the rates observed in narrow Greenland fjord settings where mélange is presumably providing some back pressure at the grounding line. Increasing the model's maximum cliff retreat values closer to those observed in Greenland (~10 km per year) increases Antarctica's simulated contribution to GMSL to more than 2m by 2100 in the RCP8.5 scenario (DeConto et al., in preparation).

Considering the implications of multiple meters of sea-level rise on century timescales, additional study of these processes and more explicit model treatments of the buttressing mélange in front of retreating ice fonts should be a priority. In reality, rates of cliff retreat depend on the details of fracture mechanics in addition to back-pressure from mélange and other processes not explicitly represented in the current generation of models. Nonetheless, observed behavior of the few tidewater glaciers thick enough to undergo this type of structural failure hints at the possibility that current ice sheet projections, including those in DeConto and Pollard (2016), could be conservative and that 2.5 m or more of total GMSL rise by 2100 cannot be ruled out.

Other Recent Antarctic Modeling

In the last year, several other modeling studies of the AIS' future were published in high profile journals (e.g., Clark et al., 2016, Golledge et al., 2015, Ritz et al., 2015, and Winkelmann et al., 2015). Among these, Ritz et al., (2015) and Golledge et al., (2015) are the most directly comparable to DeConto and Pollard (2016), because they explicitly discuss the possible state of the ice sheet in 2100.

Ritz et al. (2015) used a hybrid physical-statistical modeling approach, whereby the physical processes triggering the onset of MISI (Figure 6), which DeConto and Pollard attempt to model directly, are determined statistically rather than physically. They estimated probabilities of MISI onset in eleven different sectors around the ice-sheet margin, based on observations of places undergoing retreat today (mainly in the Amundsen Sea) and expected future climate change following the A1B emissions scenario used in IPCC AR4 (Solomon et al., 2007).[8] In places where they project MISI to begin, the persistence and rate of grounding-line retreat is parameterized as a function of the local bedrock topography (slope), grounding line thickness (Schoof et al., 2007), basal slipperiness, and one of three different model treatments of basal friction which is shown to provide considerable uncertainty.

The advantage of the approach used by Ritz et al., (2016) is that the relative simplicity of the ice sheet model allows thousands of model iterations in each of the eleven Antarctic sectors, allowing a probabilistic assessment of the results based on each ensemble member's performance relative to modern, observed retreat rates in the Amundsen Sea. While their A1B future climate scenario is not directly comparable to the RCPs used by DeConto and Pollard (2016), they concluded that Antarctica could contribute up to 30 cm (12 inches) GMSL by 2100 (95% quantile), similar to the RCP4.5 results of DeConto and Pollard (2016) but considerably less than RCP8.5 (Figure 10).

The Ritz et al., (2015) study represents a careful and statistically rigorous approach, but their conclusions may be hampered by their reliance on modern, observed rates of retreat in the Amundsen Sea to calibrate their results. Today, retreat in the Amundsen Sea is being driven by oceanic sub-ice melt. In the future, atmospheric warming may become an increasingly dominant driver of ice-sheet retreat via hydrofracturing and cliff failure, processes that recent observations in the region do not inform. Furthermore, their maximum retreat rates consider only those processes associated with MISI, and do not consider the additional potential contributions from the physical processes associated with MICI.

Golledge et al. (2015), used the PISM ice sheet model (Winkelmann et al., 2011) which is similar in its formulation to the ice-sheet model used by DeConto and Pollard (2016), but without hydrofracturing and ice-cliff physics, to simulate the future response of the AIS to simplified RCP emissions scenarios. The PISM model captures MISI dynamics, but not MICI, so again, the bulk of simulated ice-sheet retreat is driven by oceanic warming and sub-ice melt, rather than atmospheric warming. PISM's treatment of sub-ice melt in response to warming ocean temperatures (Feldmann and Levermann et al., 2015) makes PISM more sensitive to ocean warming than DeConto and Pollard's model. As a result, Golledge et al., (2015) find they can produce 39 cm (10 inches) of GMSL by 2100 from Antarctic in RCP8.5 (mainly through MISI),

[8] Greenhouse gas emissions scenario A1B is roughly intermediate between RCP4.5 and RCP8.5.

without the MICI physics used by DeConto and Pollard, (2016). Using a more conservative oceanic melt-rate parameterization in their simulations, the GMSL contribution drops from 39 to 10 cm by 2100, highlighting the ongoing uncertainty in heavily parameterized continental-scale ice sheet models, particularly with regard to their sensitivity to a warming ocean.

While Ritz et al. (2015) and Golledge et al. (2015) both simulate less ice sheet retreat by 2100 than DeConto and Pollard (2016), these studies still represent a considerable departure from IPCC AR5 (Church et al., 2013), which assessed little to no contribution to future sea level from Antarctica by 2100, even under the high-emissions RCP8.5 scenario. Furthermore, despite the enhanced sensitivity of the PISM model to a warming ocean, Golledge et al. (2015) also find that a low emissions scenario like RCP2.6 essentially eliminates the risk of a substantial future sea-level contribution from Antarctica. This important conclusion is in agreement with the findings of DeConto and Pollard (2016).

Outlook: The Science is Moving Quickly

Recent advances in monitoring and modeling the Greenland and Antarctic ice sheets are leading to steady improvements in our understanding of the underlying processes driving ice-sheet retreat, but the multifaceted complexity of the coupled ice-atmosphere-ocean-Earth system continues to hamper predictions of the ice sheet's future. A number of coordinated, international programs are either just getting underway, or are planned in the near future with the goal of reducing uncertainty in future sea-level rise. Among others, these include, the NRC ESAS 2007 Decadal Survey, which identified the following as a major science question for satellite observations of Earth over the next decade: "Will there be catastrophic collapse of the major ice sheets, including those of Greenland and West Antarctica and, if so, how rapidly will this occur? What will be the time patterns of sea-level rise as a result?" It recommended three key Earth-observation missions for ice-sheet monitoring: (i) DESDynI (now NiSAR, a synthetic aperture radar (SAR) to estimate surface deformation); (ii) Ice, Cloud and land Elevation Satellite-2 (ICESat-2) (laser altimeter to estimate ice sheet height) and (iii) a follow on to the current GRACE satellite. NISAR will launch in 2020, and the other two missions are due for launch within the next 2 years. Operation IceBridge is an airborne mission carrying instruments such as an laser altimeter and a sounding radar to bridge the gap between ICESat (ended 2009) and ICESat-2 (to be launched 2018). Internationally, there are several missions collecting relevant data: the European Space Agency has operated CryoSat-2 since 2010 to monitor the ice sheets with radar altimetry, another element in its continuous record since 1992 (ERS-1, ERS-2 and Envisat), and there are plans for a CryoSat-3. Other relevant SAR data also come from Sentinel-1a (ESA), ALOS (Japan) and TerraSAR-X (Germany). Continued availability of these types of observations will be critical for understanding processes and monitoring when and where the ice is thinning and retreating.

One of the key limitations in understanding processes driving ice sheet mass loss is the lack of observations near the ice margins and the surrounding oceans. This is challenging, as the areas are often ice covered, and are logistically difficult to reach, and so much of the region remains unmapped. A NASA Earth Ventures mission, Oceans Melting Greenland (OMG), was launched in 2015 for $30M. This mission is acquiring, via aircraft and ship, vital measurements in the ocean off Greenland's outlet glaciers to understand how the ocean conditions are changing. The same needs to be done in Antarctica. In 2016 six ALAMO floats were deployed in the Ross Sea off the Ross Ice Shelf. Observations like these are needed all around Antarctica and especially in the vulnerable Amundsen Sea region.

Constraining how much and how fast the WAIS will change in the coming decades has recently been identified as a

top priority in Antarctic research (National Academies, 2015). The U.S. National Science Foundation and the U.K. National Environmental Research Council recently announced a joint, $23M solicitation for collaborative US-UK science proposals to understand the Thwaites Glacier, how it behaved in the past, and how it might retreat in the future. This level of international coordination is required to surmount the expense and logistical challenges of doing science in the Antarctic.

While observational programs are advancing our understanding of ice-sheet processes and interactions between ice, ocean, atmosphere, and the underlying Earth, numerical models must keep pace, as it is models that will ultimately provide improved projections. While ice sheet modeling advances have been steady in recent years, some of the key limitations described above will need to be resolved before uncertainties in projections can be reduced and the possible thresholds and tipping points can be more robustly identified. Part of the challenge in modeling the ice sheets is illustrated by the number of interacting processes (Figure 13) at an ice sheet margin, or even in a single outlet glacier like Thwaites. Many of these interacting processes operate on different timescales, adding to the modeling challenge.

While detailed and highly resolved models of individual processes or local regions are being developed, the lessons learned from such detailed modeling must be 'scaled up' to the continental scale. This often requires parameterizations of the processes that cannot be resolved at the spatial resolution (5-40 km) of typical continental ice sheet models. Furthermore, the decadal to century timescales most relevant for policy decisions, are short for a whole ice sheet. The fast, dynamic behavior of individual outlet glaciers, surging or sticking ice streams, and growing or collapsing ice shelves can be thought of as the 'weather' of the ice sheet. The continental ice-sheet models now being tasked with providing useful future projections on decadal-to-century timescales are analogous to climate models, best suited to modeling long-term changes rather than short-term forecasts of the ice sheet 'weather'. Furthermore, the predictive skill of any model is not only determined by the validity of the physics represented in the model, but also the initial conditions applied at the beginning of a simulation. For an ice sheet model, this means that the bedrock topography, conditions at the bed of the ice, internal ice temperatures, ice rheology, speed of the ice, underlying ocean conditions, overlying atmospheric conditions, etc., need to be known at the spatial resolution of the model. Such details remain unresolved in parts of Greenland and Antarctica and will have to be improved before model confidence can be substantially increased at the continental ice-sheet scale.

Key continental-scale modeling challenges that must be overcome in the short term include 1) two-way ice sheet-ocean-atmosphere coupling, 2) more explicit modeling of grounding line and ice cliff physics, including the effects of mélange, and 3) firn models coupled to both the atmosphere and underlying ice physics. Advances in all of these areas are occurring steadily, and substantial advances are expected within the next decade. In the meantime, work currently underway and expected in the next one to five years includes improved understanding on the ocean and warming thresholds capable of driving substantial WAIS retreat. Furthermore, a more complete exploration of the upper-end (maximum) estimates of what is possible in terms of future sea-level rise from Antarctica (and Greenland) will be particularly valuable for California policy and planning purposes. Based on the emerging science, this extreme upper bound is likely to be higher than in the current literature or published national or international climate assessments.

It is worth emphasizing that the threat of massive sea-level rise from Antarctica is not only supported by the recent ice-sheet modeling literature, but also from basic observations and fundamental physical principles. First, lessons from the geological record show that the polar ice sheets and the AIS in particular are sensitive to modest amounts of warming (Dutton et al., 2015). Second, the amount of warming over Antarctica in high-emissions future greenhouse gas emissions scenario will produce massive amounts of meltwater on Antarctic ice shelves before the end of the century (DeConto and

Pollard, 2016; Trusel et al., 2015) and meltwater has been observed to drive ice-shelf breakup in the recent past. This includes the sudden collapse of the Larsen B ice shelf in 2002 that resulted in the speed-up of upstream glaciers, previously buttressed by the ice shelf, by a factor of eight in some instances (Rignot et a;, 2004; Scambos et al., 2004). Third, loss of Antarctic ice shelves and the associated loss of buttressing will trigger MISI on reverse-sloped bedrock as is occurring in the Amundsen Sea today. Fourth, in some locations in Antarctica, marine-terminating ice cliffs greater than 100 meters tall will emerge in some places and these cliffs will fail structurally under their own weight as observed in Greenland today. Fifth, much of the Antarctic Ice Sheet rests in deep sub-marine basins, exposing the ice-sheet margin to a warming ocean, and dynamical instabilities induced by reverse-sloped bedrock.

In summary, the current pace of global sea-level rise (1.2 inches per decade) is already impacting California ‘s coastline. New ice-sheet projections suggest the rate of rise could accelerate sharply later in this century, with the potential for two meters (6.5 feet) or more of total sea-level rise by 2100. While the uncertainty in these projections remains high, the risk is not negligible given the stakes to future society, development, and infrastructure. Given the level of uncertainty but also the potential impacts, significant investment in any major new coastal development with long lifespans needs to be carefully assessed. Similarly, responses to both long-term sea-level rise and short-term elevated sea levels for existing infrastructure and development also need to consider economic, social, and environmental impacts and costs as well as the lifespan of any approach. Increasing the reliability of future sea-level projections will be important in decision making for both existing and proposed development and infrastructure. This is a tractable problem, but it will require improved scientific understanding of mass-loss processes from the vast polar ice sheets across all the relevant spatial and temporal scales. This can only be achieved through continued and new observations from satellites and the field (both on the ice and in the surrounding atmosphere and ocean), combined with modeling to investigate key processes such as ice-ocean interactions, surface melting, and fracture mechanics of ice. This will require substantial international and inter-agency investment to support collaborations across the disciplines of glaciology, meteorology, oceanography, and computational science.

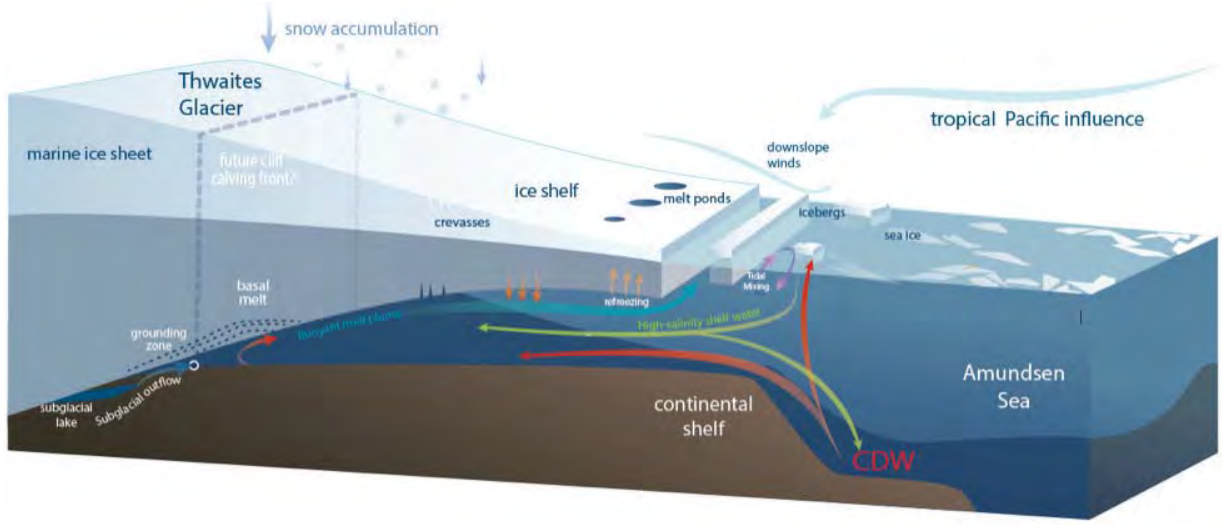

Figure 13. A schematic representation of the primary, interconnected processes operating at a marine-terminating outlet glacier like the Thwaites Glacier. Both the individual processes and their coupled interactions must be understood to be properly modeled, illustrating the grand challenge faced when trying to predict how a system like this will behave in the future. Some processes shown, like cliff collapse and extensive meltwater ponding, have not begun in the region, but could if grounding line retreat and warming continues.

References

Alley RB, Anandakrishnan S, Christianson K, Horgan HJ, Muto A, et al. 2015. Oceanic forcing of ice-sheet retreat: West Antarctica and more. Annual Review of Earth and Planetary Science Letters 43: 207-31

Bamber JL, Griggs JA, Hurkmans RTWL, Dowdeswell JA, Gogineni SP, et al. 2013. A new bed elevation dataset for Greenland. The Cryosphere 7: 499-510

Banwell AF, MacAyeal DR, Sergienko OV. 2013. Breakup of the Larsen B Ice Shelf triggered by chain reaction drainage of supraglacial lakes. Geophysical Research Letters 40: 1-5

Bassis JN, Petersen SV, Mac Cathles L. 2017. Heinrich events triggered by ocean forcing and modulated by iso static adjustment. Nature 542: 332-4

Bassis JN, Walker CC. 2012. Upper and lower limits on the stability of calving glaciers from the yield strength envelope of ice. Proceedings of the Royal Society A 468: 913-31

Bintanja R, van Oldenborgh GJ, Drijfhout SS, Wouters B, Katsman CA. 2013. Important role for ocean warming and increased ice-shelf melt in Antarctic sea-ice expansion. Nature Geoscience 6: 376-99

Bracegirdle TJ. 2012. Climatology and recent increase of westerly winds over the Amundsen Sea derived from six reanalyses. International Journal of Climatology 33: 843-51

Capron E, Govin A, Stone EJ, Masson-Delmotte V, Mulitza S, et al. 2014. Temporal and spatial structure of multi-millennial temperature changes at high latitudes during the Last Interglacial. Quaternary Science Reviews 1-3: 116-33

Church JA, Clark PU, Cazenave A, Gregory JM, Jevrejeva S, et al. 2013. Chapter 13: Sea Level Change. In Climate Change 2013: the Physical Science Basis, ed. TF Stocker, D Qin, G-K Plattner, M Tignor, SK Allen, et al: Cambridge University Press

Clark PU, Shakun JD, Marcott SA, Mix AC, Eby M, et al. 2016. Consequences of twenty-first-century policy for multi-millennial climate and sea-level change. Nature Clim. Change 6: 360-9

Committee on the Development of a Strategic Vision for the US Antarctic Program. 2015. A Strategic Vision for NSF Investments in Antarctic and Southern Ocean Research. Washington, DC: The National Academies Press

Cornford SL, Martin DF, Payne AJ, Ng EG, Le Brocq AM, et al. 2015. Century-scale simulations of the response of the West Antarctic Ice Sheet to a warming climate. The Cryosphere 9: 1579–600

Csatho BM, Schenk AF, van der Veen CJ, Babonis G, Duncan K, et al. 2014. Laser altimetry reveals complex pattern of Greenland Ice Sheet dynamics. Proceeding of the National Academy of Sciences 1111: 18478–83

Dahl-Jensen D, Neem. 2013. Eemian interglacial reconstructed from a Greenland folded ice core. Nature 493: 489-94

DeConto RM, Pollard D. 2016. Contribution of Antarctica to past and future sea-level rise. Nature 531: 591-7

Dutrieux P, De Rydt J, Jenkins A, Holland PR, Ha HK, et al. 2014. Strong sensitivity of Pine Island ice-shelf melting to climatic variability. Science: 174-8

Dutton A, Carlson AE, Long AJ, Milne GA, Clark P, et al. 2015. Sea-level rise due to polar ice-sheet mass loss during past warm periods. Science 3491

Favier L, Durand G, Cornford SL, Gudmundsson GH, Gagliardini O, et al. 2014. Retreat of Pine Island Glacier controlled by marine ice-sheet instability. Nature Geoscience 7: 874-8

Fretwell P, Pritchard HD, Vaughan DG, Bamber JL, Barrand NE, et al. 2013. Bedmap2: improved ice bed, surface and thickness datasets for Antarctica. Cryosphere 7: 375-93

Fricker HA, Siegried MR, Carter S, Scambos T. 2015. A decade of progress in observing and modelling Antarctic subglacial water systems. Philosophical Transactions of the Royal Society A 364

Goelzer H, Huybrechts P, Raper SCB, Loutre MF, Goosse H, Fichefet T. 2012. Millennial total sea-level commitments projected with the Earth system model of intermediate complexity LOVECLIM. Environmental Research Letters 7: 045401

Goldberg, DN, Holland, DM, and Schoof, C. 2009. Grounding Line Movement and Ice Shelf Buttressing in Marine Ice Sheets. Journal of Geophysical Research: Earth Surface 114: F04026

Golledge NR, Kowalewski DE, Naish TR, Levy RH, Fogwill CJ, Gasson E. 2015. The multi-millennial Antarctic commitment to future sea-level rise. Nature 526: 421-5

Gomez N, Pollard D, Holland D. 2015. Sea level feedback lowers projections of future Antarctic Ice Sheet mass loss. Nature Communications 6

Hansen J, Sato M, Hearty P, Ruedy R, Kelley M, et al. 2016. Ice melt, sea level rise and superstorms: evidence from paleoclimate data, climate modeling, and modern observations that 2 C global warming could be dangerous. Atmospheric Chemistry and Physics 16: 3761-812

Harig C, Simons FJ. 2015. Accelerated West Antarctic ice mass loss continues to outpace East Antarctic gains. Earth and Planetary Science Letters 415: 134-41

Hay C, Lau H, Gomez N, Austermann J, Powell E, et al. 2017. Sea-level fingerprints in a region of complex Earth structure: The case of WAIS. Journal of Climate 30: 1881-92

Hay C, Morrow ED, Kopp RE, Mitrovica JX. 2015. Probabilistic reanalysis of twentieth-century sea-level rise. Nature 517: 481-4

Hoffman JS, Clark PU, Parnell AC, He F. 2017. Regional and global sea-surface temperatures during the last interglaciation. Science 355(6322):276-279

Holland PR, Jenkins A, Holland D. 2008. The response of ice shelf basal melting to variations in ocean temperature. Journal of Climate 21: 2558-72

Huybrechts P. 1994. Formation and disintegration of the Antarctic ice sheet. Annals of Glaciology 20: 336-40

Huybrechts P, Goelzer H, Janssens I, Driesschaert E, Fichefet T, et al. 2011. Response of the Greenland and Antarctic ice sheets to multi-millennial greenhouse warming in the earth system model of intermediate complexity LOVECLIM. Surveys in Geophysics 32: 397-416

Jacobs SS, Jenkins A, Giulivi CF, Dutrieux P. 2011. Stronger ocean circulation and increased melting under Pine Island Glacier ice shelf. Nature Geoscience 4: 519-23

Johnson GC, Chambers DP. 2013. Ocean bottom pressure seasonal cycles and decadal trends from GRACE Release-05: Ocean circulation implications. Journal of Geophysical Research 118: 4228-40

Joughin I, Howat IM, Fahnestock M, Smith B, Krabill W, et al. 2008. Continued evolution of Jakobshavn Isbrae following its rapid speedup. Journal of Geophysical Research-Earth Surface 113

Joughin I, Smith BE, Howat IM, Floricioiu D, Alley RB, et al. 2012. Seasonal to decadal scale variations in the surface velocity of Jakobshavn Isbrae, Greenland: Observation and model-based analysis. Journal of Geophysical Research: Earth Surface 117: n/a-n/a

Joughin I, Smith BE, Howat IM, Scambos T, Moon T. 2010. Greenland flow variability from ice-sheet-wide velocity mapping. Journal of Glaciology 56: 415–30

Joughin I, Smith BE, Medley B. 2014. Marine ice sheet collapse potentially under way for the Thwaites Glacier basin, West Antarctica. Science 344: 735-8

Kopp R, DeConto RM, Bader D, Horton RM, Hay CC, et al. 2017. Implications of ice-shelf hydrofracturing and ice cliff collapse mechanisms for sea-level projections. Earth's Future in review

Kuipers Munneke P, Ligtenberg SRM, van den Broeke MR, Vaughan DG. 2014. Firn air depletion as a precursor of Antarctic ice-shelf collapse. Journal of Glaciology 60: 205-14

Le Meur E, Gagliardini O, Zwinger T, Ruokolainen J. 2004. Glacier flow modelling: a comparison of the Shallow Ice Approximation and full-Stokes solution. Comptes Rendus Physique 5: 709-22

Leuliette EW, Nerem RS. 2016. Contributions of Greenland and Antarctica to global and regional sea level change. Oceanography 29: 154-9

Leuliette EW, Scharroo R. 2010. Integrating Jason-2 into a multiple-altimeter climate data record. Marine Geology 33(sup 1): 504-17

Levitus S, Antonov JI, Boyer TP, Baranova OK, Garcia HE, et al. 2012. World ocean heat content and thermosteric sea level change (0–2000 m), 1955–2010. Geophysical Research Letters 39

Little CM, Urban NM. 2016. CMIP5 temperature biases and 21st century warming around the Antarctic coast. Annals of Glaciology 57: 68-78

MacAyeal DR. 1989. Large-scale ice flow over a viscous basal sediment: theory and application to Ice Stream B, Antarctica. Journal of Geophysical Reseach 94: 4071-87

Marshall J, Armour KC, Scott JR, Kostov Y, Hausmann U, et al. 2014. The ocean's role in polar climate change: asymmetric Arctic and Antarctic responses to greenhouse gas and ozone forcing. Philosophical Transactions of the Royal Society A 372

Marzeion B, Jarosch A, Hofer M. 2012. Past and future sea-level change from the surface mass balance of glaciers. The Cryosphere 6: 1295-1322

Masahiro W, Kamae Y, Masakazu Y, Oka A, Sato M, et al. 2013. Strengthening of ocean heat uptake efficiency associated with the recent climate hiatus. Geophysical Research Letters 40: 3175–9

Meier MF, Dyurgerov MB, Rick UK, O'Neil S, Pfeffer WT, Anderson, RS. 2007. Glaciers dominate eustatic sea-level rise in the 21st century. Science 24: 1064-1067

Millan R, Rignot E, Bernier V, Morlighem M, Dutrieux P. 2017. Bathymetry of the Amundsen Sea Embayment sector of West Antarctica from Operation IceBridge gravity and other data. Geophysical Reseach Letters 44: 1360-1368

Miller KG, Wright JD, Browning JV, Kulpecz A, Kominz M, et al. 2012. High tide of the warm Pliocene: Implications of global sea level for Antarctic deglaciation. Geology

Mitrovica J, Gomez N, Morrow E, Hay C, Latychev K, Tamisiea M. 2011. On the robustness of predictions of sea level fingerprints. Geophysical Journal International 187: 729-42

Moon T, Joughin I, Smith BE, Howat I. 2012. 21st-century evolution of Greenland outlet glacier velocities. Science 336: 576-9

Morland LW. 1987. Unconfined ice-shelf flow. In Dynamics of the West Antarctic Ice Sheet, ed. CJ van der Veen, J Oerlemans, pp. 99-116. New York: Sprinker

Mouginot J, Rignot E, Scheuchl B. 2014. Sustained increase in ice discharge from the Amundsen Sea Embayment, West Antarctica, from 1973 to 2013. Geophysical Reseach Letters 41: 1576-84

Oerlemans J. 1982. A model of the Antarctic ice sheet. Nature 297: 550-3

Pagani M, Liu J, LaRiviere JP, Ravelo AC. 2009. High Earth-system climate sensitivity determined from Pliocene carbon dioxide concentrations. Nature Geoscience 3: 27-30

Paolo FS, Fricker H, Padman L. 2015. Volume loss from Antarctic ice shelves is accelerating. Science Express

Pattyn F. 2003. A new three-dimensional higher-order thermomechanical ice sheet model: Basic sensitivity, ice stream development, and ice flow across subglacial lakes. Journal of Geophysical Research-Solid Earth 108: 2382

Pattyn F, Schoof C, Perichon L, Hindmarsh RCA, Bueler E, et al. 2012. Results of the Marine Ice Sheet Model Intercomparison Project, MISMIP. The Cryosphere 6: 573-88

Peltier WR. 2004. Global Glacial Isostasy and the Surface of the Ice-Age Earth: The ICE-5G(VM2) model and GRACE. Annual Reviews of Earth and Planetary Sciences 32

Pollard D, DeConto R. 2012. Description of a hybrid ice sheet-shelf model, and application to Antarctica. Geoscientific Model Development 5: 1273-95

Pollard D, DeConto RM. 2009. Modeling West Antarctic Ice Sheet growth and collapse through the last 5 million years. Nature 458: 329-32

Pollard D, DeConto RM, Alley RB. 2015. Potential Antarctic Ice Sheet retreat driven by hydrofracturing and ice cliff failure. Earth and Planetary Science Letters 412: 112-21

Pritchard HD, Ligtenberg SRM, Fricker HA, Vaughan DG, van den Broeke MR, Padman L. 2012. Antarctic ice-sheet loss driven by basal melting of ice shelves. Nature 484: 502-5

Radic V, Bliss A, Beedlow AC, Hock R, Miles E, Cogley JG. 2014. Regional and global projections of twenty-first century glacier mass changes in response to climate scenarios from global climate models. Climate Dynamics 42: 37-58

Rignot, Eric, G. Casassa, P. Gogineni, W. Krabill, A. U. Rivera, and R. Thomas. “Accelerated ice discharge from the Antarctic Peninsula following the collapse of Larsen B ice shelf.” Geophysical Research Letters 31, no. 18 (2004).

Rignot E, Mouginot J, Morlighem M, Seroussi H, Scheuchl B. 2014. Widespread, rapid grounding line retreat of Pine Island, Thwaites, Smith, and Kohler glaciers, West Antarctica, from 1992 to 2011. Geophysical Reseach Letters 41: 3502-9

Rignot E, Velicogna I, van den Broeke MR, Monaghan A, Lenaerts J. 2011. Acceleration of the contribution of the Greenland and Antarctic ice sheets to sea level rise. Geophysical Research Letters 38: L05503

E. Rignot, S. Jacobs, J. Mouginot, B. Scheuchl, Ice-shelf melting around Antarctica. Science 341, 266–270 (2013). Medline doi:10.1126/science.1235798

Ritz C, Rommelaere V, Dumas C. 2001. Modeling the evolution of Antarctic ice sheet over the last 420,000 years: Implications for altitude changes in the Vostok region. Journal of Geophysical Research-Atmospheres 106: 31943-64

Robinson A, Calov R, Ganopolski A. 2012. Multistability and critical thresholds of the Greenland ice sheet. 2: 429–32

Roemmich D, Gilson J. 2009. The 2004–2008 mean and annual cycle of temperature, salinity, and steric height in the global ocean from the Argo Program. Progress in Oceanography 82: 81-100

Rovere A, Raymo ME, Mitrovica JX, Hearty PJ, O’Leary MJ, Inglis JD. 2014. The Mid-Pliocene sea-level conundrum: Glacial isostasy, eustasy and dynamic topography. Earth and Planetary Science Letters 387: 27-33

Scambos TA, Bell RE, Alley B, Anandakrishnan S, Bromwich DH, et al. in review. How Much, How Fast?: A Review and Science Plan for Research on the Instability of Antarctica’s Thwaites Glacier in the 21st century. Global and Planetary Change

Scambos TA, Bohlander JA, Shuman CA, Skvarca P. 2004. Glacier acceleration and thinning after ice shelf collapse. Geophysical Research Letters 31: L18402

Scambos TA, Hulbe C, Fahnestock M, Bohlander J. 2000. The link between climate warming and break-up of ice shelves in the Antarctic Peninsula. Journal of Glaciology 46: 516-30

Schmidtko S, Heywood KJ, Thompson AF, Aoki S. 2014. Multidecadal warming of Antarctic waters. Science 346: 1227-31

Schoof C. 2007. Ice sheet grounding line dynamics: Steady states, stability, and hysteresis. Journal of Geophysical Research-Earth Surface 112: F03S28

Seddik H, Greve R, Zwinger T, Gillet-Chaulet F, Gagliardini O. 2012. Simulations of the Greenland ice sheet 100 years into the future with the full Stokes model Elmer/Ice. Journal of Glaciology 58: 427-40

Shepherd A, al. e. 2012. A reconciled estimate of ice-sheet mass balance. Science 388: 1183-9

Shepherd A, D. Wingham and E. Rignot. 2004. Warm ocean is eroding West Antarctic Ice Sheet. Goephysical Research Letters 31

Solomon S, Qin D, Manning M, Chen Z, Marquis M, et al, eds. 2007. IPCC, 2007: Climate Change 2007: The Physical Science Basis. Contribution of Working Group I to the Fourth Assessment Report of the Intergovernmental Panel on Climate Change. Cambridge, United Kingdom and New York, NY: Cambridge University Press. 996 pp.

Steig EJ, Ding Q, Battisti DS, Jenkins A. 2012. Tropical forcing of Circumpolar Deep Water Inflow and outlet glacier thinning in the Amundsen Sea Embayment, West Antarctica. Annals of Glaciology 53: 19-28

Stella FS, Stein S, Dixon TH, Craymer M, James TS, et al. 2007. Observation of glacial isostatic adjustment in ‘‘stable’’ North America with GPS. Geophysical Reseach Letters 34

Stone EJ, Lunt DJ, Annan JD, Hargreaves JC. 2013. Quantification of the Greenland ice sheet contribution to Last Interglacial sea level rise. Climate of the Past 9: 621-39

Thomas R. 2004. Force-perturbation analysis of recent thinning and acceleration of Jakobshavn Isbrae, Greenland. Journal of Glaciology 50: 57-66

Trusel LD, Frey KE, Das SB, Karnauskas KB, Munneke PK, et al. 2015. Divergent trajectories of Antarctic surface melt under two twenty-first-century climate scenarios. Nature Geoscience published online

Turner J, Lu H, White I, King JC, Phillips T, et al. 2016. Absence of 21st century warming on Antarctic Peninsula consistent with natural variability. Nature 535: 411-5

van den Broeke M, Bamber J, Ettema J, Rignot E, E. S, et al. 2009. Partitioning recent Greenland mass loss. Science 326: 984-6

van Vuuren DP, Edmonds J, Kainuma M, Riahi K, Thomson A, et al. 2011. The representative concentration pathways: an overview. Climatic Change 109: 5-31

Velicogna I, Sutterley TC, van den Broeke MR. 2014. Regional acceleration in ice mass loss from Greenland and Antarctica using GRACE time-variable gravity data. Journal of Geophysical Research Space Physics 119: 8130–7

Velicogna I, Wahr J. 2013. Time-variable gravity observations of ice sheet mass balance:Precision and limitations of the GRACE satellite data. Geophysical Research Letters 40: 3055-63

Weertman J. 1974. Stability of the junction of an ice sheet and an ice shelf. Journal of Glaciology 13: 3-11

Winkelmann R, Levermann A, Ridgwell A, Caldeira K. 2015. Combustion of available fossil fuel resources sufficient to eliminate the Antarctic Ice Sheet. Science Advances 1

Yau AM, Bender M, Robinson A, Brook E. 2016. Reconstructing the last interglacial at Summit, Greenland: Insights from GISP2. Proceeding of the National Academy of Sciences 113: 9710-5

Attachment 2
CoSMoS 3.0 Phase 2
Southern California Bight:
Summary of Data and Methods

Coastal Storm Modeling System (CoSMoS)

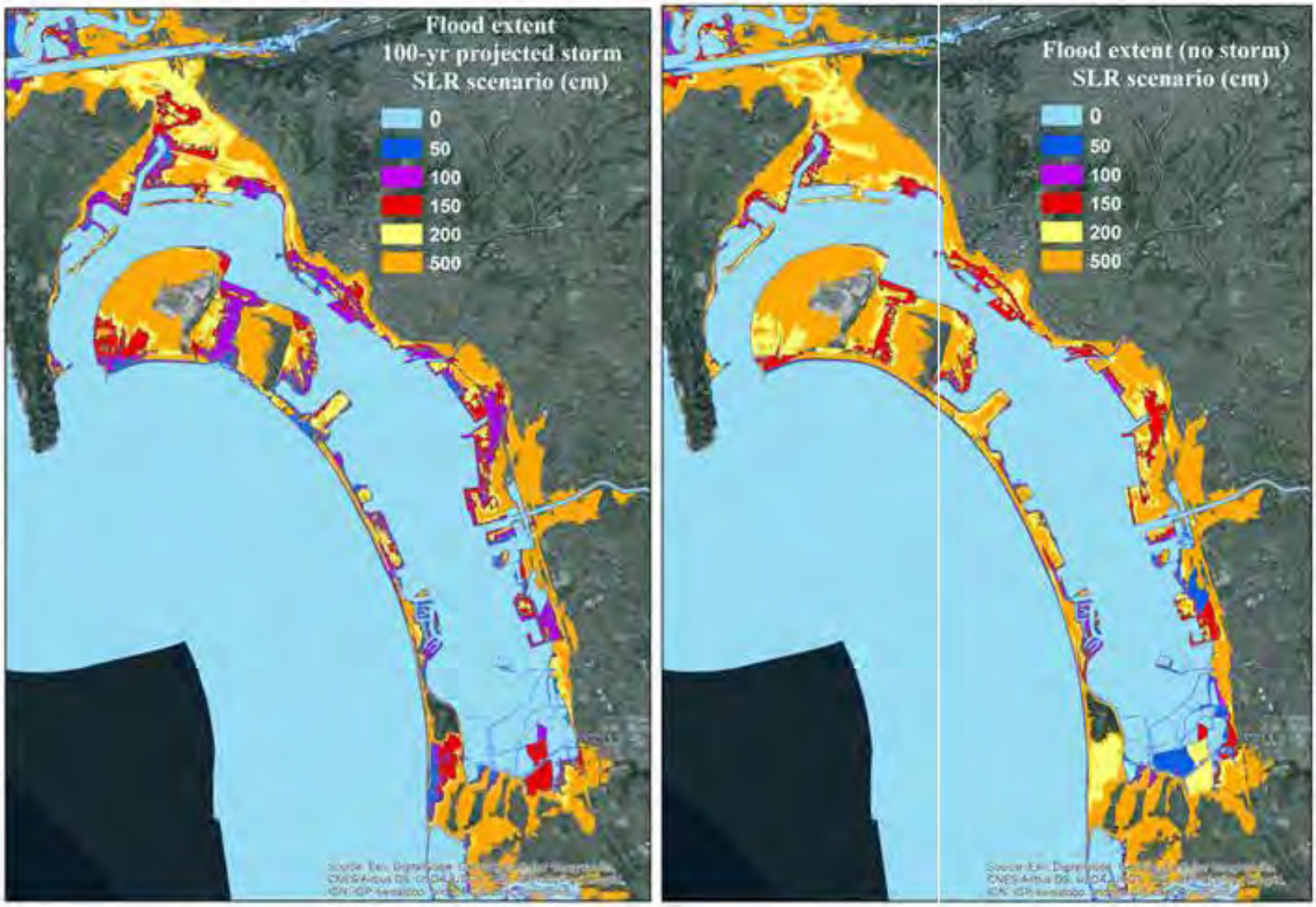

CoSMoS Coastal Storm Modeling System USGS

USGS science for a changing world

CoSMoS v3.0 Phase 2 Southern California Bight: Summary of methods

Table of Contents

CoSMoS 3.0 Phase 2 Southern California Bight: Summary of data and methods

By Li H. Erikson, Patrick L. Barnard, Andrea C. O'Neill, Sean Vitousek, Patrick Limber, Amy C. Foxgrover, Liv M. Herdman, and Jonathan Warrick

Suggested citation:

Erikson, L.H., Barnard, P.L., O'Neill, A.C., Vitousek, S., Limber, P., Foxgrover, A.C., Herdman, L.H., and Warrick, J., 2017. CoSMoS 3.0 Phase 2 Southern California Bight: Summary of data and methods. U.S. Geological Survey. http://dx.doi.org/10.5066/F7T151Q4

Executive Summary

Flood maps are regularly used for design, disaster, and hazard mitigation planning, but until relatively recently; little information exists on probable coastal flood hazards under conditions of climate change. Changes in atmospheric conditions, such as wind and pressure, can impart deviations in both magnitude and frequency of storm events compared to the past which, combined with sea-level rise (SLR) will affect coastal flood hazard projections.

With the aim of forecasting flood hazards, the USGS, in collaboration with Deltares, developed the Coastal Storm Modeling System (CoSMoS) for the Southern California Bight (Barnard and others, 2014; *http://cosmos.deltares.nl/SoCalCoastalHazards/index.html*). That first iteration of CoSMoS (version 1) focused on evaluating flood hazards associated with historical storms and two SLR scenarios; the system continues to run operationally for near-term forecasts of regional wave climate and water levels. The work presented here, extends upon the initial CoSMoS work to include 1) high resolution grids for better representation of harbors, lagoons, bays, estuaries, and overland flow, 2) fluvial discharges that might locally impede and amplify flooding associated with coastal storms, 3) long-term morphodynamic change integrated into the coastal flooding projections, 4) uncertainty associated with terrain models, numerical model errors and vertical land motion, and 5) alterations to coastal storm intensity and frequency associated with a changing climate.

This report summarizes data and methods used to develop CoSMoS version 3.0 and its application to the approximately 480 km shoreline extending from the U.S. / Mexico border to Point Conception, CA. CoSMoS 3.0 downscales 21st century ocean and coastal storms from the global to local scale. Winds, sea level pressures, and sea surface temperatures derived from global climate models, were used to compute waves, storm surges, and sea level anomalies, for the 21st century. From this projected time-series, multiple storm events for select return periods were identified along different sections of the coast; these were modeled in detail using a train of numerical models that account for the combined effects of storm intensity, direction, sea-level rise, astronomic tides, and long-term morphologic change.

A total of 40 scenarios were simulated and represent potential future flood hazards associated with 3 storms (1-year, 20-year, and 100-year) and a background atmospheric condition in combination with present day mean sea level and 9 additional SLR scenarios (0.25 meters (m) to 2 m at 0.25 m increments and 5 m). Results have been synthesized and are available for download as Google Earth kmz files,

ArcGIS shapefiles, or GeoTIFFs at *http://walrus.wr.usgs.gov/coastal_processes/cosmos/socal3.0/index.html*. See Appendix A for data and format descriptions of downloadable files. A tool for visualization, data analysis, and additional downloadable data is available at http://*ourcoastourfuture.org*.

Disclaimer: The data and maps included in these files are intended to improve flood hazard awareness and preparedness associated with climate change; however, they do not guarantee the safety of an individual or structure. The U.S. Geological Survey provides these maps as a planning tool but assumes no legal liability or responsibility resulting from the use of this information.

Section 1. Study Area

The Southern California Bight (SCB) extends from the U.S. / Mexican border northwestward to Point Conception and encompasses ~ 480 kilometers (km) of open coast shoreline, punctuated by river mouths, bays, lagoons, and estuaries (fig. 1). The coast hosts a complex mixture of beach settings variably backed by narrow to wide beaches, dunes, low to high cliffs, and urban infrastructure.

Tectonic controls along the Pacific and North American plate boundary has resulted in the region being fronted by a narrow continental shelf (< 20 kilometers, km), a series of islands (Channel Islands) that can shelter portions of the coastline from open ocean swell, and a highly irregular complex bathymetry that hosts a plethora of submerged seamounts, troughs, and canyons (Christensen and Yeats, 1992; Hogarth and others, 2007). The seamounts, knolls, canyons, and Channel Islands significantly alter the open ocean deep water wave climate to a more complicated nearshore wave field (O'Reilly and Guza, 1993; O'Reilly and others, 1999; Rogers and others, 2007; Adams and others, 2011). Swell dominate the nearshore wave energy, but locally generated wind-waves comprise ~40% of the total wave energy spectrum (Crosby, 2016).

Astronomic tides are mixed semidiurnal with a mean tide range of 1.12 m to 1.23 m depending on location within the SCB (National Oceanic and Atmospheric Administration, NOAA, 2016; stations 9410230, 9411340, 941070, and 9410840). Tides travel from southeast to northwest, with high tide taking ~30 minutes to transit from San Diego to Point Conception.

Measured sea level rise (SLR) rates range from 0.95 millimeters/year (mm/yr) to 2.22 mm/year amongst 6 tide gauges located within the SCB, each with >30 years of sea level measurements (NOAA, *https://tidesandcurrents.noaa.gov/sltrends/sltrends.html*, accessed November 2016). Extensive studies that incorporate observations and modeling of climate change-induced SLR, project an acceleration in the rate and that an upper extreme level of 2.88 m may be reached by the year 2100, with a median projection of 0.74 m and 1.37 m for the representative concentration pathway (RCP) 4.5 and RCP 8.5 scenarios, respectively (Cayan and others, 2016).

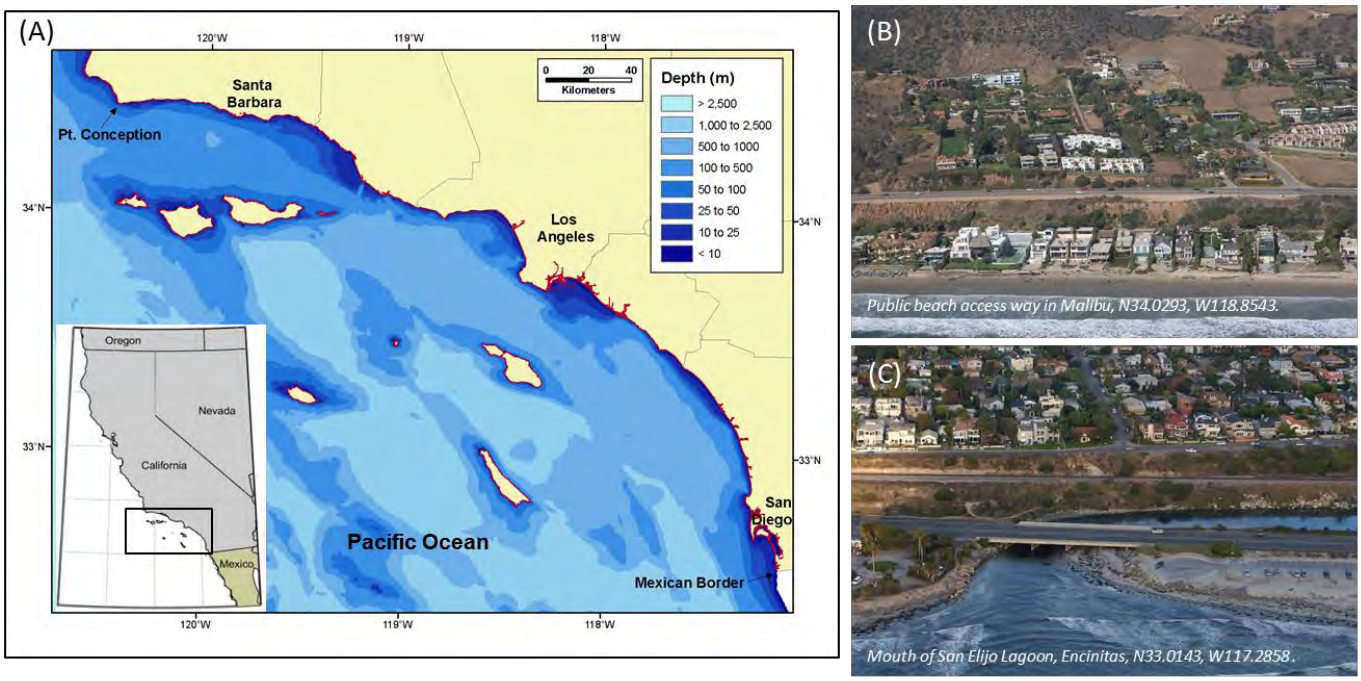

Figure 1. Map of study area and example photos of urbanized coastal sections. (A) Map of the Southern California Bight and bathymetry. (B and C) Images 200801843 and 200407620 downloaded from California Coastal Records Project, *www.californiacoastline.org*, copyright © 2002-2015 Kenneth & Gabrielle Adelman (last accessed December 2016).

Section 2. CoSMoS 3.0 model overview

CoSMoS 3.0 is comprised of one global scale wave model and a suite of regional and local scale models that simulate coastal hazards in response to projections of 21st century waves, storm surge, anomalous variations in water levels, river discharge, tides, and sea-level rise (table1; fig. 2). In CoSMoS 3.0 Phase 2, a total of 40 scenarios, resulting from the combination of 10 sea levels, 3 storm conditions, and one background condition were simulated. Sea-level rise ranged from 0 m to 2 m, at 0.25 m increments, plus an additional 5 m extreme. Future storm conditions represent the 1-year, 20-year, and 100-year return level coastal storm events, as derived and downscaled from winds, sea-level pressures (SLPs), and sea-surface temperatures (SSTs) of the RCP 4.5, GFDL-ESM2M global climate model (GCM).

Ocean waves, including both local seas and swell generated from distant storms across the Pacific Ocean, are the largest contributor to coastal flooding along the open coast of California during storm events. Thus, future wave conditions are first simulated with the global-scale WaveWatch III (WW3) model. Section 3.1 provides more detail on the global scale wave model.

Projected deep water waves computed with the global scale wave model are propagated to shore with a suite of regional (Tier I) and local (Tiers II and III) models that additionally simulate regional and local wave growth (seas) in combination with long-term and event-driven morphodynamic change and

water level changes due to astronomic tides, winds, sea-level pressure, steric effects, and sea-level rise (fig. 2).

Table 1. Models employed in CoSMoS.

Spatial scale	Model
Global scale	WaveWatch III
Regional scale (Tier I)	Delft3D FLOW and WAVE models
Local scale (Tier II)	Delft3D FLOW and WAVE models
Local scale (Tier III)	XBeach cross shore profile models

The regional Tier I model consists of one Delft3D hydrodynamic FLOW grid for computation of currents and water level variations (astronomic tides, storm surge, and steric effects) and one SWAN grid for computation of wave generation and propagation across the continental shelf. Wave conditions from the global wave model are applied at the open-boundaries of the SWAN model. The FLOW and SWAN models are two-way coupled so that tidal currents are accounted for in wave propagation and growth and conversely, that orbital velocities generated by waves impart changes on tidal currents. See Section 3.2 for more details on Tier I.

Employing high-resolution grids for fine-scale modeling of the entire study is not possible using desktop computers and therefore Tier II was segmented into 11 sections. Each sub-model consists of two SWAN grids and multiple FLOW grids. Wave and water level time-series of the Tier I model are applied at the open boundaries of each Tier II sub-model. See Section 3.3 and Section 3.5 for more details on Tier II.

Tier III consists of more than 4,000 cross-shore XBeach (eXtreme Beach) models that simulate event-driven morphodynamic change, water level variations, and infragravity wave runup every ~100 m alongshore. Wave runup is the maximum vertical extent of wave uprush on a beach or structure above the still water level, and in cases where infragravity waves exist, the reach of wave runup can be significantly further inland compared to wave runup driven by shorter incident waves (Roelvink and others, 2009). The U.S. west coast is particularly susceptible to infragravity wave runup due to the prevalence of breaking long-period swell (low wave steepness) across wide, mildly sloping (dissipative) beaches that result in a shoreward decay of incident wave energy and accompanying growth of infragravity energy.

In Phase 1 of CoSMoS 3.0, cross-shore profiles were extracted from a 2 meter (m) resolution seamless digital elevation model (DEM; USGS CoNED, 2016) and used as initial conditions for each of the >4,000 XBeach model runs, independent of the sea level scenario simulated. In Phase 2, long-term morphodynamic change resulting from SLR and changing wave conditions, was first modeled and used as initial conditions for each detailed flood simulation associated with the prescribed storm and SLR combinations. See Section 3.4 for more details on Tier III.

The methods and data presented in this report apply to both Phase 1 and 2 of CoSMoS version 3.0. Phase I differs from Phase II in that 1) long-term morphodynamic change was not included in the simulations and 2) only the 100-year storm (in combination with all SLR scenarios) was simulated.

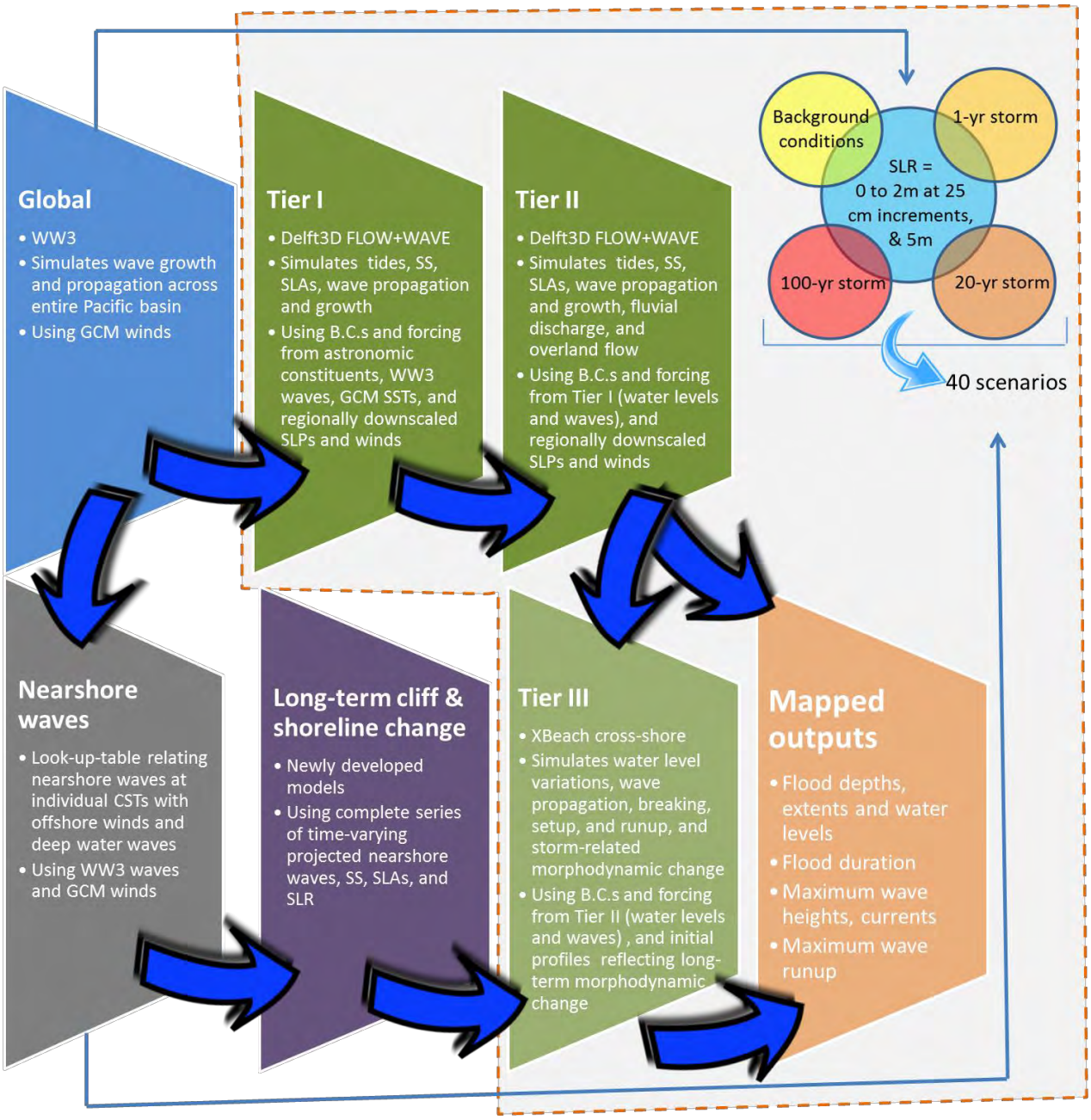

Figure 2. Schematic of CoSMoS version 3.0 Phase 2 numerical model approach for simulating coastal storm flooding under the influence of climate change. Each trapezoid represents individual components in the model train. Thin blue arrows denote the use of global climate data for *a priori* determination of coastal storm events; events were subsequently modeled in detail with Tiers I through III (grouped and shown with dashed line). The approach applies to CoSMoS version 3.0 Phase 1 as well, except that long-term morphodynamic change was not included and only the 100-year storm was simulated. Abbreviations: WW3: WaveWatch3; CST: cross shore transect; SLR: sea-level rise; SLP: sea-level pressure; GCM: global climate model; SLA: sea level anomalies; SS: storm surge; B.C.s: boundary conditions.

Section 3. Models and data

3.1 Global scale wave model

Grids, model settings, and bathymetry

The third-generation, spectral wave model WaveWatch III (WW3, version 3.14, Tolman, 2009) was used to project future wave conditions. The model was applied over a near-global grid (NWW3, latitude 80°S–80°N) with 1°x 1.25° spatial resolution, and a one-way nested Eastern North Pacific (ENP) grid with 0.25° spatial resolution (~27 km at latitude 37°N). Bathymetry and shoreline positions were populated with the 2-minute Naval Research Laboratory Digital Bathymetry Data Base (DBDB2) v3.0 and National Geophysical Data Center Global Self-Consistent Hierarchical High-Resolution Shoreline (GSHHS, Wessel and Smith, 2006). Wave spectra were computed with 15° directional resolution and 25 frequency bands ranging non-linearly from 0.04 to 0.5 Hz. Wind-wave growth and whitecapping was modeled with the Tolman and Chalikov (1996) source term package and nonlinear quadruplet wave interactions were computed with the Hasselmann and others (1985) formulation. Bulk wave parameter statistics (significant wave height, H_s; peak wave period, T_p; and peak wave direction, D_p) were saved hourly at points in deep water, offshore of the continental shelf. Time-series model outputs from a point coincident with the Scripps Institution of Oceanography California Data Information Program (CDIP) buoy 067 (33.221ºN, 119.881ºW) were used as deep water boundary conditions for running Tier I storm event and SLR scenarios for CoSMoS ver. 3.0.

Boundary forcing

Wind speeds and directions for years 2010 through 2100 computed with the National Oceanographic and Atmospheric Administration (NOAA) Geophysical Fluid Dynamics Laboratory earth systems global climate model (GCM) GFDL-ESM2M (Dunne and others, 2012; data download available at *http://nomads.gfdl.noaa.gov:8080/DataPortal/cmip5.jsp*) were used to drive the WW3 wave model. GFDL-ESM2M simulations employ coupling between global-scale atmosphere and ocean circulation models. The atmospheric component includes physical features such as aerosols (both natural and anthropogenic), cloud physics, precipitation, and evaporation; the oceanic model includes such processes as water fluxes, currents, sea ice dynamics and a representation of ocean mixing.

GFDL-ESM2M near-surface wind data are available at 10 m, neutrally stable fields on a 2.5º x 1.5º grid at a 3 hour time-step. Prior to running the WW3 model, east-west and north-south directed wind fields were linearly interpolated to the WW3 grid resolutions. The GFDL-ESM2M model was selected amongst the various GCMs available because 1) of the relatively high temporal model output resolution (3- hourly) of atmospheric fields, 2) the time-series included the entire 21st century as opposed to just the mid- and end-of century as was the case for most of the GCMs at the onset of the CoSMoS study, and 3) relatively good agreement between downscaled historical wave conditions compared to observations, particularly for the extreme events along this coastline (Erikson and others, 2015).

Whereas a complete time-series for the 21st century was modeled with WW3 and used for selection of storm events, deep water wave conditions for the mid- (2026-2045) and end-of-century (2081-2100) time-periods were also simulated and compared to the RCP 8.5 climate scenario. Comparisons between

modeled hind-casts (1976-2005) and the mid- and end- of century time-slices showed that for both climate scenarios, wave height is projected to slightly decrease offshore of Southern California and that a greater decrease is expected with RCP 8.5 (Erikson and others, 2015). Thus, this study was limited to the more conservative RCP 4.5, the climate scenario with likely higher future wave heights in the study area.

The climate scenarios were defined by the fifth phase of the Coupled Model Inter-comparison Project (CMIP5) and represent trajectories of increasing global radiative forcing that reach 4.5 W/m^2 and 8.5 W/m^2 by the year 2100, relative to pre-industrial (1850) radiative forcing (Hibbard and others, 2007). RCP 8.5 represents a high radiative forcing (Moss and others, 2010), and is roughly equivalent to the A2 emission scenarios of the IPCC CMIP3 Special Report on Emission Scenarios (SRES) (Meinshausen and others 2011). RCP 4.5 represents a scenario of medium radiative forcing with the onset of stabilization by mid-century, and is roughly equivalent to the B1 IPCC CMIP3 scenario.

3.2 Regional scale wave and hydrodynamic model - Tier I

Grids, model settings, and bathymetry

The WAVE and FLOW modules of the Delft3D version 4.01.00 were used to simulate waves and hydrodynamics, respectively. The WAVE module allows for two-way coupling (communication) between wave computations and FLOW hydrodynamics and simulates waves with the numerical model SWAN (Simulating Waves Nearshore, Delft University of Technology). SWAN is a commonly used third-generation spectral wave model specifically developed for nearshore wave simulations that account for propagation, refraction, dissipation, and depth-induced breaking (Booij and others, 1999; Ris, 1999). The SWAN model was run in a stationary mode, with settings identical to Rogers and others (2007): JONSWAP spectrum with peak enhancement factor of 3.3 at the open boundary forcing, 36 directional bins (i.e., 10° discretization), and 35 frequencies with logarithmic spacing from 0.0418 Hz to 1.00 Hz. Depth induced breaking was computed with the Battjes and Janssen (1978) formulation and a breaking index of 0.73; whitecapping is described with the default Komen and others (1994) expression. Bottom friction is based on the JONSWAP formulation, with the friction coefficient set at 0.067 m^2/s (Hasselmann and others, 1973).

Delft3D-FLOW, developed by WL/Delft Hydraulics and Delft University of Technology, is a widely used numerical model that calculates non-steady flows and transport phenomena resulting from tidal and meteorological forcing (Lesser and others, 2004).The Tier I FLOW model was run with the following settings: water density equal to 1025 kg/m^3, uniform Chezy bed roughness of 65, the Fredsoe stress formulation due to wave forces, a uniform horizontal viscosity of 1 m^2/s, and a linear wind drag model with coefficients of 6.3e-4 and 7.2e-3 at breakpoints of 0 m/s and 100 m/s wind speeds. FLOW models are run with a 30 second time-step and communication with the WAVE module every 20 minutes.

Tier I SWAN and FLOW models consist of identical structured curvilinear grids that extend from shore to ~200 km offshore in water depths > 1,000 m and range in resolution from 1.2 km x 2.5 km in the nearshore to 3.5 km x 5 km in the offshore. The two-way coupled model was run in a spherical coordinate system and with FLOW in a vertically-averaged mode (2DH). Bathymetry was derived from the National Geophysical Data Center (NGDC) Coastal Relief Model (*http://www.ngdc.noaa.gov/mgg/coastal/coastal.html*).

Boundary forcing

Tidal forcing

Spatially varying astronomic tidal amplitudes and phases derived from the Oregon State University (OSU) TOPEX/Poseidon global tide database (Egbert and others, 1994) were applied along all open boundaries of the Tier I FLOW grid. A total of 13 constituents were represented: M2, S2, N2, K2, K1, O1, P1, Q1, MF, MM, M4, MS4, and MN4.

Sea level anomalies

Sea level anomalies due to large-scale meteorological and oceanographic processes unrelated to storms, were applied along all open boundaries of the Tier I FLOW grid. Elevated sea-level anomalies (SLAs) are often observed in conjunction with El Niño events (Flick, 1998; Storlazzi and Griggs, 1998; Bromirski and others, 2003) and yield water levels of 10-20 cm above normal for several months (Cayan and others, 2008).

In an effort to maintain simplicity, correlations of SLAs with sea surface temperature anomalies (SSTAs) were developed. Both observed and GCM SSTAs are readily available (making it simple to use) and are physically linked to SLAs via direct correspondence to thermal expansion (i.e., thermosteric) and indirectly to changes in large scale wind patterns. SSTAs were computed by subtracting out the long term mean (1971 to 2000; Reynolds and others, 2002) from a satellite-derived SST time-series spanning the years 1981 through 2014 (NOAA/OAR/ESRL PSD). A linear least-square fit through the upper envelope of mean monthly SSTAs and SLAs measured at La Jolla resulted in the empirical equation (r = 0.90, fig. 3),

$$SLA = C_0 + C_1 \cdot \text{SSTA} \qquad (3)$$

where the empirical coefficients C_0 and C_1 were found to equal 0.0546 and 0.0745, respectively. The upper envelope was defined by the maximum SLA within 0.25° SSTA bins from -2.0°C to +2.5°C. A fit through the upper envelope, rather than all the data, was done ensuring a positive SLA for higher SSTAs. Due to scatter in the data and relatively small SLAs, a fit through all data would yield only a slight positive SLA (~0.10 m) for the maximum observed SSTA.

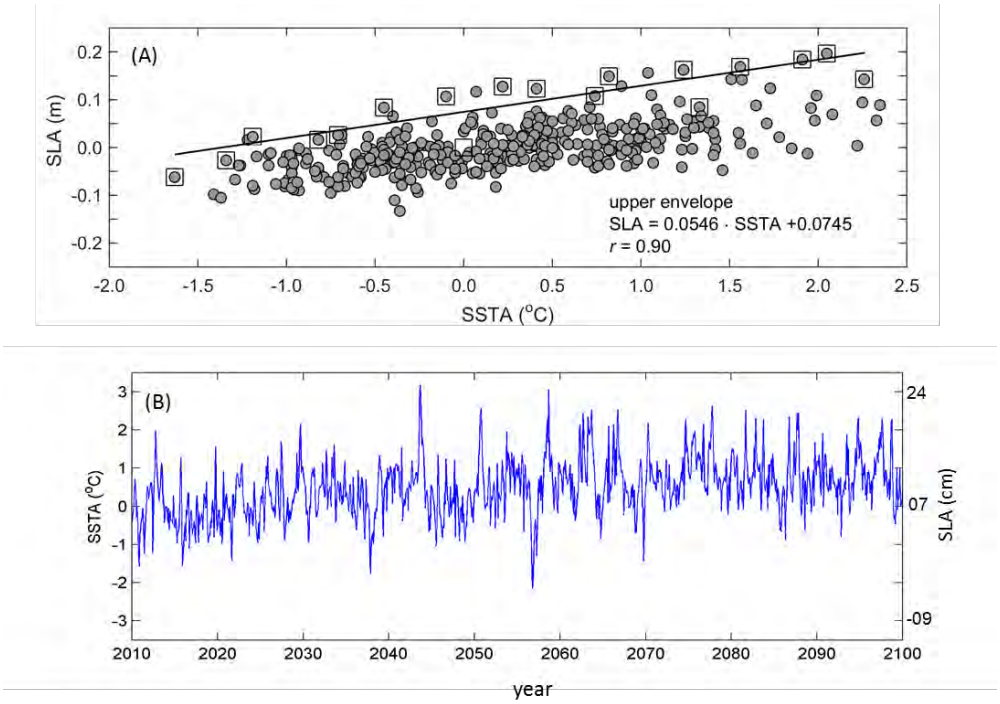

Figure 3. Plots illustrating the empirical relationship and results of sea level anomalies (SLAs) used in model simulations. (A) Linear regression model relating sea surface temperature anomalies (SSTA) and SLAs at La Jolla, CA. Squares highlight the data points of the upper envelope that were used to derive the linear model (solid line). (B) Projected SSTAs (left-hand y-axis) and SLAs (right-hand y-axis).

Atmospheric forcing

Space- and time-varying wind (split into eastward and northward components) and sea level pressure (SLP) fields were applied to all grid cells at each model time-step. The wind and SLP fields were input as equidistant points spaced 10 km apart and interpolated within the Delft3D model to the SWAN and FLOW grids. An average pressure of 101.3 kiloPascals (kPa) was applied to the open boundaries of the meteorological grid.

Winds and SLPs stem from a recently (2015) derived 10 km resolution dataset of hourly winds and sea level pressures. The California Reanalysis Downscaling at 10km (CaRD10) is a reconstruction of the high-spatial resolution / high-temporal scale analysis of atmosphere and land covering the state of California for global change studies (Kanamitsu and Kanamaru, 2007; SIO, 2015). CaRD10 data is generated by dynamically downscaling coarse atmospheric data using Scripps' Experimental Climate Prediction Center Hydrostatic Global to Regional Spectral Model (G-RSM). The downscaling includes scale-selective bias corrections to suppress large scale errors, yet stay true to the large scale forcing fields, and does not use any observations except sea surface temperatures (SSTs) to adjust the results. Two sub-sections of the CaRD10 database were used for CoSMoS application to the Southern California study region: 1) a hindcast period derived from dynamical downscaling of the National Centers for Environmental Prediction (NCEP) Global Forecast System (GFS) model Global Reanalysis (available years 1975 to 2010 at 32 km, 3 hourly resolution) and 2) a future period (2011 – 2100 at 2.5° x 1.5°, 3 hourly resolution) derived from the same RCP4.5 GFDL-ESM2M GCM used in the global-scale wave downscaling.

Deep water wave forcing

Deep water wave parameters (H_s, T_p, and D_p), obtained with the WW3 model for the CDIP067 buoy were applied along all open boundaries of the Tier I SWAN grid. Alongshore variations in deep water wave forcing available with the WW3 model outputs were small, particularly with respect to incident wave directions, which are critical to accurate computations of wave propagation from deepwater to the SCB nearshore region where sheltering effects are important (Rogers and others 2007).

3.3 Local scale 2D wave and hydrodynamic model – Tier II

Grids, model settings, bathymetry and topography

Tier II consists of 11 local-scale sub-models, each consisting of two SWAN grids and multiple FLOW grids (fig. 4). San Diego and Los Angeles Counties each include three sub-models, Orange and Ventura Counties two sub-models, and Santa Barbara was comprised of one sub-model (Table 2). Physical overlap exists between sub-models along-shore extents in order to avoid erroneous boundary effects in regions of interest.

Each Tier II hydrodynamic FLOW sub-model consists of one 'outer' grid and multiple two-way coupled 'domain decomposition' (DD) structured grids. DD allows for local grid refinement where higher resolution (~10 m - 50 m) is needed to adequately simulate the physical processes and resolve detailed flow dynamics and overland flood extents. Communication between the grids takes place along internal boundaries where higher-resolution grids are refined by 3 or 5 times that of the connected grid. This DD technique allows for two-way communication between the grids and for simultaneous simulation of multiple domains (parallel computing), reducing total computation time while maintaining high resolution computations.

In the landward direction, Tier II DD FLOW grids extend to the 10 m topographic contour; exceptions exist where channels (e.g., the Los Angeles River) or other low-lying regions reach very far inland. The number of DD FLOW grids ranges from 4 to 13, depending on local geography, bathymetry, and overall setting. Grid resolution ranges from approximately 130 m x 145 m (across and along-shore, respectively) in the offshore region to as fine as 5 m x 15 m in the nearshore and overland regions.

Wave computations are accomplished with the SWAN model using two grids for each Tier II sub-model: one larger grid covering the same area as the 'outer' FLOW grid and a second finer-resolution two-way coupled nearshore nested grid. The nearshore SWAN grids extend from at least the 30 m isobath to well inland of the present day shoreline. The landward extension is included to allow for wave computations of the higher SLR scenarios.

All model settings of the Tier II domains are identical to those used for Tier I runs, with the exception of the time-step (10 seconds) and threshold depth (1 cm) in the hydrodynamic FLOW models. The threshold depth is used within the model to assign a grid cell as either wet or dry. For the flooding and drying scheme, the bottom is assumed to be represented as a staircase of tiles centered around the grid cell water level points. If the total water level drops below 1 cm, then the grid cell is set to dry. The grid cell is again set to wet when the water level rises and the total water depth is greater than the threshold.

Table 2. Tier II sub-model extents, number of grids, and grid resolutions.

Sub-model name	Geographic extents* (north to south)	Counties**	Number of DD grids	Grid resolution (m)	
				Most coarse*	Finest
gc	Point Conception to Carpinteria	SB	6	70 x 90	18 x 16
ve	Carpinteria to Oxnard Beach	SB / VE	13	100 x 110	5 x 15
is	Oxnard Beach to Point Mugu	VE	6	90 x 90	5 x 15
pm	Point Mugu to Malibu	VE /LA	8	100 x 110	20 x 20
mk	Malibu to Palos Verdes	LA	4	130 x 145	30 x 40
la	Palos Verdes to Seal Beach	LA / OR	4	90 x 115	25 x 45
oc	Seal Beach to Huntington Bch.	OR	12	7 x 11	35 x 65
np	Huntington Bch to San Clemente	OR	9	70 x 85	5 x 8
cb	San Clemente to Encinitas	OR / SD	9	30 x 60	10 x 15
ty	Encinitas to La Jolla	SD	6	30 x 60	10 x 20
sd	La Jolla to Punta Bandera	SD	9	90 x 140	10 x 13

* excluding the 'outer' FLOW grid but including grids where XBeach is used for flooding calculations
** SB: Santa Barbara; VE: Ventura; LA: Los Angeles; OR: Orange; SD: San Diego

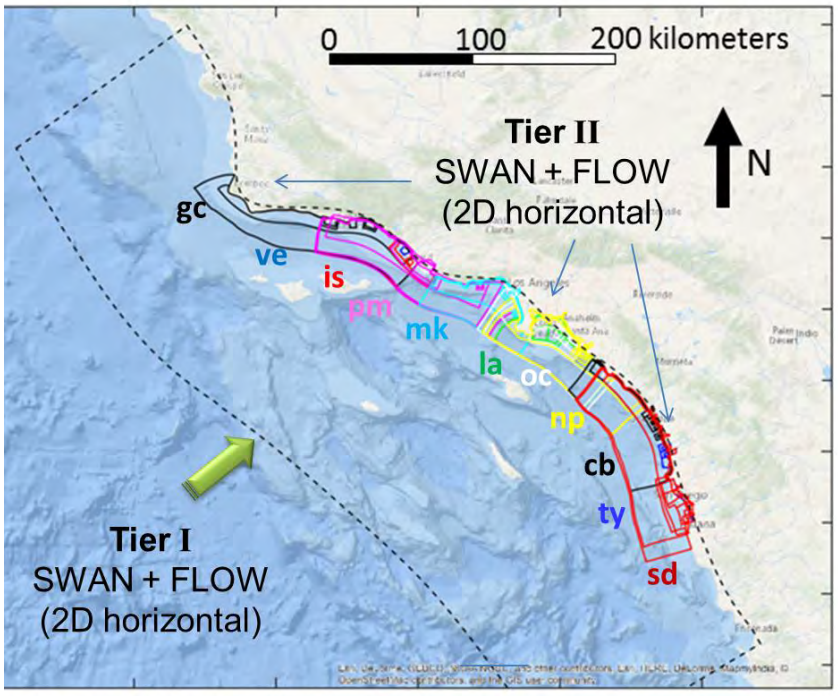

Figure 4. Map showing Tier II model grid extents.

Bathymetry and topography is represented with a seamless digital elevation model (DEM) constructed by the USGS Coastal National Elevation Database (CoNED) team using the most recent, high-resolution topographic and bathymetric datasets available (http://topotools.cr.usgs.gov/coned/index.php). Topography is composed of bare-earth data derived from topographic and bathymetric light detection and ranging (Lidar) data and bathymetry from multi-and single-beam sonars. The DEM was constructed to define the shape of nearshore, beach, and cliff surfaces

as accurately as possible, utilizing dozens of bathymetric and topographic data sets. The vast majority of the data was derived from the Coastal California Data Merge Project which includes lidar data collected from 2009 through 2011 and multi-beam bathymetry collected between 1996 and 2011 extending out to the three nautical mile limit of California's state waters (NOAA, 2016; *https://catalog.data.gov/dataset/2013-noaa-coastal-california-topobathy-merge-project*). Harbors and some void areas in the nearshore were filled in with bathymetry from either more recent multi-beam surveys, 1/3 arc-second (~10 m resolution) NOAA coastal relief model data, or single-beam bathymetry. In deeper waters offshore of the three nautical mile limit (~5.6 km) the 10 m resolution NOAA coastal relief models were used (*http://www.ngdc.noaa.gov/dem/squareCellGrid/map*). Following compilation of the topography and bathymetry data, the DEM was 'hydro-enforced' to provide water flow connectivity between open sluices, canals, and under bridges and piers. The final nearshore DEM consists of 2 m resolution data extending from the 20 m isobath to the 20 m elevation contour. These data were used to populate the majority of the Tier II grids and generate initial profiles for the 0 m SLR of the nearly 4,500 cross-shore transects (CSTs) used for Tier III XBeach modeling. A second DEM of 10 m gridded resolution is used to represent deeper water conditions extending seaward of the three nautical mile limit. All data are referenced to the NAD83 and NAVD88 horizontal and vertical datums, respectively, and both Tier II and Tier III models run in projected UTM (zone 11 S) coordinates.

Boundary forcing

Water level and Neumann time-series, extracted from Tier I simulations, were applied to the shore parallel and lateral open boundaries of each Tier II 'sub-model outer' grid, respectively. Several of the sub-models proved to be unstable with lateral Neumann boundaries; for those cases one or both of the lateral boundaries were converted to water level time-series or left unassigned. The open boundary time-series were extracted from completed Tier I simulations so that there is no communication from Tier II to Tier I (i.e. one-way communication).

The water level time-series extracted from Tier I and applied at the open boundaries of the 'nested' sub-models included variations due to tides, SLAs and storm surge, the latter of which is computed with spatial and time-varying winds and SLPs across the continental shelf. In order to account for further contributions of winds and SLPs to storm surge related wind-setup at the shore and local inverse barometer effects (IBE, rise or depression of water levels in response to atmospheric pressure gradients), the same 10 km hourly resolution winds used in Tier I are also applied to each grid cell in the Tier II sub-models.

A set of gauged and ungauged rivers and tributaries considered most relevant in influencing coastal flooding were selected and included in the Tier II sub-models. A total of 41 time-varying fluvial discharges are applied either at the closed boundaries or distributed as point sources across grid cells within the relevant model domains (table 3). See Section 3.6 for explanations of how the time-series were derived.

Table 3. Fluvial discharge points included in Tier II model runs.

River or creek	Longitude (DD)	Latitude (DD)	Tier II sub-model	River or creek	Longitude (DD)	Latitude (DD)	Tier II sub-model
Jalama	-120.49939	34.51268	gc	Los Angeles	-118.18076	33.80757	la, np
Gaviota	-120.23122	34.47670	gc	San Gabriel	-118.07196	33.77822	la
Refugio	-120.06830	34.46742	gc	Bolsa Chica	-118.03087	33.71205	oc
El Capitan	-120.02231	34.46286	gc	Newport Bay	-117.83347	33.66012	np
Goleta3	-119.83536	34.43268	gc	Santa Ana	-117.94888	33.65797	la
Goleta4	-119.81935	34.43188	gc	San Juan	-117.66907	33.45832	sd
Goleta	-119.85164	34.43088	gc	San Mateo	-117.57813	33.38536	cb
Goleta2	-119.85164	34.43088	gc	San Onofre	-117.57183	33.37625	cb
Devereux	-119.86817	34.41682	gc	Santa Margarita	-117.38939	33.23724	cb
Arroyo Burro	-119.74090	34.40523	gc	San Luis Rey	-117.37455	33.20970	cb
Carpinteria SM1	-119.52549	34.40462	gc	Buena Vista	-117.33367	33.18381	cb
Carpinteria SM2	-119.52549	34.40462	gc	Agua Hedionda	-117.30445	33.14778	cb
Rincon	-119.47326	34.37774	gc	Batiquitos	-117.26057	33.09203	cb, ty
Ventura	-119.30830	34.28100	gc, is	San Elijo	-117.25114	33.01976	ty
Santa Clara	-119.25637	34.24017	is, ve	Del Mar	-117.23189	32.97878	ty
Calleguas	-119.08061	34.11838	is	Pensaquitos	-117.20610	32.91575	ty
Mailbu	-118.68000	34.04093	mk, pm	San Diego	-117.19646	32.76264	sd
Mission	-118.08840	34.01668	gc	Sweetwater	-117.05831	32.63631	sd
Ballona	-118.42808	33.97935	mk	Otay	-117.08671	32.59734	sd
Carbon Creek	-124.03430	33.87050	la, np	Tijuana	-117.10233	32.56456	sd
Dominguez	-118.25991	33.81453	la				

Time- and space-varying 2D wave spectra extracted from completed Tier I simulations were applied approximately every km along the open boundaries of the 'outer' Tier II sub-model SWAN grids. Space and time-varying wind fields were also applied to both Tier II SWAN grids to allow for computation of local wave generation.

3.4 Local scale 1D wave and hydrodynamic model – Tier III

Grids, model settings, bathymetry and topography

Nearshore hydrodynamics, wave setup, total wave runup and event-based erosion were simulated with the XBeach (eXtreme Beach) version 1.21.3667 (2014) model (Roelvink and others, 2009). XBeach is a morphodynamic storm impact model specifically designed to simulate beach and dune erosion, overwash, and flooding of sandy coasts. XBeach was run in a profile mode, at 4,466 CSTs numbered consecutively from 1 at the U.S. / Mexico border to 4,802, north of Point Conception. Profiles across harbor mouths, inlets, etc. were excluded from the XBeach simulations. Each of the profiles extend from the approximate -15 m isobath to at least 10 m above NAVD88 but are truncated in cases where a lagoon

or other waterway exists on the landward end of the profile. Two meter resolution bathymetry and topography were extracted from the seamless DEM (see section 3.3) along each of the CSTs and resampled to generate a cross shore grid with relatively larger grid cells offshore, hence reducing run times. In simulations with increased SLR, the original profiles were modified to represent long-term morphodynamic change (see section 3.5). Cross shore grid resolution ranged from 5 m onshore and in shallow water depths to between 25 m and 35 m in the offshore, depending on long wave resolution at the offshore boundary, depth to grid size ratio, and grid size smoothness constraints.

Sediment transport was computed in XBEACH with the Soulsby-van Rijn (Soulsby, 1997) transport formula and bore averaged equilibrium sediment concentrations. A median grain diameter of 0.25 mm and sediment thickness of 2 m was assumed for all profile models. Bottom roughness is set to a uniform Chezy value of 65, horizontal background viscosity of 0.01 m^2/s, and a flooding and drying threshold depth of 1 cm, similar to Tier II. Initial profile sections of steepness in excess of 32° (angle of repose of natural sand) are assumed to be hard structures or cliffs and set to be immobile (not allowed to erode or accrete during the storm). All simulations are run with a morphological acceleration factor of 10 to speed up the morphological time scale relative to the hydrodynamic timescale and thus reduce computation time.

With regards to wave computations, the XBeach model was run with an instationary wave solver but in a hydrostatic (no vertical pressure gradients) mode, and thus computed hydrodynamics and morphodynamic change associated with wave groups rather than individual waves. Wave breaking and dissipation is modeled after Roelvink (1993) where dissipation is proportional to the wave height to the third order divided by local water depth.

Boundary forcing

Hourly time-series of water levels extracted from completed Tier II runs were applied at the seaward ends (-15 m isobaths) of each of the profile models. These water level variations represented the cumulative effect of astronomic tides, storm surge (including IBE and wind setup), SLAs, and SLR. Neumann boundaries set to zero were used along the lateral boundaries: a condition that has been shown to work well with quasi-stationary situations where the coast can be assumed to be uniform alongshore outside the model domain (Roelvink and others, 2009).

Time series of H_s, T_p, and D_p saved at 20 minute intervals from the nested high resolution Tier II SWAN grid were also applied at the offshore boundary of each profile model. Sensitivity tests comparing the use of these bulk parameters versus full 2-dimensional spectral descriptions output from SWAN showed little difference in the modeled runup, and thus the simpler, and less memory-intensive, approach employed in this study was use of bulk statistical representation of wave conditions as forcing. Bulk parameters extracted from the Tier II simulations were converted to parametric Jonswap spectra by the XBeach model using a 3.3 peak enhancement factor and a cosine law directional spreading coefficient of 10.

3.5 Long-term morphodynamic change models

To better characterize and incorporate the impact of long-term morphologic change on flood hazards, a cliff recession model and a sandy coast shoreline change model were developed for this study (purple trapezoid in fig. 2). Both models are transect based, one-line models, that were used to predict cliff

top recession and lateral movement of the mean high water (MHW) position at the CSTs used to simulate wave setup and runup with the Tier III XBeach model.

The cliff recession model (Limber and others, 2015) employs a suite of models, including 2-D process-based soft rock (loosely consolidated sediment deposits) and hard rock (indurated lithologies such as sandstone or granite) models, and several empirical 1-D models that relate wave impacts and water level variations (e.g. storm surges, sea level anomalies) directly to cliff edge retreat through time (Trenhaile, 2000, 2009, 2011; Walkden and Hall, 2005; Walkden and Dickson, 2008; Hackney and others, 2011; Revell and others, 2011).

The sandy coast shoreline change model (CoSMoS Coastal One-line Assimilated Simulation Tool CoSMoS-COAST; Vitousek and others, 2015) incorporates historical trend analysis and three process-based models that compute both long- and cross-shore transport of sandy shores (Pelnard-Considere, 1956; Bruun 1962; Larson and others, 1997; Davidson-Arnott, 2005; Yates and others, 2009; Long and Plant, 2012; Anderson and others, 2015; Vitousek & Barnard, 2015). Historical shoreline positions and a Kalman filter were used to auto-tune the model parameters (Long and Plant, 2012) and to implicitly account for unresolved sediment transport processes and inputs, such as sediment loading from rivers and streams, regional sediment supply, and long-term erosion.

The cliff and shoreline models were used to project cliff top recession and movement of the MHW line, respectively, for nine SLR scenarios (0.25 m to 2 m, at 0.25 m increments, and 5 m). Projected time-series of SLR and waves (height, period, and incident direction) at the offshore ends of the CSTs served as boundary conditions for both the cliff recession (2,017 profiles) and shoreline change (4,011 profiles) models.

SLR was represented with a second-order polynomial curve that reached 1 m or greater by the year 2100, relative to 2000. For SLR rates of 0.25 m, 0.50 m and 0.75 m, long-term morphodynamic change simulations were run up through Jan 01, 2044, 2069, 2088, respectively, based on the National Research Council (2012) values for Southern California (2012).

Projected wave time-series were derived from a look-up-table constructed from numerical simulations. The look-up-table relates deep-water waves to nearshore wave conditions and was developed from a 30-year hindcast (Hegermiller and others, 2016). Using this look-up-table and dynamically downscaled GFDL-ESM2M RCP4.5 wave projections (see Section 3.1), 100+ year long time-series of 3-hourly nearshore wave conditions were generated at each of the CSTs and used as boundary conditions to the long-term morphodynamic change models (gray trapezoid in fig. 2). This approach of developing and using a look-up-table, was done because of the high computational expense associated with computing long (100+ years) continuous time-series within the large geographic extent of the SCB.

Several different management scenarios involving beach nourishment and the existence and maintenance of hard structures to limit erosion were simulated with both the cliff recession and sandy shoreline change models. Two management scenarios were investigated for the cliff recession projections: (1) cliff recession unlimited by cliff armoring, and (2) no cliff recession where armoring currently (2016) exists. For the sandy shoreline projections, four management scenarios were simulated, representing all combinations of: (1) no beach nourishment or continued rates of historical beach nourishment were investigated for the sandy shoreline simulations, and (2) the existence or non-existence of hard structures that limit erosion. This “hold-the-line” hard-structures scenario was achieved by limiting erosion to an 180,000-point polyline digitized from aerial photos (Google Earth, 2015/2016) that represents the division of beach and urban infrastructure.

Feedback between the cliff and shoreline change models was not incorporated for this application. However, the cliff recession model did include foreshore accretion in cases of failed cliff material. In future model applications, the CoSMoS-COAST and cliff retreat models will be coupled together.Incorporating long-term morphodynamic change with the flood modeling

Incorporating long-term morphodynamic change with the flood modeling in CoSMoS 3.0 Phase 2, was done by evolving the original (0 m SLR) cross-shore profiles by the projected long-term cliff recession and MHW positions associated with each SLR. The selected long-term management scenario assumed that beach nourishment would cease but that existing cliff armoring and flood/beach protection infrastructure remains in place (i.e., the "hold-the-line" scenario). The resulting 'evolved' profiles were then used to simulate inundation and runup with the Tier III XBeach model (Section 3.4). No adjustments were made to the depth and topography representations in the Tier II Delft3D high-resolution grids that were used to simulate inland flooding (Section 3.3).

Profile changes incorporated recession of the cliff top and consequential retreat of the cliff face, lateral migration of the MHW position, and vertical translation in keeping with SLR (fig. 5). These shoreline modifications were made only within the active beach region and up to the urban development boundary used to "hold-the-line".

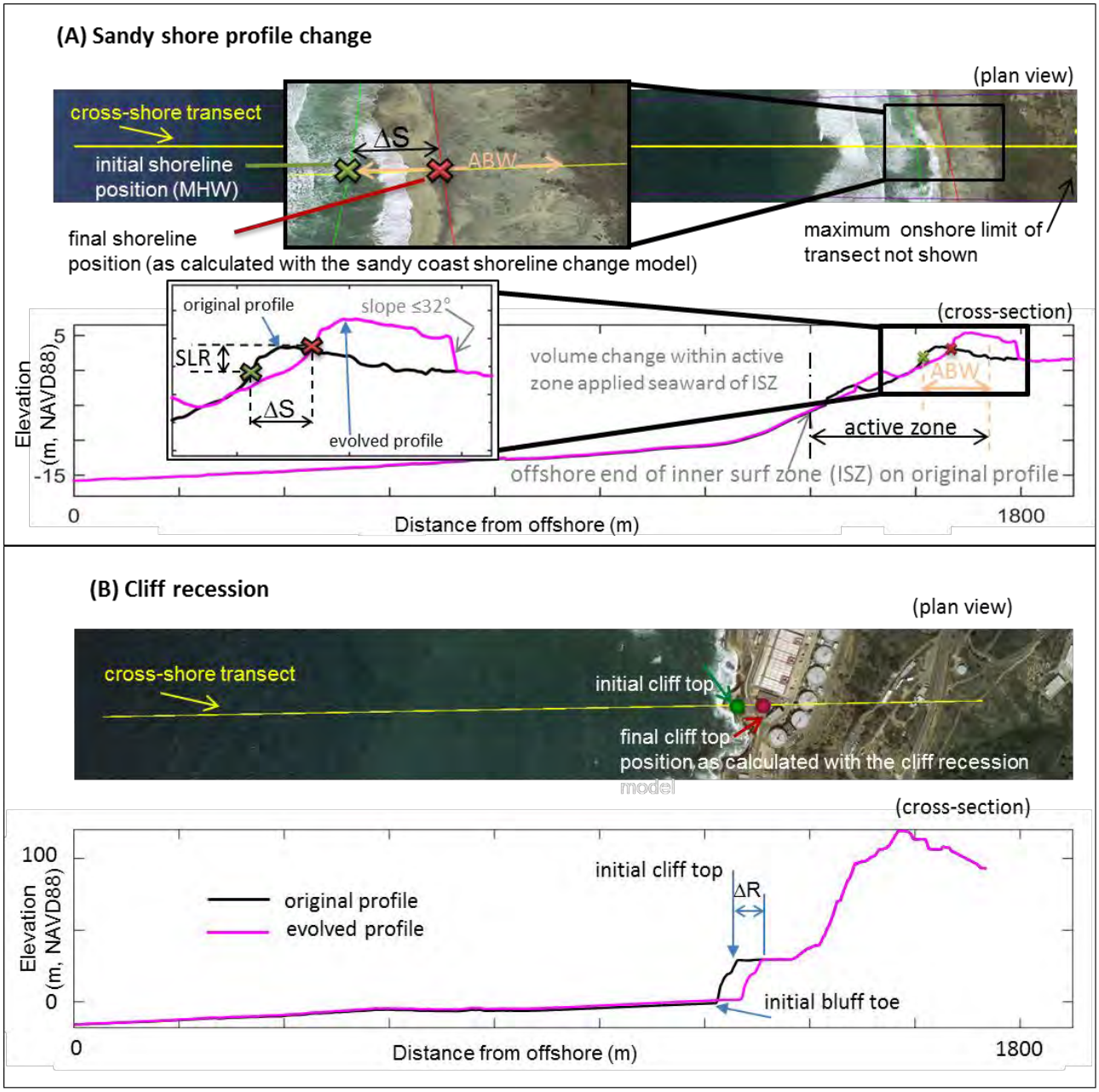

Figure 5. Example profile types considered in merging cliff and shoreline model projections. (A) Schematic of key parameters used in the evolution of soft (sand and gravel) beaches (ΔS: = change in mean-high-water position; ABW: active beach width). (B) Schematic of key parameters used in the evolution of cliff profiles (ΔR: = cliff recession).

3.6 Fluvial discharge model

At the time of this study, there were no available time-series of 21st century discharge rates associated with the RCP 4.5 scenario, and therefore idealized hydrographs were constructed. Idealized hydrographs were generated by parameterization of peak discharge rates and estimation of the duration and rate of increase and decrease of discharges associated with coastal storm events.

Peak discharge rates

Fluvial discharge points considered most relevant in influencing coastal flooding and used within the Tier II model domains were separated into two groups: 1) gauged streams and rivers for which we were able to identify a relationship between peak flows and an independent atmospheric variable available as part of GCM model outputs (which after testing turns out to be SLP gradients, ∇SLP), and 2) subordinate rivers and tributaries. Variants of SLPs, a readily available parameter in GCM outputs, were tested against peak discharge rates measured at 18 USGS gauging sites. Peak discharge rates were defined as the 99.95th percentile flow rate from records that were at least 40 years long and sampled at 15 minute intervals (http://waterdata.usgs.gov/ca/nwis/rt). Reasonably strong linear relationships ($0.42 < r < 0.92$, *p*-values between 0.003 and 0.731) were found between maximum sea level pressure gradients (∇SLP) and peak discharge at 7 stations (table 4). ∇SLP were computed with the CaRD10 hindcast covering 3 days prior to peak discharge and within a 0.67° to 1° radius of the gauging station. Time periods within 1, 3, and 5 days preceding an event and within 0.67°, 1°, and 5° search radii were tested. Best fits were obtained with the 3 day window and 0.67° search radius for all sites but Santa Ana and Santa Margarita for which a 1° search radius gave the best results. Whereas the correlation for Ventura and Santa Margarita Rivers were somewhat poor (correlation coefficients, $r = 0.49$ and $r = 0.42$, respectively, see table 4) these discharge points were kept because of the lack of alternative major surrogate rivers in these locations.

The linear relationship established between measured peak fluvial discharge rates and ∇SLP allows for an estimate of peak discharge events associated with future storms. In CoSMoS, ∇SLP were calculated for each primary discharge site from GCM pressure fields associated with a particular storm. These values were used in the linear model with appropriate coefficients (last columns in table 4) to estimate peak discharge rates (in m^3/s) for a given storm.

Table 4. Primary fluvial discharges: gauged stations for which linear relationships between fluvial discharge (Q) and sea level pressure gradients (∇SLP) were established.

USGS gauging station ID	station name	Drainage area (km^2)	*r*	*p*-val	best fits Q=m·∇SLP+b	
					m	b
11119750	Mission Ck	22	0.82	0.022	1.577E-07	2.234E-07
11120000	Atascadero	49	0.92	0.003	2.060E-07	-4.621E-08
11118500	Ventura River	487	0.48	0.274	1.503E-07	-2.131E-07
11106550	Calleguas Creek	642	0.74	0.058	6.303E-08	-1.909E-08
11102300	Rio Hondo (L.A. trib.)	321	0.78	0.040	7.094E-08	1.376E-06
11078000	Santa Ana	4403	0.66	0.103	1.662E-08	-2.358E-08
11046000	Santa Margarita	1873	0.42	0.731	2.702E-08	-1.208E-08

Sub-ordinate rivers and tributaries were assigned to one of the nine primary discharges (table 5; fig. 6) based on proximity and location relative to the primary watersheds as well as previous studies that have evaluated similar relationships (Warrick and Farnsworth, 2009). Peak discharge rates associated with individual storm events were estimated by assuming that the runoff rates of the subordinate discharges,

defined as the fluvial discharge rate divided by the drainage area, are equal to the runoff rate of the primary discharge (see flow chart in fig. 6). Drainage areas upstream of each gauging station were derived from USGS 12-digit and 8-digit (where necessary) watershed boundaries, local water district maps (for verification and inclusion of all necessary tributaries), and other published sources.

Table 5. Sub-ordinate rivers and tributaries, drainage areas, and associated primary discharges.

Sub-ordinate river/tributary	Drainage area (km^2)	USGS gauging station
Primary discharge: Atascedero		
Jalama	64	11120000
Gaviota	52	11120000
Refugio	21	11120000
El Capitan	16	11120000
Devereux	10	11120000
Goleta	15	11120000
Goleta2	15	11120000
Goleta3	15	11120000
Goleta4	24	11120000
Goleta5	51	11120000
Primary discharge: Mission Creek		
Arroyo burro	25	11119750
Mission	30	11119750
Carp_SM1	1	11119750
Carp_SM2	7	11119750
Rincon	38	11119750
Primary discharge: Ventura		
Ventura R	487	11118500
Santa Clara R	4,128	11118500
Primary discharge: Calleguas		
Mailbu	284	11106550
Primary discharge: Santa Margarita		
San Juan	303	11046000
San Mateo	346	11046000
San Onofre	111	11046000
Los Flores	69	11046000
Santa Margarita R	1,916	11046000
San Luis Rey	1,442	11046000
Buena Vista	56	11046000
Agua Hedionda	77	11046000
Batiquitos	138	11046000
San Elijo	219	11046000
Del Mar	894	11046000
Pensaquitos	244	11046000
San Diego	976	11046000
Sweetwater	564	11046000
Otay	367	11046000
Tijuana	4,390	11046000
Primary discharge: Rio Hondo		
Ballona	332	11102300
Dominguez	175	11102300
Bolsa Chica	5	11102300
Newport Bay	306	11102300
Primary discharge: Santa Ana		
Los Angeles R	2,156	11078000
San Gabriel R	1,658	11078000

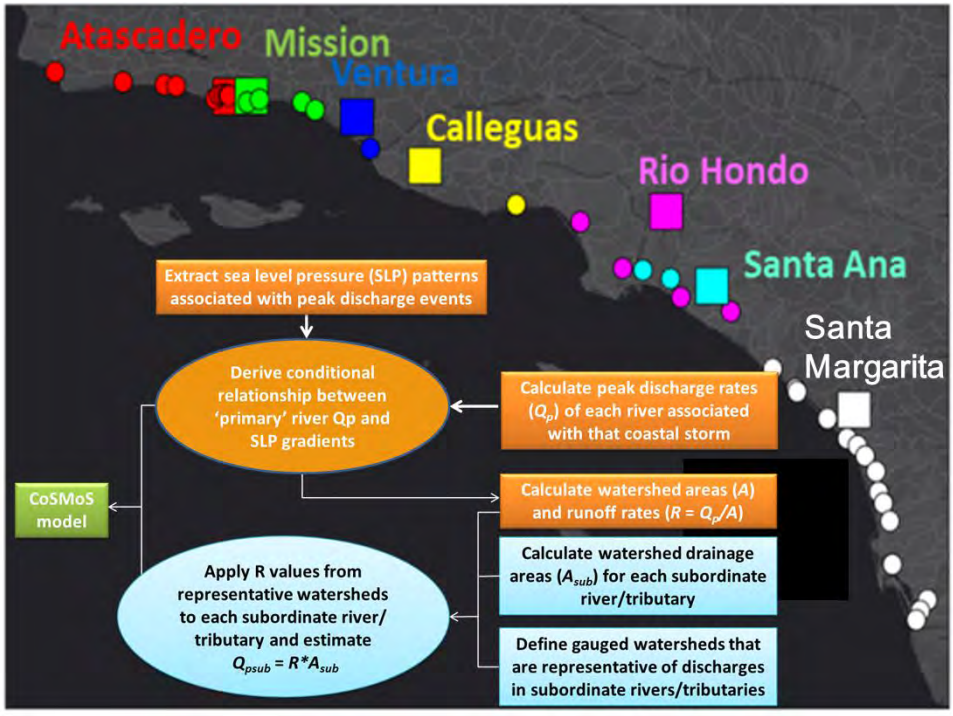

Figure 6. Schematic of approach used to estimate peak fluvial discharge rates associated with atmospheric storm patterns for coastal storms simulated with CoSMoS ver. 3.0. Primary discharges and sub-ordinate rivers and tributaries are color coded in the map figure. The flow chart details the method used to derive a conditional relationship between atmospheric storm patterns and peak fluvial discharge rates of 'primary discharges' (filled squares) and the method used to derive peak flows of sub-ordinate discharges (filled circles).

Idealized hydrograph

An idealized hydrograph was developed with the aim of estimating the duration and rate of increase and decrease of peak discharge events. Stations where data were available at 15 minutes or better sampling resolution, and for which at least 4 events exceeded the 99.95th percentile during the record period, were used to develop the hydrograph. Nine stations within the study area met these criteria (table 6). Events that exceeded the 99.95th percentile (column 7 in table 6) were selected, normalized, and used to develop the hydrograph assuming a lognormal distribution. The shape of the idealized hydrograph is skewed toward rapid initial increases in flow and subsequent slower rates of decreasing discharge rates (fig. 7). The total duration is on the order of 0.7 days (17 hours) for flows that exceed 10% of the peak discharge.

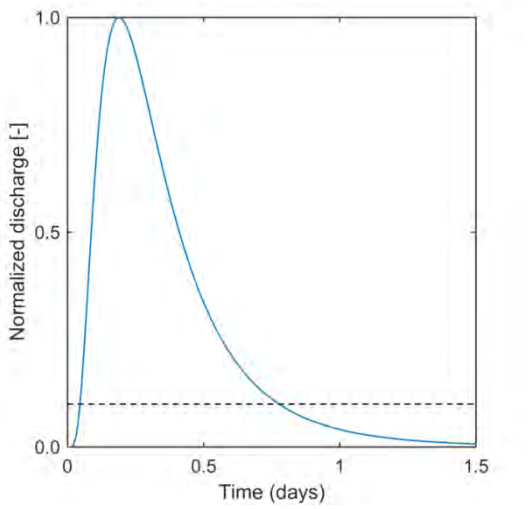

Figure 7. Idealized hydrograph. Dashed horizontal line indicates 10% peak discharge rates.

Table 6. Gauging stations and details of each for development of unit hydrograph.

USGS gauging station ID	Lat (°N) (NAD27)	Lon (°E) (NAD27)	Length of record (years)	Mean flow (m^3/s)	Median flow (m^3/s)	99.95th per-centile (m^3/s)	# events ≥99.95th per-centile	Lognormal mean (days)	Lognormal variance (days)
11119750	34.428	-119.725	44	0.06	0.00	13	5	-1.51	0.84
11120000	34.425	-119.812	73	0.14	0.00	38	5	-3.66	1.80
11109000	34.404	-118.739	87	1.67	1.08	77	5	-1.11	0.80
11119500	34.401	-119.487	74	0.05	0.00	14	4	-1.30	0.79
11106550	34.179	-119.040	46	0.97	0.31	120	3	-1.48	0.90
11092450	34.162	-118.467	83	2.90	1.84	290	6	-2.12	1.51
11048600	33.645	-117.861	14	0.05	0.02	9	8	-3.27	1.46
11047300	33.498	-117.666	42	0.45	0.08	61	5	-3.10	1.42
11046000	33.311	-117.347	92	0.89	0.13	98	5	-2.15	1.01
		mean	61.73	0.80	0.38	80	5	-2.19	1.17
		min.	13.51	0.05	0.00	9	3	-3.66	0.79
		max.	91.89	2.90	1.84	290	8	-1.11	1.80

Section 4. Identification of storm events

The model system, which aims to account for the most relevant atmospheric and oceanic processes that might contribute to future flooding and associated coastal hazards and the inter-related non-linear physics of each of these, requires downscaling from the global to local level and is computationally expensive. Because of the long simulation times, it is not feasible to run all Tiers for the entire 21st century time-

period. Instead, a hybrid numerical-analytical downscaling approach was developed to estimate total water levels (TWL), inclusive of storm-wave and surge impacts and long-term climatic variation, in the SCB nearshore region. From this, relevant return period storm events were selected and used for Tiers I through III detailed modeling.

TWL time-series up through the year 2100 were computed at 4,802 coastal points within the SCB using downscaled waves (Hegermiller and others, 2016) and SLPs and SSTs from the GFDL-ESM2M RCP 4.5 GCM. The 1-year, 20-year, and 100-year future coastal storm events were identified at each location and clustered with a *k*-means algorithm to delineate coastal segments where individual storms result in similar return period water levels. Clustering of extreme events showed that the more severe but rare coastal flood events (e.g., the 100-year event) occur for most of the region from the same storm. In contrast, different storms from varying directions were responsible for the less severe, but more frequent, local coastal flood events. To this end, two 100-year storms were identified (February 2044 and March 2059), two 20-year storms (February 2025 and February 2095), and three 1-year storms (March 2020, December 2056, and January 2097)). Upon completion of 1-year storm simulations using the entire train of models (resolving detailed flow dynamics and wave-current interaction) for a range of SLRs, results showed a single 1-year storm (March 2020) consistently yielded the highest water levels throughout the SCB; thus, Phase 2 1-year projections use contributions from only that storm. Deep water waves, SLAs, and maximum and minimum wind speeds and SLPs within the entire model domain, are summarized for each of the identified storm events in table 7.

Table 7. Boundary conditions associated with each modeled scenario. Deep water wave conditions (Hs, Tp, and Dp) applied at all open boundaries of the Tier I wave grid. Sea level anomalies (SLA) applied uniformly to all model domains. Sea level pressures (SLPs) and wind speeds vary in time and space. Those shown are the minimum and maximum values, respectively, attained somewhere within Southern California Bight domain.

Scenario	Hs (m)	Tp (s)	Dp (degrees)	SLA (m)	Minimum SLP (kPa)	Maximum wind speed (m/s)
background	1.75	12	286	0	NA	NA
1-year storm #1	4.39	16	284	0.16	100.56	22.8
20-year storm#1	5.86	18	281	0.18	100.79	22.3
20-year storm#2	6.13	18	292	0.24	100.41	28.7
100-year storm#1	6.20	16	264	0.19	100.43	26.6
100-year storm#2	6.80	18	287	0.23	98.67	30.3

NA: not applicable

Section 5. Scenarios and Timing of Events

Individual coastal storm events, as represented by high waves, strong winds, low sea level pressures, and large scale phenomenon that produce month long changes in water levels, were modeled in conjunction with a spring tide and various states of sea level rise to simulate the impacts of a ‘scenario’. In CoSMoS version 3.0, each storm is represented by dynamically downscaled waves, winds, and sea-level pressures from the same GCM model, resulting in realistic representations of passing storm systems and internally consistent timing of these processes. However, because storm events and astronomic tides are independent phenomena, a given storm event can occur during any part of the tide cycle. A storm that occurs during high tide may result in substantial flooding and damage, but conversely may impart very

little destruction if the storm were to occur during low tide. For less computationally intensive modeling systems, a probabilistic approach can be taken to evaluate coastal impacts from storms that occur during different stages of the tide, but with the deterministic process-based CoSMoS model that aims to resolve details and non-linear processes, this is not presently feasible. Instead, it is assumed that each storm coincides with a high spring tide (tide levels that occur approximately twice every month for a total of ~8 days). This represents a near-worst case scenario, with the 'King Tide' being slightly higher but much less frequent, occurring typically only during two ~3-4 day time periods per year.

Each scenario is simulated over a 24 hour time-period with Tiers II and III (fig. 8). Tier I is run for 28 days to allow for model 'spin-up'. Sea-level rise and SLA are held constant and uniform through the duration of the scenario. Deep water wave forcing are also held constant throughout the simulation at the open boundary of Tier I, but consequently vary in height and direction as they approach the shore in response to changes in both bathymetry and water levels. SLP fields are shifted in time so that the lowest pressure anywhere within the Tier I model domain aligns in time with the high tide at the Los Angeles tide station (approximate center of the study area, hour 17 in fig. 8), thus "synching" the storm arrival with the high tide level. The wind fields are similarly time-shifted since these are physically linked to the pressures and share a common time-stamp. For fluvial discharges, the peak of the hydrograph is placed 1hour following the high tide. The timing of the hydrograph was selected based on comparisons between peak fluvial discharge rates at gauging stations close to shore (e.g. Malibu) and hindcast time-series of nearshore wave conditions. Comparisons of these time-series revealed that the peak storm H_s consistently preceded the peak in fluvial discharge rates due to the lag in response time of the associated watersheds.

Forcing / boundary	Timing
tides	varies spatially and temporally and is identical for each scenario
SLR	constant for duration of scenario (but differs between scenarios)
SLA	constant for duration of scenario (but differs between scenarios)
deep water waves	constant for duration of scenario (but differs between scenarios)
SLPs	varies spatially and temporally, timing assigned such that the lowest SLP anywhere within the SoCal Bight aligns with high tide
winds	varies spatially and temporally linked to the timing of SLPs
river discharge	varies temporally at each established USGS gauging site via a idealized hydrograph and derived peak discharge rate based on SLP gradients; timing is hardwired to occur with peak 1hr after high tide

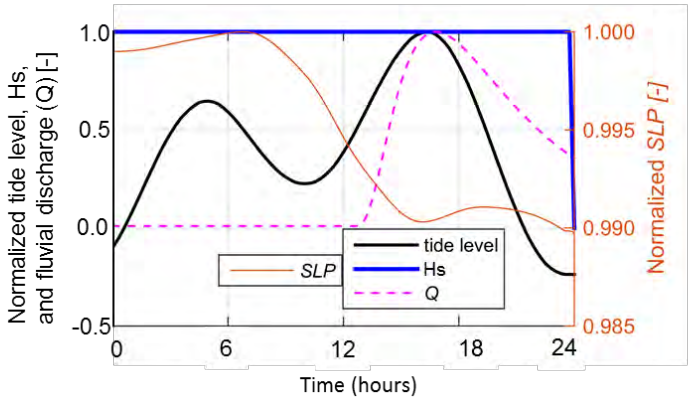

Figure 8. Summary list and plot illustrating timing of individual forcing agents used in model simulations. Abbreviations: SLR: sea-level rise; SLA: sea level anomalies; SLPs: sea-level pressure.

Section 6. Determination of flood extents and uncertainty estimates

Flood extents were determined in two ways: 1) from the landward-most wet grid cell in the high-resolution Delft3D grids, and 2) from maximum wave setup calculated with XBeach cross-shore models along the open coast. Wave setup is the increase in mean water level above the still water line due to the transfer of momentum by waves that are breaking or otherwise dissipating their energy. Wave setup can last from several to ten or more times the length of the incident wave period. Storm-related T_p in southern California are typically on the order of 14 s (CDIP092 for two storm events: Dec 2005 and Jan 2010 storm events); assuming 5 times the dominant incident period of 14s means setup lasts a little less than a minute ($3 \cdot 14$ s) to nearly 5 minutes ($20 \cdot 14$ s). With this in mind, a two minute 8^{th} order Butterworth low-pass filter is applied to water level time-series computed with the XBeach model at the position of the present day MHHW line (1.57 m to 1.63 m above NAVD88). The intersection between the maximum 2-minute sustained water level and landward position of the eroded XBeach profile is then identified and set as the maximum flood extent (fig. 9). Note that except where overtopping occurs or at a narrow beach that fronts a near vertical cliff or wall, this method results in a flood extent that is seaward of the maximum runup in most areas. Maximum runup is also output as part of the CoSMoS results, but are mapped as single points rather than included in the flood extent. This is because runup levels are of shorter duration, and depending on the beach slope, may only constitute a couple of centimeters of intermittent standing water. The event-based erosion extent is dependent on the runup extent.

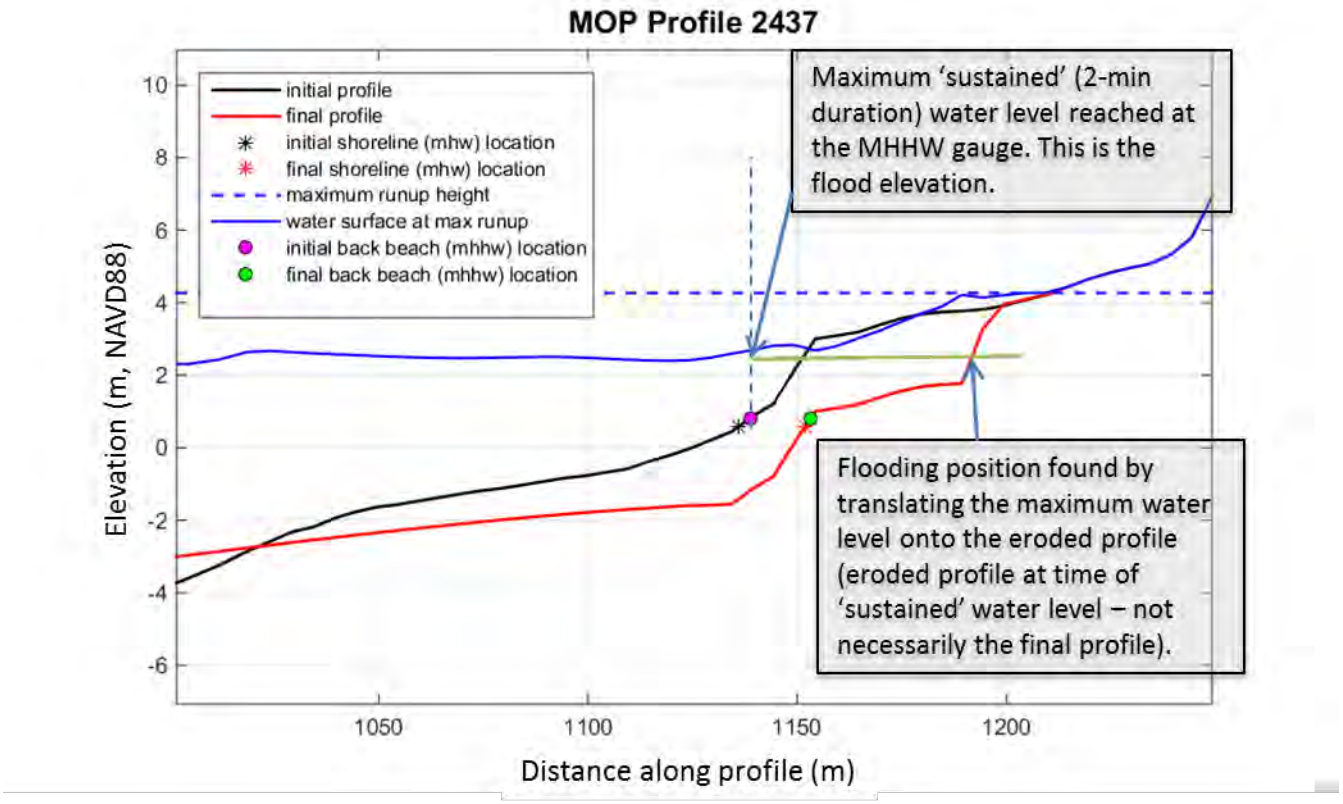

Figure 9. Illustration of method used to determine the flood extent at XBeach cross-shore profile models.

Melding of flood extents simulated with the XBeach and Delft3D high resolution models was done by interpolating (linear Delaunay Triangulation) resulting water level elevations onto a common 2 m resolution square mesh (within the Mathworks Matlab environment). In some areas, such as Mission Beach in San Diego County, where both XBeach and high resolution grids exist to capture flooding from either or both the landward or seaward side, XBeach results were given precedence (fig. 10).

This post-processing step was done for all storms simulated as part of a given scenario. For the 20-year storm for example, two individual storm events were modeled in order to ensure that local effects, such as shoreline orientation with respect to incident storm direction, were taken into account. For those cases where more than one storm was modeled, all resulting 2 m gridded flood maps were overlain and maximum water levels saved at each grid cell to generate a single, composite flood map for a given scenario (fig. 11).

Resulting water elevation surfaces were differenced from the high resolution DEM to isolate areas where the water level exceeds topographic elevations, indicating flooding. For scenarios that include SLR, 2 m DEMs that incorporate long-term morphodynamic changes were used. These DEMs were constructed by replacing original DEM data within the active beach zone with results of the long-term morphodynamic models (Section 3.5). The active beach zone was populated with data from the evolved >4,000 CSTs and additionally with data from sub-profiles spaced ~10 m apart in between the primary CSTs. Shoreline and cliff profile changes of the primary CSTs were projected onto 2 m cross-shore resolution sub-profiles; all CST and sub-CST data (Easting, Northing, elevation(ΔZ)) were then spatially interpolated within the active beach zone of the original DEM, to portray total morphological change.

The resulting flood maps were then processed to exclude isolated wetted areas not hydraulically connected to the ocean; these disconnected areas were flagged as low-lying vulnerable areas below the flood elevation.

Maps of associated maximum flood durations, velocities, and wave heights were processed in a similar manner to that of the flood depths and extents in that they were gridded onto a common 2 m mesh and then combined as illustrated in figure 10. Data that fell outside the flood map extents were removed so that the foot prints of all maps are identical.

Uncertainty bands of the final flood extents take into account numerical model errors, DEM uncertainty, and vertical land motion (VLM). Overall, tidal amplitudes, water levels, wave heights, and wave setup are reasonably well represented by the numerical models (data and comparisons are out of the scope in this document but will be provided in upcoming publications). The area and number of storms tested are however, small in relation to the large geographic scope and thus model error is estimated to be ±0.50 m. The vertical accuracy of the baseline DEM is estimated to be ±0.18 m, the 95% confidence level for topographic lidar measurements in open terrain (Dewberry, 2012). Spatially variable measurements of vertical land motion attributed to tectonic movement of the San Andreas Fault System from Howell and others (2016) were also incorporated. Maximum rates of uplift (0.4mm/yr) and subsidence (0.6mm/yr) within our study area equate to a maximum of 3.4 cm of uplift and 5.2 cm of subsidence for the 1m SLR scenario based on the National Research Council (2012) SLR projections for Southern California (2012) of 1m of SLR by the year 2100. The VLM uncertainty for the 1m SLR scenario was also applied for scenarios > 1m. Uncertainty bands were applied to the final flood maps by raising and lowering the evolved DEMs (or baseline DEM for 0 SLR scenarios) by ± 0.68 m plus elevation uplift or subsidence resulting from VLM. The flood extent uncertainty bands do not take into account additional uncertainty resulting from cliff recession and shoreline change projections in the evolved DEMs. Uncertainties in cliff retreat and shoreline change projections are provided within their respective data files.

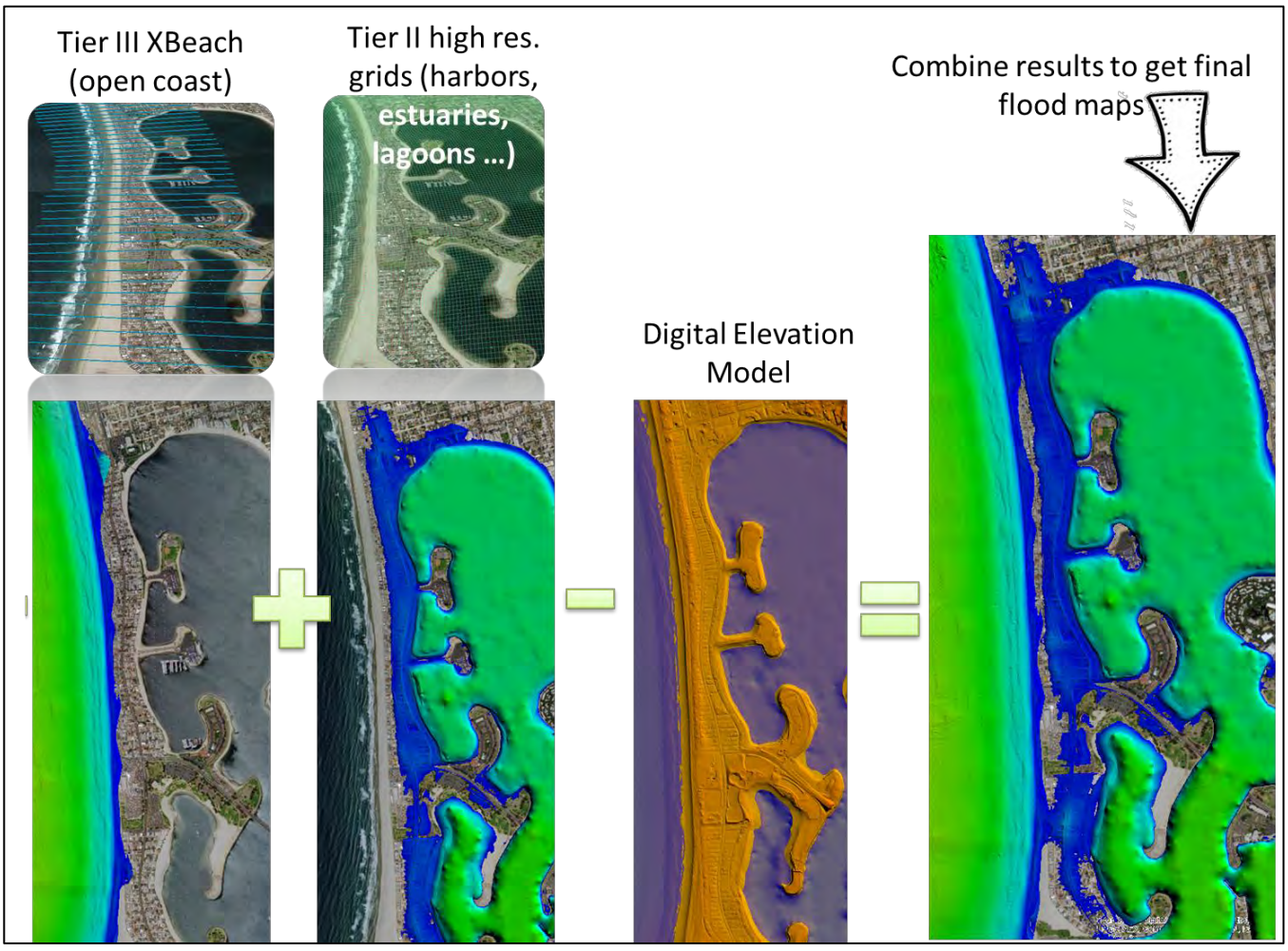

Figure 10. Schematic illustrating melding of Tier II and Tier III flood elevations and extents. Example shown is of Mission Beach, San Diego County.

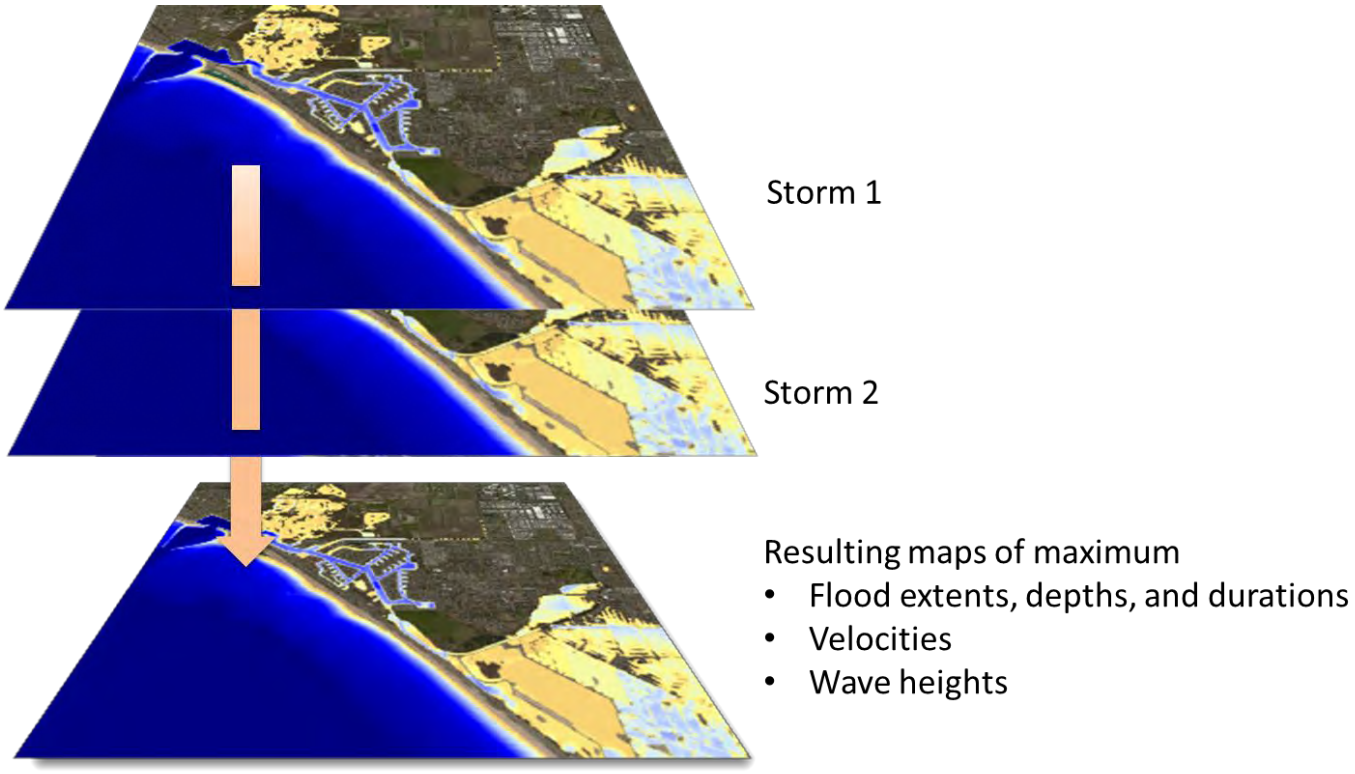

Figure 11. Schematic illustrating the combination of multiple model results from several storm simulations to attain one single map of local maximum values.

Acknowledgements

This work was funded by the USGS Coastal and Marine Geology Program and carried out under the USGS Climate Change Impacts to the U.S. Pacific and Arctic Coasts Project. The initial funding for CoSMoS 3.0, primarily from the California State Coastal Conservancy with additional support from the City of Imperial Beach, California Department of Fish & Wildlife, and Tijuana River National Estuarine Research Reserve (TJNERR), and substantial support from within USGS, was for the preliminary construction of CoSMoS 3.0, including shoreline and cliff model development and the delivery of 5 SLR scenarios (i.e., 0, 50, 100, 150 and 200 cm) in combination with the 100-year coastal storm. Here we report on the data and methods utilized in the continuation of this effort, Phase 2. Phase 2, to include all 40 storm (no storm, annual, 20-year and 100-year) and SLR scenarios (0-2 m in 25 cm increments, plus 5 m) is funded by California's 4th Climate Assessment.

References

Adams, P. N., Inman, D.L., and Lovering, J.L., 2011. Effects of climate change and wave direction on longshore sediment transport patterns in Southern California. Climatic Change, 103,, S211-S228.

Anderson, T. R., Fletcher, C. H., Barbee, M. M., Frazer, L. N., and Romine, B. M., 2015. Doubling of coastal erosion under rising sea level by mid-century in Hawaii. Natural Hazards, 78(1), 75-103.

Barnard, P.L., van Ormondt, M., Erikson, L.H., Eshleman, J., Hapke, C., Ruggiero, P., Adams, P.N. and Foxgrover, A.C., 2014. Development of the Coastal Storm Modeling System (CoSMoS) for predicting

the impact of storms on high-energy, active-margin coasts. Natural Hazards, Volume 74 (2), p. 1095-1125, *http://dx.doi.org/10.1007/s11069-014-1236-y*

Booij, N., Ris, R.C., and Holthuijsen, L.H., 1999. A third generation model for coastal regions, Part I – Model description and validation. Journal of Geophysical Research, 104(C4), 7649-7666

Bromirski, P.D., Flick, R.E., and Cayan, D.R., 2003. Storminess variability along the California coast: 1858–2000, Journal of Climate, 16(6), 982–993.

Bruun, P., 1962. Sea-level rise as a cause of shore erosion, Proceedings of the American Society of Civil Engineers, Journal of the Waterways and Harbors Division, 88, 117 – 130.

Cayan, D.R., Bromirski, P.D., Hayhoe, K., Tyree, M., Dettinger, M.D., Flick, R.E., 2008. Climate change projections of sea level extremes along the California coast. Climate Change, S57-S73.

Christiansen R.L., Yeats, R.S., 1992. Post-Laramide geology of the U.S. Cordilleran region. In: Burchfiel BC, Lipman PW, and Zoback ML (eds), The Cordilleran orogen: conterminous U.S.: the geology of North America [DNAG] Vol. G-3: geological society of America, 261–406 .

Crosby, S.C., O'Reilly, W.C., and Guza, R.T., 2016. Modeling long period swell in southern California: practical boundary conditions from buoy observations and global wave model predictions. J. Atm. Ocean Technology, in press.

Davidson-Arnott, R. G., 2005. Conceptual Model of the Effects of Sea Level Rise on Sandy Coasts, J. of Coastal Res., 21, 6, 1116-1172.

Dewberry, 2012. LiDAR Quality Assurance (QA) Report California, LiDAR and Imagery QA submitted to: NOAA Coastal Services Center, *https://coast.noaa.gov/htdata/lidar1_z/geoid12a/data/1124/supplemental/ca2009_2011_ca_coastal_conservancy_m1124_qareport.pdf*

Donat, M.G., Leckebusch, G.C., Wild, S., and Ulbrich, U., 2010. Benefits and limitations of regional multi-model ensembles for storm loss estimations: Climate Research, v. 44, p. 211–225.

Dunne, J.P., John, J.G., Adcroft, A.J., Griffies, S.M.m Hallberg, R.W., Shevliakova, E., Stougger. R.J., Cooke, W., Dunne, K.A., Harrison, M.J., Krasting, J.P., Malyshev, S.L., Milly, P.C.D., Phillipps, P.J., Sentman, L.T., Samuels, B.L., Spelman, M.J., Winton, M., Winttenberg, A.T., and Zadeh, N., 2012. GFDL's ESM2M global coupled climate-carbon earth system models. Part I: physical formulation and baseline simulation characteristics, Journal of Climate, 25, 6646-6665.

Flick, R. E., 1998. Comparison of California tides, storm surges, and mean sea level during the El Niño winters of 1982–1983 and 1997–1998. Shore & Beach 66(3):7–11.

Egbert, G., Bennet, A., Foreman, M., 1994. TOPEX/POSEIDON tides estimated using a global inverse model. Journal of Geophysical Research 99 (C12), 821–824.

Erikson, L.H., Hegermiller, C.A., Barnard, P.L., Ruggiero, P. andvan Ormondt, M., 2015. Projected wave conditions in the Eastern North Pacific under the influence of two CMIP5 climate scenarios. Journal of Ocean Modelling, (0000)1-15, *http://dx.doi.org/10.1016/j.ocemod.2015.07.004*

Cayan, D., Kalansky, J., Iacobells, S., Pierce, D., Franco, G., Anderson, J., Wilhelm, S., Bedsworth, L., Anderson, M., 2016. Sa level rise scenarios for California's fourth climate assessment. Early release, subject to revision.

Hackney, C., Darby, S. E., & Leyland, J., 2013. Modelling the response of soft cliffs to climate change: A statistical, process-response model using accumulated excess energy. Geomorphology, 187, 108-121.

Hasselmann, S., Hasselmann, K., Allender, J. H., Barnett, T. P. , 1985. Computations and parameterizations of the nonlinear energy transfer in a gravity-wave spectrum. Part II: parameterizations of the nonlinear energy transfer for application in wave models, J. Physical Oceanography, 15, 1378–1391.

Hegermiller, C.E., Erikson, L.H., and Barnard, P.L., 2016. Nearshore waves in the Southern California Bight: A 30-year hindcast and 90-year projected time series for the 21st century. U.S. Geological Survey summary of methods to accompany data release.

Hibbard, K. A., G. A. Meehl, P. Cox, and Friedlingstein, P., 2007. A strategy for climate change stabilization experiments. Eos, Trans. Amer. Geophys. Union, 88, doi:10.1029/2007EO200002.

Howell, S., Smith-Konter, B., Frazer, N., Tong, X., and D. Sandwell. 2016. The vertical fingerprint of earthquake cycle loading in southern California. Nature Geoscience, 9,611-614. http://dx.doi.org/10.1038/ngeo2741

Kanamaru H., and Kanamitsu, M., 2007. Fifty-seven-year California reanalysis downscaling at 10 km (card10). Part ii: comparison with North American regional reanalysis. J. Climate, 20, 5572–5592.

Larson, M., Hansen, H. and N. C. Kraus, 1997. Analytical solution of one-line model for shoreline change near coastal structures, Journal of Waterway, Port, Coastal, and Ocean Engineering 123 (4):180-191.

Lesser, G., Roelvink, J., Van Kester, J., Stelling, G., 2004. Development and validation of a three-dimensional morphological model. Coastal Engineering, 51, 883–915.

Limber, P., Barnard, P.L. and Hapke., C., 2015. Towards projecting the retreat of California's coastal cliffs during the 21st Century. In: P. Wang, J.D. Rosati and J. Cheng (Eds.), The Proceedings of the Coastal Sediments 2015, World Scientific, 14 pp., doi:10.1142/9789814689977_0245

Long, J. W. and Plant, N. G., 2012. Extended Kalman Filter framework for forecasting shoreline evolution, Geophys. Res. Lett., 39, L13603, doi:10.1029/2012GL052180.

Meinshausen, M., and Coauthors, 2011. The RCP greenhouse gas concentrations and their extensions from 1765 to 2300. Climate Change, 109**,** 213-241.

Moss, R. H., and Coauthors, 2010: The next generation of scenarios for climate change research and assessment. Nature, 463, 747-756.

National Oceanic and Atmospheric Administration (NOAA), 2016. National Ocean Service, Data Catalog, Retrieved from https://data.noaa.gov/dataset/2009-2011-ca-coastal-california-topobathy-merged-project-digital-elevation-model-dem on 09 January 2014.

National Research Council (NRC), 2012. Sea-level rise for the coasts of California, Oregon, and Washington: past, present, and future. Committee on Sea Level Rise in California, Oregon, and Washington. The National Academies Press, Washington, 260 p.

O'Reilly W.C., Guza, R.T., 1993. Comparison of two spectral wave models in the Southern California Bight. Coastal Engineering, 19(3):263–282.

O'Reilly W.C., Guza, R.T., and Seymour, R.J., 1999. Wave prediction in the Santa Barbara Channel. Proc. 5th California Islands symposium, mineral management service, Santa Barbara CA, March 29–31.

Pelnard-Considere, R. ,1956. Essai de theorie de l'evolution des formes de rivage en plages de sable et de galets. 4th Journees de l'Hydraulique, Les energies de la Mer, Paris, 3(1), 289-298.

Revell, D. L., Battalio, R., Spear, B., Ruggiero, P., & Vandever, J., 2011. A methodology for predicting future coastal hazards due to sea-level rise on the California Coast. Climatic Change, 109(1), 251-276.

Reynolds, R.W., N.A. Rayner, T.M. Smith, D.C. Stokes, and W. Wang, 2002. An improved in situ and satellite SST analysis for climate. J. of Climate, 15, 1609-1625.

Ris, R.C., Booij, N., and Holthuijsen, L.H., 1999. A third-generation wave model for coastal regions: Part II –Verification.: Journal of Geophysical Research, 104(C4), 7667-7682.

Roelvink, J.A., 1993. Dissipation in random waves groups incident on a beach, Coastal Eng., 19 (1-2), 127-150.

Roelvink, D., Reniers, A., van Dongeren, A., de Vries, J.T. and McCall, R., 2009. Modeling storm impacts on beaches, dunes, and barrier islands, Coastal engineering 56 (11), 1133-1152

Rogers, W.E., Kaihatu, J.M., Hsu, L., Jensen, R.E., Dykes, J.D., Holland, K.T., 2007. Forecasting and hindcasting waves with the SWAN model in the Southern California Bight. Coastal Engineering, 54, 1-15.

Scripps Institution of Oceanography (SIO), 2016. Data retrieval by personal communication.

Soulsby, R. L., 1997. Dynamics of Marine Sands, Thomas Telford, London.

Storlazzi, C.D., Griggs, G.B., 1998. The 1997–98 El Niño and erosion processes along the central coast of California. Shore and Beach , 66(3):12–17.

Tolman, H. L., and D. Chalikov, 1996. Source Terms in a Third-Generation Wind Wave Model. Journal of Physical Oceanography, 26, 2497-2518.

Tolman, H.L., 2009. User manual and system documentation of WAVEWATCH III version 3.14. NOAA/NWS/NCEP/MMAB Technical Note 276:194 p

Trenhaile, A. S., 2000. Modeling the development of wave-cut shore platforms. Marine Geology, 166(1), 163-178.

Trenhaile, A. S., 2009. Modeling the erosion of cohesive clay coasts.Coastal Engineering, 56(1), 59-72.

Trenhaile, A. S., 2011. Predicting the response of hard and soft rock coasts to changes in sea level and wave height. Climatic Change, 109(3-4), 599-615.

U.S. Geological Survey (USGS), 2015. Coastal National Elevation Database (CoNED) Project – Topobathymetric Digital Elevatio Model. Sioux Falls, South Dakota. https://lta.cr.usgs.gov

Vitousek, S. and Barnard, P.L., 2015. A non-linear, implicit one-line model to predict long-term shoreline change. In: P. Wang, J.D. Rosati and J. Cheng (Eds.), The Proceedings of the Coastal Sediments 2015, World Scientific, 14 pp., doi:10.1142/9789814689977_0215

Walkden, M. J. A., & Hall, J. W., 2005. A predictive mesoscale model of the erosion and profile development of soft rock shores. Coastal Engineering,52(6), 535-563.

Walkden, M., & Dickson, M., 2008. Equilibrium erosion of soft rock shores with a shallow or absent beach under increased sea level rise. Marine Geology, 251(1), 75-84.

Warrick, J.A., and Farnsworth, K.L., 2009, Sources of sediment to the coastal waters of the Southern California Bight, in Lee, H.J., and Normark, W.R., eds., Earth science in the urban ocean--The Southern California Continental Borderland: Geological Society of America Special Paper 454, p. 39-52.

Yates, M. L., R. T. Guza, and W. C. O'Reilly, 2009. Equilibrium shoreline response: Observations and modeling, J. Geophys. Res., 114, C09014, doi:10.1029/2009JC005359.

Appendix A: Downloadable data files

CoSMoS v3.0 Phase 2 URL:	https://www.sciencebase.gov/catalog/item/57f1d4f3e4b0bc0bebfee139	
Description of CoSMoS v3.0 data (*per county unless stated otherwise*)	**Format**	**File name (compressed)**
CoSMoS Phase 2 flood hazard projections (flood extents, low-lying vulnerable areas, and flood uncertainty [max/min flood potential]): all SLRs for 1-year storm	shapefile	CoSMoS_v3_Phase2_1year_flood_hazards.zip
- all SLRs for 20-year storm	shapefile	CoSMoS_v3_Phase2_20year_flood_hazards.zip
- all SLRs for 100-year storm	shapefile	CoSMoS_v3_Phase2_100year_flood_hazards.zip
- all SLRs for background conditions	shapefile	CoSMoS_v3_Phase2_average_conditions_flood_hazards.zip
CoSMoS Phase 2 flood depth (centimeters) and duration (number hours of 24.85 hrs) projections: all SLRs for 1-year storm	GeoTIFF	CoSMoS_v3_Phase2_1year_flood_depth_and_duration.zip
- all SLRs for 20-year storm	GeoTIFF	CoSMoS_v3_Phase2_20year_flood_depth_and_duration.zip
- all SLRs for 100-year storm	GeoTIFF	CoSMoS_v3_Phase2_100year_flood_depth_and_duration.zip
- all SLRs for background conditions	GeoTIFF	CoSMoS_v3_Phase2_average_conditions_flood_depth_and_duration.zip
CoSMoS Phase 2 water level (total water level; relative to NAVD88) projections: all SLRs for 1-year storm	GeoTIFF	CoSMoS_v3_Phase2_1year_storm_water_elevation.zip
- all SLRs for 20-year storm	GeoTIFF	CoSMoS_v3_Phase2_20year_storm_water_elevation.zip
- all SLRs for 100-year storm	GeoTIFF	CoSMoS_v3_Phase2_100year_storm_water_elevation.zip
- all SLRs for background conditions	GeoTIFF	CoSMoS_v3_Phase2_average_conditions_water_elevation.zip
CoSMoS Phase 2 wave height projections: all SLRs for 1-year storm	GeoTIFF	CoSMoS_v3_Phase2_1year_storm_wave_height.zip
- all SLRs for 20-year storm	GeoTIFF	CoSMoS_v3_Phase2_20year_storm_wave_height.zip
- all SLRs for 100-year storm	GeoTIFF	CoSMoS_v3_Phase2_100year_storm_wave_height.zip
- all SLRs for background conditions	GeoTIFF	CoSMoS_v3_Phase2_average_conditions_wave_height.zip
CoSMoS Phase 2 ocean current projections: all SLRs for 1-year storm	GeoTIFF	CoSMoS_v3_Phase2_1year_storm_currents.zip
- all SLRs for 20-year storm	GeoTIFF	CoSMoS_v3_Phase2_20year_storm_currents.zip
- all SLRs for 100-year storm	GeoTIFF	CoSMoS_v3_Phase2_100year_storm_currents.zip
- all SLRs for background conditions	GeoTIFF	CoSMoS_v3_Phase2_average_conditions_currents.zip
CoSMoS-COAST Phase 2 projections of shoreline change for Southern California (all counties)	KMZ	CoSMoS_v3_Phase2_shoreline_projections.zip

CoSMoS Phase 2 projections of coastal cliff retreat for Southern California (all counties)	KMZ	CoSMoS_v3_Phase2_cliff_retreat_projections.zip

Appendix B: Abbreviations, figures, and tables

BCC	Beijing Climate Center, China
CDIP	Coastal Data Information Program
CMIP5	Fifth Phase of the Coupled Model Inter-Comparison Project
D_m	mean wave direction
D_p	peak wave direction
DBDB2	Digital Bathymetric Data Base
GCM	global climate model
GFDL	Geophysical Fluid Dynamics Laboratory, NOAA, USA
GSHHS	Global Self-consistent Hierarchical High-resolution Geography Database
H_s	significant wave height
INMCM	Institute of Numerical Mathematics climate model, Russia
MIROC	Model for Interdisciplinary Research on Climate, Japan
NDBC	National Data Buoy Center, NOAA, USA
NOAA	National Oceanic and Atmospheric Administration, USA
RCP	representative concentration pathway
SLR	sea-level rise
T_m	mean wave period
T_p	peak wave period
WW3	WAVEWATCH–III wave model

Figures

Tables